2022-12-01

In Vitro Characterization Of Novel Compounds With Anti-Cancer Activity

Edgar Alonso Borrego Puerta
University of Texas at El Paso

IN VITRO CHARACTERIZATION OF NOVEL COMPOUNDS WITH ANTI-CANCER ACTIVITY

EDGAR ALONSO BORREGO PUERTA

Doctoral Program in Biosciences

APPROVED:

Renato J. Aguilera Ph.D., Chair

Manuel Miranda-Arango, Ph.D.

Charles T. Spencer, Ph.D.

Sourav Roy, Ph.D.

Md Nurunnabi, Ph.D.

Stephen Crites, Ph.D.
Dean of the Graduate School

Dedication

I dedicate this to my parents, sister, brothers, nieces, nephew, and Mono for all their support and endless love.

IN VITRO CHARACTERIZATION OF NOVEL COMPOUNDS WITH ANTI-CANCER ACTIVITY

By

Edgar Alonso Borrego Puerta,

DISSERTATION

Presented to the Faculty of the Graduate School of

The University of Texas at El Paso

in Partial Fulfillment

of the Requirements

for the Degree of

DOCTOR OF PHILOSOPHY

Department of Biological Sciences

THE UNIVERSITY OF TEXAS AT EL PASO

December 2022

Acknowledgments

First, I would like to thank my parents for their support and motivation throughout my career. You always motivate me to be a better person. To my dad for always inspiring me and encouraging me to pursue my dreams, thank you for showing me the path to a scientific career. To my mom for all her love and support, your advice has always helped me to continue. There are not enough words to describe how proud I am to be your son. To my sister, Citlaly, you always helped me during this journey, thank you for guiding me and opening the doors of your home. To my brother, Rafael, you have guided me through all my life and even though I have taken some bad decisions in my life, you have always been there to support me. Mono, thank you for motivating me and supporting me, you have always been there for me unconditionally. Thank you for everything.

I would like to thank Dr. Aguilera; you are an amazing mentor. I will be forever grateful to you for taking me as your student and guiding me to fulfill my dream to become a scientist. Thank you so much Dr. for everything you have done for me, you have provided me with skills that I always wanted to have. Being part of your lab enhanced my love for science. Also, thank you to Dr. Spencer, Dr. Nurunnabi, Dr. Roy, and Dr. Miranda for being part of my committee, mentoring me, and for all their advice. To Dr. Dimmock, thank you for our collaboration and for allowing me to test your compounds.

Dr. Varela, Thank you so much! I will never forget all your support and kindness. I am thankful to you for teaching me a lot of things, for always motivating me to learn more, and for helping me to develop my critical thinking. To Denisse, thank you so much for helping me during my time here at UTEP. I appreciate that you were always there to help

me and give me advice. I also want to thank Gladys for helping me and supporting me since day one. I have learned a lot of different topics from you.

My deepest gratitude goes to Dr. Lisett Contreras. You have helped in many aspects that I would need another chapter of my dissertation just to thank you. You have helped me to develop myself as a researcher. Thank you for teaching me and helping me to adapt to the lab. My time in El Paso has been easier and more fun because of you. I hope that every new Edgar finds someone like you to help him. You are amazing Lisa!

Cristina Guerena and Yareli Schiaffino, I appreciate your help so much. Thank you so much for being very patient with me and for helping me during this project. I know that you both are going to become excellent researchers. You are the best!

Dr. Paulina Villanueva, thank you so much for all the laughs and support, definitely sharing time with you has been one of the best experiences. Luca, cuate, thank you for all your help and for accepting me as your roommate, it was a great experience. I also want to thank Gaby for all her time and for believing in me, we always have a great time. To all my lab mates Dr. Hess, Lenore, Stephi, Alexa, and Dr. Swain, thank you so much for everything, you definitely made the lab to be more enjoyable. I also want to thank Carlos for helping with the in silico analysis.

Diana, I sincerely appreciate everything you have done for me, we had many adventures and I hope we continue having more. Thank you for helping me, I will be forever grateful to you.

To all the people who have helped me during the entire journey, here at UTEP and in El Paso, thank you so much!

Abstract

Two libraries of chemical compounds were analyzed for their cytotoxic activity against cancer and non-cancerous cell lines. In chapter 1, fourteen novel piperidones were tested on a panel of different cell lines to identify their cytotoxic activity. These compounds were found to have cytotoxic activity toward cancer cells with a cytotoxic concentration 50 (CC_{50}) in the micromolar range. Furthermore, these fourteen compounds have selectivity preferentially towards cancer cells. Based on selectivity, and cytotoxicity, four compounds were selected for further characterization in the HL-60 cell line. The four compounds elicit apoptosis as measured by the externalization of the phospholipid phosphatidylserine (PS), the activation of caspase 3, and DNA fragmentation. In addition, the chemical compounds induce the overproduction of Reactive Oxygen Species and the depolarization of the mitochondrial membrane. Cell cycle analyses show that the 4 compounds mainly arrest HL-60 cells in the G0/G1 phase. Finally, Western Blots indicate that the treatment with the four compounds produces the accumulation of polyubiquitinated proteins suggesting that the protein degradation pathway was affected. Additionally, the four compounds overexpressed the HMOX-1 gene that encodes a protein that is overexpressed by proteasome inhibitors treatment. In Chapter 2, more than 5000 compounds from a commercial library were analyzed to find a potent chemical compound against cancer cells. A new pyrazole, referred to as B6, was discovered for having the highest cytotoxic activity at the low micromolar range. B6 was found to be cytotoxic in a panel of twenty-three different cell lines including leukemias and cell lines derived from different solid tumors. The MDA-MB-231 cell line was chosen due to its sensitivity to various anti-cancer compounds. B6 was found to induce apoptosis as

measured by PS externalization, the activation of caspase 3, and DNA fragmentation. However, B6 did not overproduce reactive oxygen species (ROS) nor the depolarization of the mitochondria membrane, suggesting another apoptotic pathway. To get an insight into the mechanism of action we performed transcriptomic analyses. After 6 h of treatment, we observed the up-regulation of 116 genes and the down-regulation of 87 genes; while after 24 hours of treatment, we observed 198 up-regulated and 532 down-regulated. A comparison to Connectivity Map (CMap) revealed that cells treated with the B6 compound displayed a gene expression pattern similar to the gene signatures expressed by tubulin inhibitors. Moreover, molecular docking analyses revealed that B6 interacts with tubulin in an in silico model. Thus, we hypothesized that B6 could be a tubulin inhibitor. Tubulin inhibitors disturb the organization of microtubules; therefore, we captured images by using fluorescent microscopy. The images showed that B6 disrupts microtubule organization. In addition, the B6 compound arrests the cell cycle in the G2/M phase. Finally, a microtubule polymerization assay revealed that B6 inhibits tubulin polymerization. The findings presented in this dissertation show promising results for these compounds as they can potentially be used as they can feasibly be used in cancer therapy.

Table of Contents

List of Tables

List of Figures

Chapter 1: Introduction

1.1 Cancer

Cancer is defined as any disease that is characterized by abnormal and uncontrolled cell growth [1,2]. Cancer can be classified depending on where it begins. There are three main types of cancer: (1) carcinomas, which begin in the tissue or skin that covers the organs, (2) sarcomas, solid tumors from connective tissue, and (3) lymphomas and leukemias, cancers that arise from blood-forming and immune system cells[2]. The most important characteristic of cancer cells is the ability to sustain long-lasting proliferation[3]. Virtually, every cell in the human body has the potential to become a cancer cell. Normal cells turn into cancer cells when they stop responding properly to the signals that control conventional cell behavior[4]. After a cell becomes cancerous, it will divide indefinitely and invade, metastasizing, and killing the host if it is left untreated[5]. This aberrant behavior of cancer cells is caused by molecular and cellular reprogramming happening in both, the intracellular and extracellular environment[6]. Many factors attribute to the formation of cancer. Ninety to ninety-five percent of all cancer cases are attributed to environmental and lifestyle factors whereas the remaining five to ten percent are due to genetic factors[7]. Environmental and lifestyle factors that affect the development of cancer include diet, tobacco and alcohol consumption, infectious agents, exposure to environmental pollutants, and radiation[7,8]. In a majority of cases cancers typically arise after mutations occur, nonetheless, these mutations are related to environmental and lifestyle factors[5,7,8]

1.2 Cancer Statistics

Cancer is a growing health problem that represents a major public concern and it is responsible for one out of six deaths worldwide[9,10]. It is a leading cause of death worldwide[11] and the second leading cause of death in the United States[12]. GLOBOCAN estimates that there were 19.3 million new cases of cancer and almost 10 million new deaths due to cancer occurred worldwide in 2020[10]. In the US, 1,918,030 new cancer cases are expected in 2022, with a projection of 609,360 new deaths[12] resulting in more than 1,600 average deaths per day. Overall, the rates of new cancer cases and deaths due to cancer are rapidly increasing worldwide[12]. In men, prostate cancer is the most diagnosed cancer, however, the leading cause of cancer death is lung cancer. In women, the most diagnosed cancer is breast cancer but the leading causes of cancer death are breast and cervical cancer[10]. In addition to representing a health problem, cancer has an enormous impact on the economy. The total annual monetary cost of cancer care in 2010 was estimated to be $124.57 billion in the US[13]. In 2020, the monetary cost of cancer care was projected to be $165.21 billion[13] and by the year 2030, it is expected to increase to $246 billion in the US alone[14].

1.3 Cancer Treatments

Cancer can be treated by using different approaches despite it being largely categorized as a deadly disease. The main goal of treatment in cancer is to kill cancerous cells while minimizing the killing of normal cells[15]. Nowadays, cancer treatments include the use of surgery, radiation, chemotherapy, and immunotherapy, among others alone or in combination [16–18]. Surgery, the physical removal of cancerous tissue from the body, is the first therapy in most solid cancers[18]. Radiotherapy is the use of radiation to kill cancer

cells by damaging the DNA enough to prevent it from being repaired[19] and it is used in at least two-thirds of western countries as part of the treatment regimen for cancer[20]. Naturally, the immune system recognizes and eliminates many threats including cancer to keep homeostasis in the body[21]. By definition, immunotherapy is the use of different approaches such as antibodies, cytokines, immunological checkpoint inhibitors, and/or vaccines to increase and restore the immune system's capability to fight cancer[22]. Chemotherapy is the use of drugs to kill or stop the progression of cancer cells which can be administered in multiple ways[23]. Chemotherapeutic agents are divided into various types: antimetabolites, alkylating agents, mitotic spindle inhibitors, and topoisomerase inhibitors, among others[24]. Even though a wide repertoire of new treatments against cancer has been developed, chemotherapy is still the regular treatment for all cancers[25]. However, the effects of chemotherapy are systemic, meaning that it kills normal and cancer cells equally[26]. In addition to killing normal cells in the body, cancer cells can become resistant to chemotherapeutic agents[24]. Therefore, there is an urgent need for new molecules that can be specific for cancer and less toxic to normal cells.

1.4 Anti-Cancer Drug Discovery

The main goal of drug screening in cancer is to discover novel chemotherapeutic agents that are capable of killing and/or stopping cell proliferation while reducing damage to normal cells[27]. One of the most common methods in drug discovery is high throughput screening (HTS). HTS consists of the screening of random large chemical libraries aiming at the discovery of hit molecules effective against biological targets in a certain disease[27,28]. In this process, chemical compounds are tested in primary screenings to determine if there is any cell death activity. If a compound displays cytotoxic activity, then

it is selected to be tested in a secondary screening where inhibitory concentrations 50 (IC_{50}s) and cytotoxic concentrations (CC_{50}s) are determined[29]. Once a hit (lead) molecule has been identified, this compound becomes a candidate for testing that will progress from preclinical to clinical trials[30].

1.5 Curcumin Piperidone and Pyrazole Derivatives

The improvement via chemical synthesis and modification of previously reported compounds is commonly used to produce better drugs[31]. Curcumin is a polyphenol obtained from the plant *Curcuma longa* (also known as turmeric). Curcumin has been demonstrated to have therapeutic effects in many biological activities including several cancers[32–35], for this reason, it is a potential candidate drug to be used in anti-cancer drug research[35]. However, curcumin has poor bioavailability due to its poor absorption and rapid metabolism[31]. Therefore, Curcumin derivatives such as piperidones have been synthesized which have been reported to have good cytotoxicity on many cancers[32]. In addition to curcumin derivatives, pyrazoles have also gained attention due to their pharmacological properties[36]. Pyrazole is a five-membered aromatic ring containing two adjacent nitrogen atoms[37]. Pyrazole and its derivatives are a class of compounds that exhibit a wide range of pharmacological properties[37]. Anti-cancer properties have been documented among the pharmacological activities exhibited by pyrazoles[37]. Additionally, many compounds used in the clinic contain the pyrazole moiety[38,39]. For this reason, pyrazoles are potential candidate structures in anti-cancer research[38].

1.6 Research Rationale

Cancer remains a deadly disease. Many approaches have been developed to treat cancer: surgery, radiation, chemotherapy, and immunotherapy, however, chemotherapy is still the regular cancer treatment. Nonetheless, chemotherapeutic agents can lead to the production of drug resistance in cancer cells. In addition, chemotherapy can be systemic, meaning that it kills cancer and non-cancerous cells indiscriminately. Therefore, there is a need for the discovery of new chemical compounds to be used as anti-cancer agents. One traditional approach that leads to the discovery of new agents is the testing of large chemical libraries to get hit compounds through HTS. Those hit compounds are then tested to unveil the mechanism of action, which helps provide enough information about the safety of the drug and how it behaves in the body. For this reason, this project focuses on characterizing novel molecules with anti-cancer activity and determining their mode of action. Despite the limitations of this study due to the lack of *in vivo* data, we hope these data can serve to help develop novel therapies and provide better weapons to win the fight against cancer in the future.

1.7 Specific Aims

The main goal of this project is to identify novel compounds with the potential to be used in anti-cancer research and to describe their mechanism of action.

Chapter 2: Evaluation of the Cytotoxicity of Novel Piperidones and Characterization of Hit Compounds

Specific Aim 1:

Cytotoxicity evaluation of novel piperidones on a panel of different cancer cell lines.

1.1. To determine which concentration of the compounds kills 50% of the cell population

1.2. To identify the most potent compounds and the compounds with the highest selective cytotoxic index (SCI)

Specific Aim 2:

Characterization of novel piperidones.

2.1. To identify which cell death mechanism is induced by the lead compounds

2.2. To determine the mode of action of the lead compounds

Chapter 3: Evaluation of cytotoxicity of a commercial chemical library, identification, and characterization of one lead compound

Specific Aim 1:

Cytotoxic analysis of a commercial chemical library to identify a potent novel compound.

1.1. Analyze more than 5000 compounds from ChemBridge DIVERset library and identify the most potent compound

1.2. Evaluate the cytotoxic activity of the most potent compound on a panel of different cell lines

Specific Aim 2:

Characterization of B6 (2-{4-[4-methoxy-3-(trifluoromethyl)phenyl]-1H-pyrazol-1-yl}-N-(2-methyl-2H-1,2,3-triazol-4-yl)acetamide) compound.

2.1. Determine if the cell death mechanism of apoptosis is induced by the hit compound

2.2. Identify the mechanism of action of the novel compound through transcriptomics, bioinformatics analysis, and proof-of-concept experiments

Chapter 2: Evaluation of Cytotoxicity of Novel Piperidones and Characterization of Hit Compounds

2.1 Evaluation of Cytotoxicity of Novel Curcumin Derivative Piperidones

Screening of chemical compounds as potential anti-cancer therapy needs the continuous growth of cell lines. Different cell lines were utilized during the analysis of the experimental chemical compounds. Hematological cancer cell lines used were HL-60, acute promyelocytic leukemia, and CCRF-CEM, which is acute lymphoblastic leukemia. Solid tumor cancer cell lines included: HT-29, a colorectal adenocarcinoma, COLO 205, a colorectal adenocarcinoma cell line, and MCF7 a breast cancer adenocarcinoma cell line. Two non-cancerous cell lines were used as controls: CCD-112CoN, a fibroblast from colon tissue, and Hs27, a fibroblast that is derived from the foreskin. All the cell lines were grown under aseptic conditions in incubators at 37°C in a humidified 5% CO_2 environment. RPMI-1640 culture media was used for HL-60, CCRF-CEM, and COLO 205. For HL-60, the complete media was prepared with 20% Fetal Bovine Serum (FBS), whereas for CEM and COLO 205, 10% FBS was used. Hs27 and MCF-7 cells were grown using Dulbecco's Modified Eagle's Medium (DMEM) media with 10% FBS, additionally, 10 µg/ml of insulin was added to the medium for MCF7. Eagle's Minimum Essential Medium (EMEM) with 10% FBS was used to grow CCD-112CoN. For HT-29, McCoy's medium supplemented with 10% FBS was utilized. Consistently, the FBS was heat inactivated. Additionally, 100 U/ml of penicillin and 100 µg/ml of streptomycin were added to all the culture mediums. All cell lines were regularly monitored, avoiding high levels of confluence. The media was replenished every two to three days. For adherent cell lines, 1X trypsin was added to detach them. For non-adherent cell lines, media was changed

by removing old media and replenishing it with new media. Before preparing an experimental multi-well plate, cell viability was tested through flow cytometry by adding 5 µg/ml of propidium iodide (PI) to a 400 µL of cell suspension aliquot. Only cells with ≥95% viability were used to run cytotoxicity experiments.

Initially, a screening to determine the cytotoxic concentration that kills 50% of the entire cell population (CC_{50}) was performed with fourteen different compounds. These compounds were chemically synthesized in the laboratory of Dr. Jonathan R. Dimmock from the University of Saskatchewan in Canada and were analyzed on a panel of different cell lines. To determine the cytotoxic activity on different cancerous and non-cancerous cell lines of the compounds, the Differential Nuclear Staining (DNS) assay was used[40]. To perform the DNS assay, $1X10^4$ Cells were seeded in 96-well plates at a volume of 100 µL of media per well and were left overnight under cell culture conditions. Cells were treated with different concentrations of the compounds: 10 µM, 7.5 µM, 5 µM, 2.5µM, 1 µM, 0.5 µM, 0.25 µM, and 0.1µM. DMSO at 1% was used as the vehicle control and untreated cells as a negative control. 1.6 millimolar (mM) of H_2O_2 was added to the cells to induce cell death as a positive control. To calculate the average of the compounds three technical replicates were used. For DMSO and untreated cells, six technical replicates were used. After treatment cells were left for a period of 24 or 48 h. Two hours before the period of incubation elapsed, a mixture of Hoechst 33342 and propidium iodide (PI) in Phosphate-buffered saline (PBS) was added to each well. When time passed, plates were read by using IN Cell Analyzer 2000 system (GE Healthcare, Pittsburg PA, USA). Four adjacent images per well were captured and analyzed with the IN Cell Analyzer Workstation 3.2 software (GE Healthcare). The following equation was used to

normalize the cytotoxicity of each treatment to the DMSO control: *(((average cell count of DMSO - total cell count of treatment well) + dead cell count of treatment well) / (average cell count of DMSO)) *100*[41]. The CC_{50} was calculated by extrapolating two concentrations, one that kills more than 50% of the population and one that kills less than 50%. The extrapolation was accomplished by using an online tool (https://www.johndcook.com/interpolator.html). To determine if a compound has selectivity toward cancer and not non-cancerous cell lines the selective cytotoxic index (SCI) is calculated. The SCI is calculated by dividing the CC_{50} value of the control cell line Hs27 by the CC_{50} value of the cancer cell lines (i.e. 4/0.16= 25). The calculation of the SCI of the compounds was performed by using the two hematological cancer cell lines. High SCI values mean that the compound kills cancer cells better than normal cells.

The effect of exposure for 24 and 48 h of the chemical compounds was analyzed in different cell lines to calculate the CC_{50} values in these specific types of cancer. A low CC_{50} value means a potent compound since it can kill cells with a lower concentration of molecules. Hematological cancer cell lines were the most sensitive to the fourteen compounds having CC_{50} values in the nanomolar range and more specifically, the HL-60 cell line was the most sensitive (**Table 1**). The most potent compounds in these cell lines were NC2564 (**Figure 1b**) with a CC_{50} value of 0.14 μM in HL-60 and NC 2559 (**Figure 1a**) with a CC_{50} value of 0.17 μM in CCRF-CEM (**Table 1**).

Table 1. CC_{50} values of fourteen compounds after 48 h of treatment in hematological cancer cell lines.

Cell Line	**HL-60**		**CCRF-CEM**	
Compound	**CC50**	**Standard Deviation**	**CC50**	**Standard Deviation**
NC2067	0.16 µM	0.043205	0.23 µM	0.015275
NC2559	0.16 µM	0.040415	0.17 µM	0.034641
NC2560	0.23 µM	0.111505	0.52 µM	0.035355
NC2561	0.26 µM	0.017321	0.41 µM	0.028284
NC2562	0.59 µM	0.075056	0.40 µM	0.035355
NC2563	1.96 µM	0.070711	3.62 µM	0.127279
NC2564	0.14 µM	0.041633	0.20 µM	0.038297
NC2565	0.19 µM	0.078102	0.46 µM	0.007071
NC2566	0.17 µM	0.041633	0.28 µM	0.028868
NC2567	0.25 µM	0.040415	0.27 µM	0.050662
NC2569	0.23 µM	0.005774	0.25 µM	0.016330
NC2570	0.18 µM	0.057735	0.20 µM	0.021229
NC2571	0.16 µM	0.028284	0.30 µM	0.045092
NC2572	0.18 µM	0.051962	0.35 µM	0.058595

The cytotoxic activity of these compounds was also analyzed in colon and breast cancer cell lines. In all three cell lines, the most potent compound was NC2564 (**Figure 1a**). Most of the compounds have CC_{50} values in the low micromolar range, however, NC2564 has CC_{50} values of 0.73 µM in HT-29 and 0.88 µM in COLO 205 (**Table 2**). Even though MCF7 was more resistant than the other cell lines, NC2564 is still the most potent compound having a CC_{50} of 1.47 µM. These data provide evidence that NC2564 is the most potent compound of this set of chemical compounds.

Table 2. CC_{50} values of fourteen compounds after 48 h of treatment in colon and breast cancer cell lines.

Cell Line	**HT-29**		**COLO 205**		**MCF 7**	
Compound	**CC50**	**Standard Deviation**	**CC50**	**Standard Deviation**	**CC50**	**Standard Deviation**
NC2067	4.30 µM	0.073711	1.72 µM	0.015275	5.44 µM	0.250067
NC2559	1.87 µM	0.251462	0.94 µM	0.034641	3.37 µM	0.466083
NC2560	2.12 µM	0.245425	1.52 µM	0.035355	3.93 µM	0.195704
NC2561	1.20 µM	0.162635	0.90 µM	0.028284	4.60 µM	0.305996
NC2562	1.48 µM	0.028284	1.40 µM	0.035355	4.03 µM	0.756042
NC2563	9.58 µM	0.441059	6.71 µM	0.127279	8.22 µM	0.252256
NC2564	0.73 µM	0.223961	0.88 µM	0.038297	1.47 µM	0.204042
NC2565	2.13 µM	0.405134	1.68 µM	0.007071	1.91 µM	0.120208
NC2566	2.25 µM	0.085440	1.53 µM	0.028868	3.13 µM	0.403774
NC2567	2.04 µM	0.118462	1.79 µM	0.050662	3.50 µM	0.317648
NC2569	1.92 µM	0.088882	1.40 µM	0.016330	3.70 µM	0.527091
NC2570	2.56 µM	0.506853	1.31 µM	0.021229	5.93 µM	0.312983
NC2571	1.67 µM	0.117898	1.82 µM	0.045092	5.37 µM	0.276225
NC2572	0.90 µM	0.043493	1.59 µM	0.058595	4.14 µM	0.657609

Compounds used as chemotherapeutic agents must have more cytotoxic activity towards cancer cells and not non-cancerous cells, showing anti-cancer selectivity. To prove that these compounds have selectivity, two non-cancerous cell lines were used. **Table 3** shows the CC_{50} values of these compounds in Hs27, which is a fibroblast cell line derived from the human foreskin, and CCD-112CoN a fibroblast cell line derived from colon tissue. Almost all the compounds have CC_{50} values in the micromolar range in both cell lines, except for NC2564 which has a CC_{50} value of 0.73 µM in Hs27.

Table 3. CC_{50} values of fourteen compounds after 48 h of treatment in normal cell lines from colon tissue and fibroblast from the foreskin.

Cell Line	**CCD-112CoN**		**Hs27**	
Compound	**CC50**	**Standard Deviation**	**CC50**	**Standard Deviation**
NC2067	5.83 μM	0.468010	5.39 μM	0.393234
NC2559	2.61 μM	0.435852	4.00 μM	0.556447
NC2560	3.39 μM	0.395011	4.36 μM	0.478574
NC2561	3.48 μM	0.132035	4.31 μM	0.085049
NC2562	2.69 μM	0.325410	2.17 μM	0.297433
NC2563	8.16 μM	0.386264	6.56 μM	1.140132
NC2564	1.30 μM	0.086168	0.73 μM	0.140475
NC2565	2.52 μM	0.047871	2.59 μM	0.132256
NC2566	2.99 μM	0.156312	2.62 μM	0.200749
NC2567	2.75 μM	0.147422	2.40 μM	0.323161
NC2569	1.81 μM	0.014142	2.83 μM	0.339559
NC2570	2.80 μM	0.113137	2.91 μM	0.069282
NC2571	2.04 μM	0.406735	3.33 μM	0.354730
NC2572	1.10 μM	0.084853	2.80 μM	0.323161

The selective cytotoxicity index (SCI) is calculated to indicate that a compound selectively kills cancer cells. The formula to calculate the SCI is *SCI = CC_{50} of non-cancerous cells/CC_{50} of cancer cells* and it was used to detect the SCI of our compounds[42]. If a compound has an SCI value greater than 1, it means that the compound has selective toxicity toward cancer cells compared to non-cancerous cells[42]. For this reason, any anti-cancer drugs must have a high SCI. Because hematological cancer cell lines were the most sensitive, it was decided to compare the values of these cancer cell lines to the values in the Hs27 cell line.

Table 4. Selective cytotoxic index (SCI) of hematological cancer cell lines compared to control cell line Hs27.

Cell Line	**HL-60**	**CCRF-CEM**
Compound	**SCI**	**SCI**
NC2067	33.68	23.43
NC2559	25.00	23.52
NC2560	18.95	8.38
NC2561	16.57	10.51
NC2562	3.67	5.42
NC2563	3.34	1.81
NC2564	5.21	3.65
NC2565	13.63	5.63
NC2566	15.41	9.35
NC2567	9.60	8.88
NC2569	12.30	11.32
NC2570	16.16	14.55
NC2571	20.81	11.10
NC2572	15.55	8.00

As shown in **Table 4**, all the compounds have SCIs greater than 1 meaning that these compounds have cytotoxicity preferentially to cancer cells and not non-cancerous cells. Based on the SCI values, three compounds, NC2559, NC2570, and NC2571(**Figure 1**), were selected for further analyses. These three compounds have SCIs of 25, 16.16, and 20.81, respectively (**Table 4**). Additionally, NC2564 was chosen for further analysis due to its high cytotoxic activity. The HL-60 cell line was chosen because it was the most sensitive cell line to compound treatment. NC2068 was not chosen because it will be investigated as part of a different project. There were other compounds such as NC2560

and NC2561 that had better SCI than NC2570, however, NC2570 was chosen because it has a good SCI and a lower CC_{50} value than NC2560 and NC2561 in HL-60 cells.

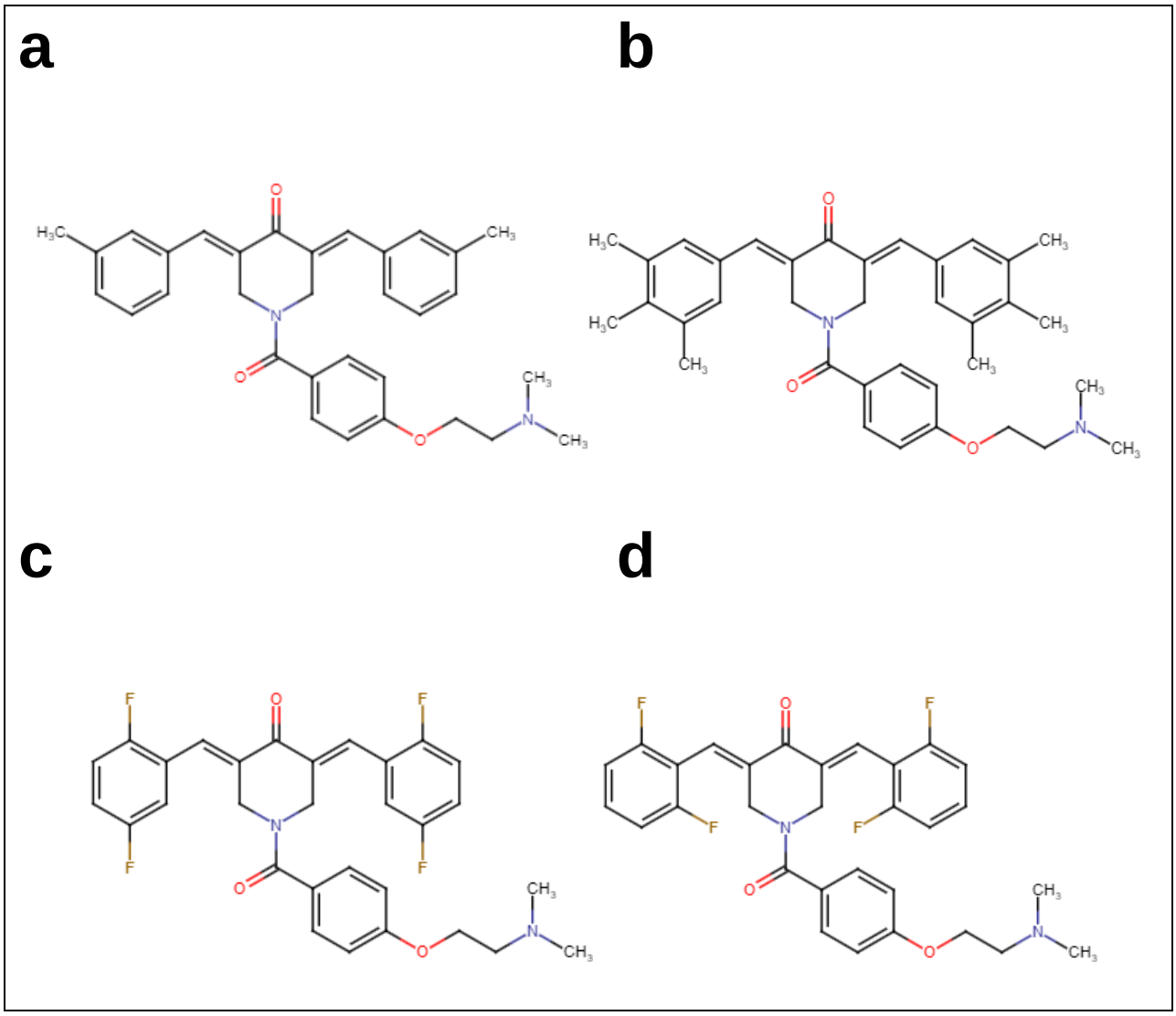

Figure 1. Chemical structure of novel compounds. Chemical structure of **(a)** NC2559, **(b)** NC2564, **(c)** NC2570 and **(d)** NC2571.

Cell death events occur during the first 24 hours, therefore, CC_{50} values at 24 hours of each compound of interest were calculated (**Table 5**). As anticipated, NC2564 has the lowest CC_{50} (0.22 μM) at 24 hours, whereas NC2559, NC2570, and NC2571 have CC_{50}s

of 0.26 μM, 0.33 μM, and 0.29 μM, respectively. Nonetheless, there was not a big difference between the four compounds (**Table 5**).

Table 5. CC_{50} values of NC2559, NC2564, NC2570, and NC2571 in HL-60 cells at 24 h.

Cell Line	**HL-60**	
Compound	**CC50**	**Standard Deviation**
NC2559	0.26 μM	0.043205
NC2564	0.22 μM	0.015000
NC2570	0.33 μM	0.010000
NC2571	0.29 μM	0.075498

2.2 NC2559, NC2564, NC2570, and NC2571 Induce Phosphatidylserine Externalization in HL-60 Cells

Based on previously published results of compounds with similar structures[42,43] it was investigated if apoptosis was the cell death mechanism executed by these compounds. The Annexin V-FITC assay is used to measure apoptosis based on the externalization of a phospholipid known as phosphatidylserine (PS)[44]. Normally PS is present in the inner side of healthy cell membranes but when cells are undergoing apoptosis PS is externalized[44]. PS externalization is an “eat me” signal that facilitates the process of removal of dead and dying cells by phagocytes in a process known as efferocytosis[45,46]. To measure phosphatidylserine externalization, the Annexin V-FITC kit was used (Beckman Coulter, Miami, FL, USA). HL-60 Cells were seeded at $1X10^5$ density in a volume of 1000 μL of growth media per well in 24-well plates and were left overnight under cell culture conditions. Cells were treated with 0.1% v/v DMSO as vehicle control,

and untreated cells were used as a negative control. As a positive control of cytotoxicity, cells were treated with 1.6 mM H_2O_2. After 24 h of exposure to the experimental compounds, cells were collected in flow cytometry tubes (5 ml tubes) and centrifuged at 1200 rpm for 5 minutes at 4°C, the supernatant was discarded, and cells were gently resuspended with a mixture of 100 µL of 1X binding buffer containing 1 µL of Annexin V-FITC and 2.5 µL of propidium iodide (PI), as previously described[47]. The cells were then incubated for 15 minutes on ice in the dark. After incubation, 300 µL of 1X binding buffer was added to each tube and examined by flow cytometry (Gallios, Beckman Coulter). To capture the fluorescence signal emitted by FITC and PI, FL1 and FL2 detectors were used, respectively[48]. Cells positive for just FITC were considered early apoptotic cells, whereas cells stained by PI alone indicate necrotic cells. The double positive FITC and PI cells represent late apoptosis. The four compounds induced PS externalization at CC_{50} values and two times CC_{50} values (**Figure 2**). There were 59.2% of cells undergoing apoptosis after treatment with 0.22 µM of NC2564 and 82.9% with 0.45µM of NC2564 (**Figure 2a**). NC2559 at 0.26 µM and 0.52 µM induced apoptosis of 28.4% and 37.3% HL-60 cells, respectively (**Figure 2b**). Treatments with 0.33 µM and 0.66 µM of NC2570 elicited apoptosis in 25.5% and 33.9% of the cell population whereas treatment with 0.29 µM and 0.58 µM of NC2571 in 27.2% and 38.4% cells (**Figure 2b**). Cells treated with DMSO induced apoptosis in less than 6% of the cell population, meaning that the compounds by themselves are responsible for the increase in the percentage of apoptotic cells.

a

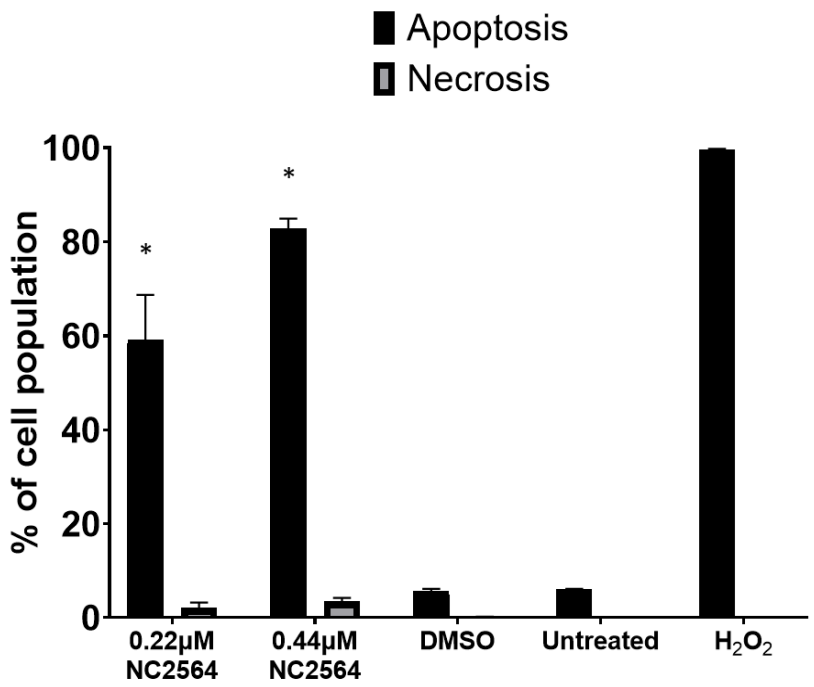
Apoptosis
Necrosis
% of cell population
100
80
60
40
20
0
*
*
0.22μM NC2564
0.44μM NC2564
DMSO
Untreated
H_2O_2

b

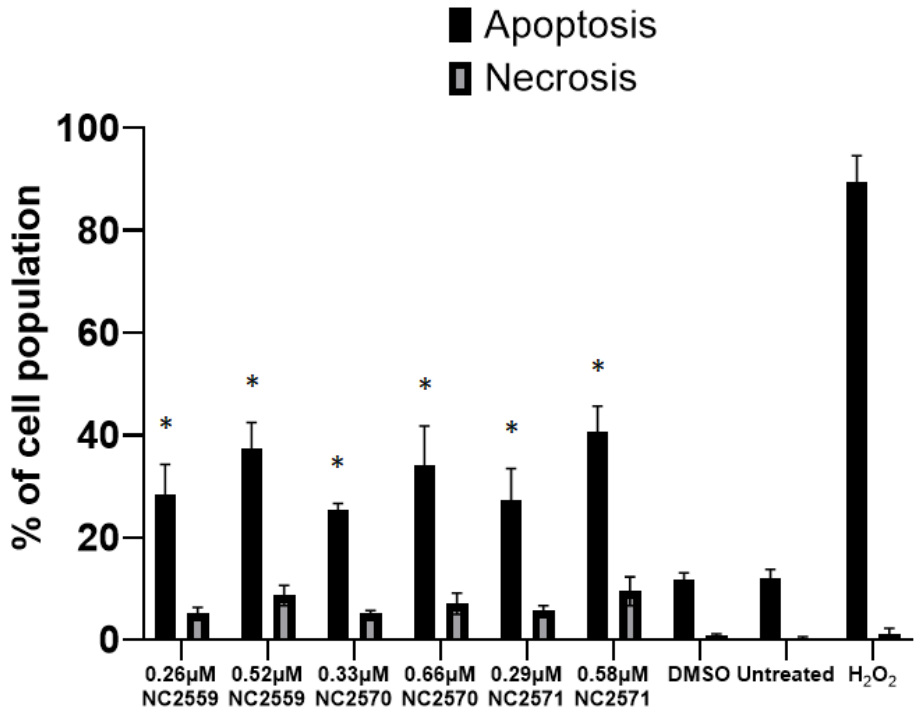
Apoptosis
Necrosis
% of cell population
100
80
60
40
20
0
0.26μM NC2559
0.52μM NC2559
0.33μM NC2570
0.66μM NC2570
0.29μM NC2571
0.58μM NC2571
DMSO
Untreated
H_2O_2

Figure 2. NC2559, NC2564, NC2570, and NC2571 induce apoptosis. HL-60 cells were treated for 24 h with **(a)** 0.22 µM, 0.45µM of NC2564, **(b)** 0.26 µM, 0.52 µM of NC2559, 0.33 µM, 0.66 µM of NC2570 and 0.29 µM, 0.58 µM of NC2571 and compared to the vehicle DMSO. **(a, b)** The four compounds induce apoptosis as measured by PS externalization. The total average of apoptosis was calculated by adding early and late apoptotic events. Each bar graph depicts the average of three technical replicates with standard deviation. * Represents *p*-value = ≤ 0.00686 compared to DMSO.

There were also cells undergoing necrosis after treatment with the four compounds. Treatment with 0.22 µM and 0.45 µM of NC2564 induced necrosis in 1.43% and 3.49% of the cell population (**Figure 2a**). NC2559 treatment at 0.26 µM and 0.52 µM induced necrosis in 5.11% and 8.6% of the cells. 0.33 µM and 0.66 µM of NC2570 caused necrosis in 5.2% and 8.2% of the cell population while treatment with 0.29 µM and 0.58 µM of NC2571 in 5.1% and 10.6% (**Figure 2b**). Even though the compounds also promote necrosis in some of the cells, it is pretty evident that cells were dying preferentially due to apoptosis. Taken together these data suggest that the four compounds induce apoptosis more positively than necrosis.

2.3 NC2559, NC2564, NC2570, and NC2571 Activate Caspase 3

Apoptosis is executed by the action of the caspase family of proteins which is a group of cytosolic cysteine enzymes with proteolytic activity. Caspases are very specific; they cleave proteins only after aspartic acid residue[49]. Caspase 3 is regularly activated during apoptosis, playing an important role as a catalyst in the cleaving of many cellular proteins[50]. Caspase 3 is required to inactivate ICAD, an inhibitor of the CAD (Caspase-Activated DNase) which is required for DNA fragmentation during apoptosis[51]. To assess the live-cell detection of the activation of the caspase 3 enzyme, the fluorogenic reagent NucView 488 caspase 3 substrate assay kit (Biotium, Hayward, CA) was used to detect caspase 3 via flow cytometry. For this assay, HL-60 cells were seeded in 24-well plates at a density of $1X10^5$ cells in 1 ml per well. Plates were left under normal cell growth conditions overnight and treated with the experimental compounds for 7 h. DMSO was used as the vehicle control and untreated cells as the negative control. As a positive caspase 3-activating control, cells were treated with 1.6 mM of H_2O_2. After treatment, cells were harvested in flow cytometer tubes and centrifuged at 1200 rpm for 5 minutes. The supernatant was discarded, and cells were resuspended in a mixture of 200 µL of PBS containing 5 µL NucView 488 Caspase 3 substrate (5 µM final concentration) and then incubated in the dark for 30 minutes at room temperature. Subsequently, cells were washed with PBS and resuspended with 300 µL of PBS, then immediately analyzed by flow cytometry. To observe the activation of caspase 3 in live cells, the same two concentrations as in the Annexin V-FITC assay for each of the four compounds were used. NC2564 at the concentrations of 0.22 µM and 0.45µM generated caspase 3 activation in 16% and 17.8% of the total cells resulting in a significant difference in

activation in comparison with DMSO solvent which only caused activation in 9% of the cell population (**Figure 3a**). The treatments with NC2559 at 0.26 µM, NC2570 at 0.33 µM, and NC2571 at 0.29 µM induced the activation of caspase 3 in 18.7%, 16.6% and 19.3% of cells, respectively (**Figure 3b**). Whereas treatments with 0.52 µM of NC2559, 0.66 µM of NC2570 and 0.58 µM of NC2571 generated the activation of caspase 3 in 43.2%, 48.5% and 46.3% of the cell population (**Figure 3b**). The vehicle control, DMSO, induced the activation in 13.6% of the cells (**Figure 3b**). There is a significant difference between the highest concentration of the NC2559, NC2570, and NC2571 and the DMSO (**Figure 3b**), as well as both concentrations of NC2564 (**Figure 3a**), suggesting that the four compounds induced the activation of the caspase 3 enzyme, thus, corroborating apoptosis as the main cell death mechanism.

a

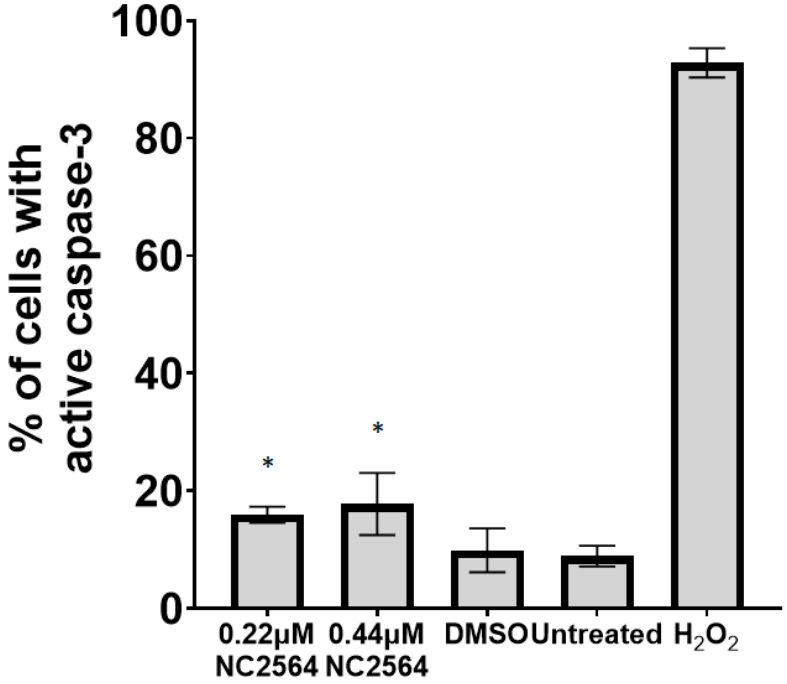
% of cells with active caspase-3
100
80
60
40
20
0
*
*
0.22µM NC2564
0.44µM NC2564
DMSO
Untreated
H_2O_2

b

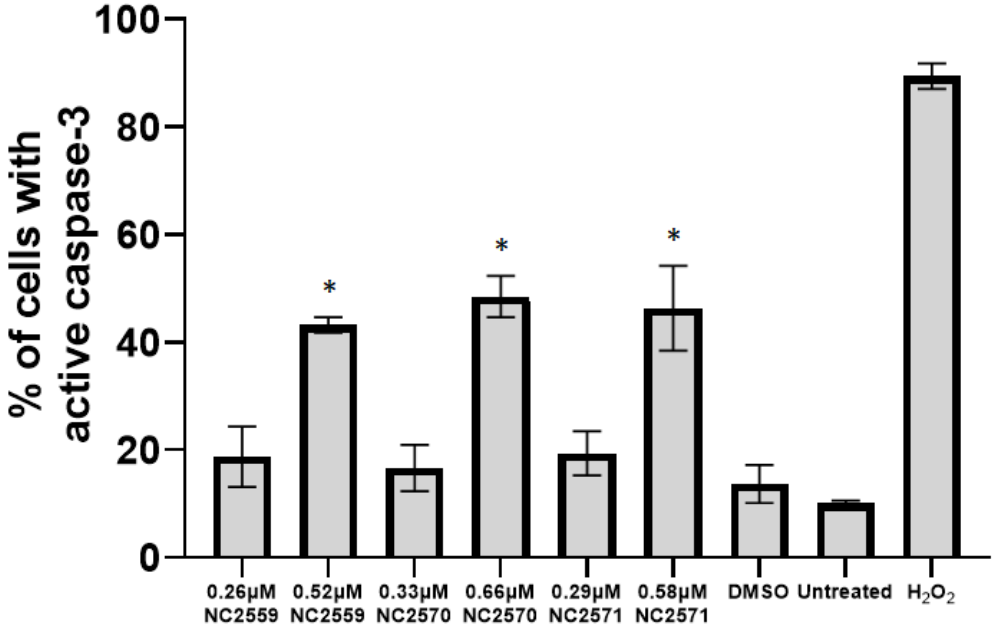
% of cells with active caspase-3
100
80
60
40
20
0
*
*
*
0.26µM NC2559
0.52µM NC2559
0.33µM NC2570
0.66µM NC2570
0.29µM NC2571
0.58µM NC2571
DMSO
Untreated
H_2O_2

Figure 3. NC2559, NC2564, NC2570, and NC2571 activate caspase 3. Cells treated with the four compounds were positive for caspase 3 activation. HL-60 cells were treated for 7 h and analyzed via flow cytometry. **(a)** NC2564 activated caspase 3 at both concentrations whereas **(b)** NC2559, NC2570 and NC2571 activated caspase 3 at the highest concentrations. Each bar graph indicates the average of three treatments with standard deviation represented as error bars. * = *p*-value ≤ 0.003513 in comparison with DMSO

2.4 NC2559, NC2564, NC2570, and NC2571 Elicit Mitochondrial Membrane Depolarization

After demonstrating that NC2559, NC2564, NC2570, and NC2571 induced apoptosis, we sought to investigate which apoptotic pathway was elicited by the compounds. There are two main apoptotic vias, the extrinsic and the intrinsic apoptotic pathways. The intrinsic pathway is mediated by internal signals in the cell and is dependent on the mitochondria. In contrast, the extrinsic pathway is mediated by extracellular signals and depends on cell death receptors[52]. One of the major events during the intrinsic pathway is the depolarization of the mitochondrial membrane potential[53,54]. The mitochondria-dependent pathway is mediated through internal signals that can be induced through insults such as those caused by chemotherapeutic agents[52]. Using this information and our experience with chemical compounds[43,55], we hypothesized that the four compounds could be inducing apoptosis via the intrinsic pathway. To test this hypothesis, we performed the JC-1 assay, which measures the depolarization of the mitochondrial membrane potential with the use of a cationic dye known as JC-1[56]. The assay was accomplished by using the MitoProbe JC-1 assay kit (Molecular Probes, M34152). $1X10^5$ HL-60 cells were

seeded in 24-well plates at a volume of 1000 µL of media per well and left under cell culture conditions overnight. Cells were incubated for 7 h with compound concentrations and controls as mentioned above. Again, the same concentrations used in the previous assays were used, CC_{50} and $2XCC_{50}$s for each compound. After incubation, cells were collected in 5 ml tubes and were spun down at 1200 rpm for 5 minutes at room temperature. The supernatant was discarded, and cells were resuspended with 400 µL of PBS containing 2 µM of JC-1 and incubated under normal cell culture conditions for 45 minutes. After incubation, cells were washed with 2600 µL of warm PBS (37°C) and centrifuged as above. The supernatant was removed, and cells were resuspended in 400 µL of warm PBS to be read immediately by flow cytometry. **Figure 4** shows the results for the mitochondrial membrane potential depolarization for the four compounds. Treatment with 0.22 µM of NC2564 induced the depolarization of the mitochondrial membrane in 4.5% of the cells, and 0.44 µM in 9.6% (**Figure 4a**). As expected, the positive control H_2O_2 at 1.6mM and the untreated cells provoked mitochondrial membrane depolarization in 95.2% and 2.6% of the cells, respectively (**Figure 4a**). In addition, DMSO at 0.1% caused mitochondrial membrane potential depolarization in 3.6% of the cells (**Figure 4a**). The results of NC2564 at its highest concentration were significantly different from those of the DMSO, meaning that NC2564 provokes mitochondrial membrane depolarization (**Figure 4a**). Exposure of HL-60 cells to NC2559 at 0.33 µM and 0.66 µM produce mitochondria membrane depolarization in 16% and 17.8% of the cells (**Figure 4b**). Additionally, Treatments with 0.33 µM and 0.66 µM of NC2570 and 0.29 µM and 0.58 µM of NC2571 produced it in 15.26%, 19%, 16.1%, and 19.4%, respectively (**Figure 4b**).

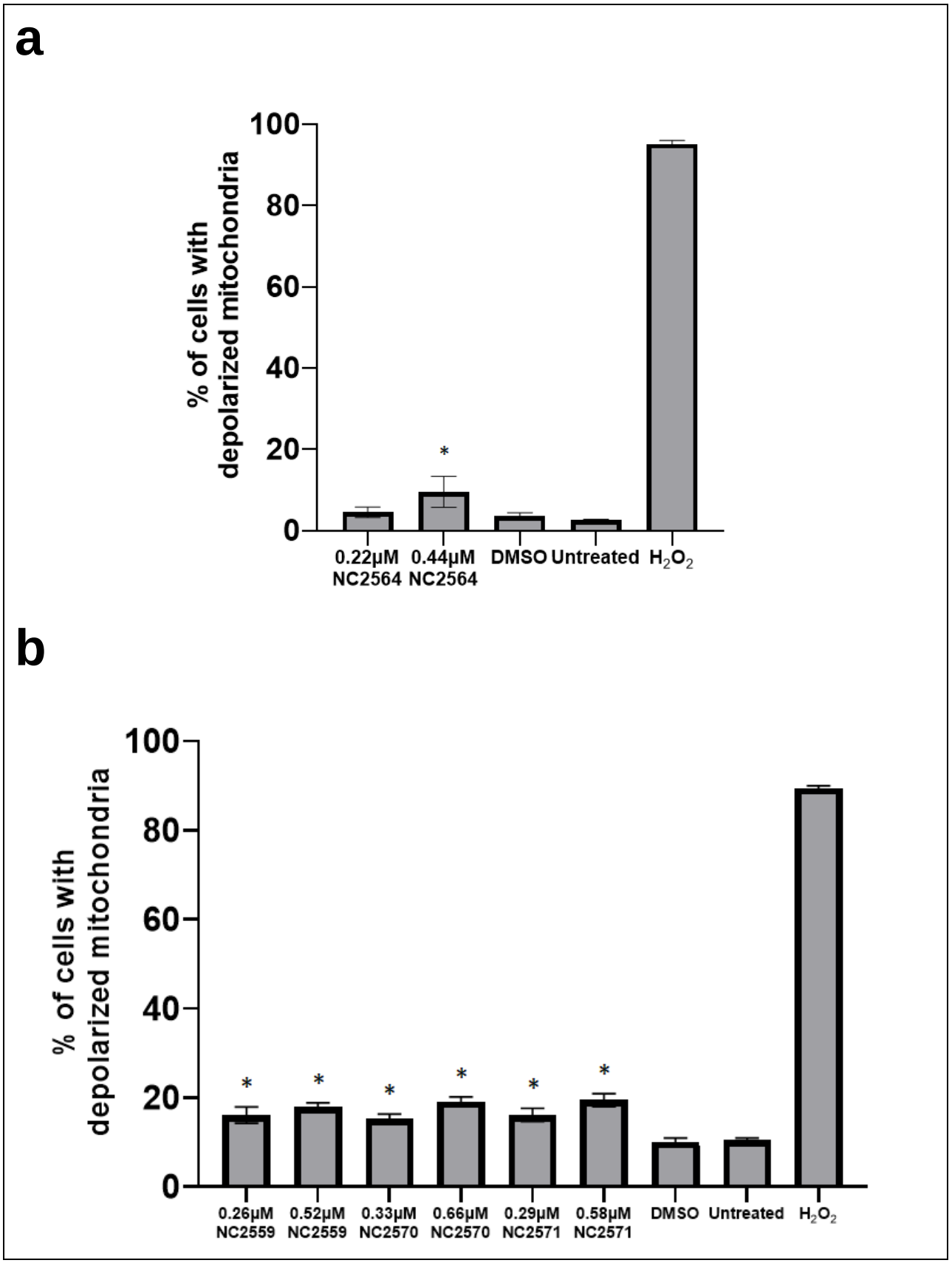
a
% of cells with depolarized mitochondria
100
80
60
40
20
0
*
0.22μM NC2564
0.44μM NC2564
DMSO
Untreated
H2O2
b
% of cells with depolarized mitochondria
100
80
60
40
20
0
*
*
*
*
*
*
0.26μM NC2559
0.52μM NC2559
0.33μM NC2570
0.66μM NC2570
0.29μM NC2571
0.58μM NC2571
DMSO
Untreated
H2O2

Figure 4. NC2559, NC2564, NC2570, and NC2571 elicit mitochondrial membrane depolarization. Treatment after 7 h with the compounds produced mitochondrial membrane depolarization as shown by the JC-1 assay. **(a)** NC2564 was significant just at the highest concentration (0.44 µM) that was used. **(b)** Treatment with NC2559, NC2570, and NC2571 significantly produced higher percentages of cells with mitochondrial membrane depolarization compared to DMSO. ***** Indicates *p*-value = ≤ 0.003236 when compared to DMSO.

As it was anticipated, H_2O_2 cells induced mitochondrial membrane depolarization in 89.4% of the cells. In contrast, 10.3% of the untreated cells were positive for the event (**Figure 4b**). In addition, 10% of the cells that were exposed to 0.1% of DMSO were positive for JC-1 accumulation (**Figure 4b**). The comparison of the results from NC2559, NC2570, and NC2571 to the DMSO, showed that these are significantly different from the DMSO, meaning that these compounds induced the depolarization of the mitochondria membrane (**Figure 4b**). Overall, these results show that treatment with the four compounds caused the depolarization of the mitochondrial membrane potential in the HL-60 cells.

2.5 NC2559, NC2564, NC2570, and NC2571 Cause ROS Overproduction

Excess generation of reactive oxygen species (ROS) can lead to the initiation of programmed cell death[57]. Increases in ROS production can impair mitochondrial function and reduce the viability of cells[58]. To investigate ROS overproduction, the DCF assay was used. This assay uses 2′,7′-dichlorodihydrofluorescein diacetate (H2DCFDA), an acetylated compound that can penetrate the cell's membrane. Once in the cytoplasm, cellular esterases remove the acetate groups to produce a non-fluorescent compound

that interacts with intracellular ROS to form a fluorescent product[59]. To perform the assay, $1X10^5$ HL-60 cells were seeded in 24-well plates at a volume of 1000 µL of media per well. Plates were left overnight under cell culture conditions and treated with 0.26 µM, 0.52 µM of NC2559, 0.33 µM, 0.66 µM of NC2570, and 0.29 µM, 0.58 µM of NC2571 for 5 h. DMSO at 0.1% was included as the vehicle control and untreated cells as a negative control. H_2O_2 at 1.6mM was included as a positive control. Following incubation, cells were collected in 5 ml tubes and centrifuged at 1200 rpm for 5 minutes at room temperature. The supernatant was discarded and cells were incubated with 10 µM of 2', 7' dichlorodihydrofluorescein diacetate (H_2DCFDA) dissolved in PBS for 45 minutes under cell culture conditions. Subsequently, cells were spun down at 1200 rpm for 5 minutes at room temperature to remove the excess dye, and 500 µL of pre-warm PBS was added to each tube to be analyzed through flow cytometry. All four compounds significantly induced the overproduction of ROS in HL-60 cells. 10.93% and 10.72% of the cells treated with 0.22 µM and 0.45 µM of NC2564, respectively, were positive for ROS, and 4.4% were positive in DMSO (**Figure 5a**). NC2559 at 0.33 µM caused the production of ROS in 8.13% of the cells and NC2559 at 0.66 µM in 12.14%. Treatments with 0.33 µM and 0.66 µM of NC2570 and 0.29 µM and 0.58 µM of NC2571 produced ROS in 12.3%, 10.5%, 9.6%, and 11.5% of the total cell population, respectively, and the DMSO, vehicle control in 4.1% of the cell population (**Figure 5b**). Collectively, these findings suggest that the four novel piperidones provoke the overproduction of ROS in HL-60 cells.

a

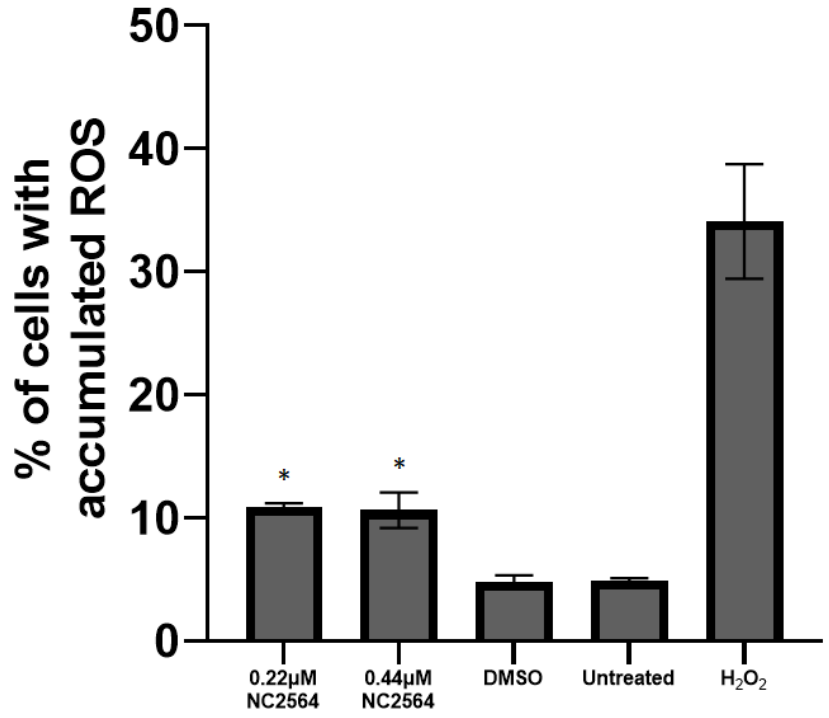
% of cells with accumulated ROS
50
40
30
20
10
0
*
*
0.22μM NC2564
0.44μM NC2564
DMSO
Untreated
H_2O_2

b

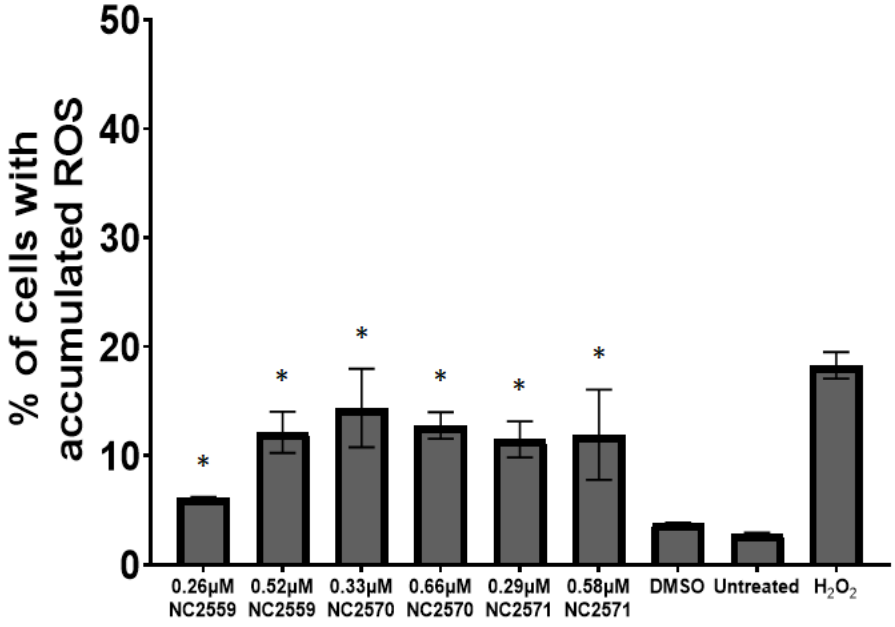
% of cells with accumulated ROS
50
40
30
20
10
0
*
*
*
*
*
*
0.26μM NC2559
0.52μM NC2559
0.33μM NC2570
0.66μM NC2570
0.29μM NC2571
0.58μM NC2571
DMSO
Untreated
H_2O_2

Figure 5. NC2559, NC2564, NC2570, and NC2571 cause ROS overproduction in HL-60 cells. Treatment with the four compounds was found to overproduce ROS after 5 h in the HL-60 cell line. Cells treated with **(a)** NC2564 **(b)** NC2559, NC2570, and NC2571 significantly produced more ROS than cells treated with the vehicle DMSO. Each bar graph represents the average of three technical replicates and the standard deviation. ***** Represents *p*-value = ≤ 0.003513 in comparison to DMSO.

2.6 NC2559, NC2564, NC2570, and NC2571 Alter the HL-60 Cell Cycle

The cell cycle is referred to as the series of events in which a cell duplicates its components to produce a daughter cell[60,61]. Cell division consists mainly of two stages: mitosis with all the known phases and the interphase which divides into G1, S, and G2 phases[61]. The final objective of any drug is to kill and/or stop cell proliferation. Therefore, compounds that influence cell cycle progression are useful to stop cell proliferation[62]. To analyze if the compounds affect the cell cycle $1X10^5$ cells were seeded in 24-well plates at a volume of 1ml of media and were left overnight under cell culture conditions. The next day cells were treated with the compounds' respective CC_{15} and CC_{30}: 0.08 µM and 0.16 µM of NC2559, 0.07 µM and 0.14 µM of NC2564, 0.1 µM and 0.2 µM of NC2570, and 0.11 µM and 0.22 µM of NC2571 for 96 h. After incubation time, cells were collected in flow cytometry tubes, centrifuged for 5 minutes at 1200 rpm, and the supernatant was discarded. Next, cells were resuspended with a mixture containing 200 µL of NIM-DAPI and 200 µL of PBS and were read via flow cytometry. **Figure 6** shows the results for the cell cycle. The four compounds at their respective CC_{15} and CC_{30} values produced the fragmentation of the DNA as measured by the population of cells in the Sub G0/G1 (**Figure 6a**).

a

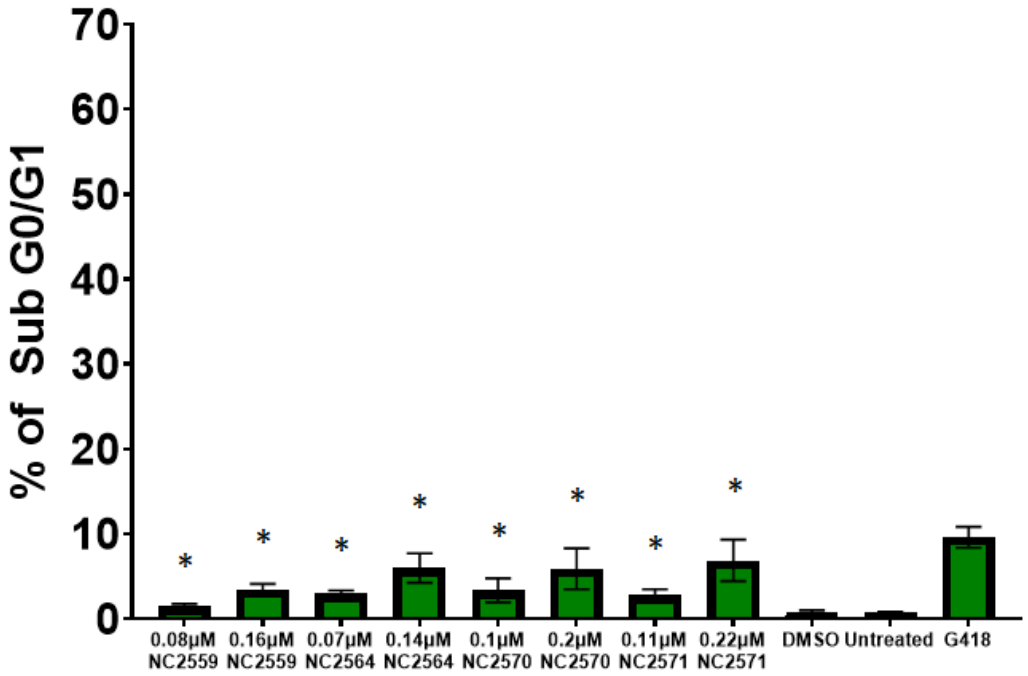
% of Sub G0/G1
70
60
50
40
30
20
10
0
0.08μM NC2559
0.16μM NC2559
0.07μM NC2564
0.14μM NC2564
0.1μM NC2570
0.2μM NC2570
0.11μM NC2571
0.22μM NC2571
DMSO
Untreated
G418

b

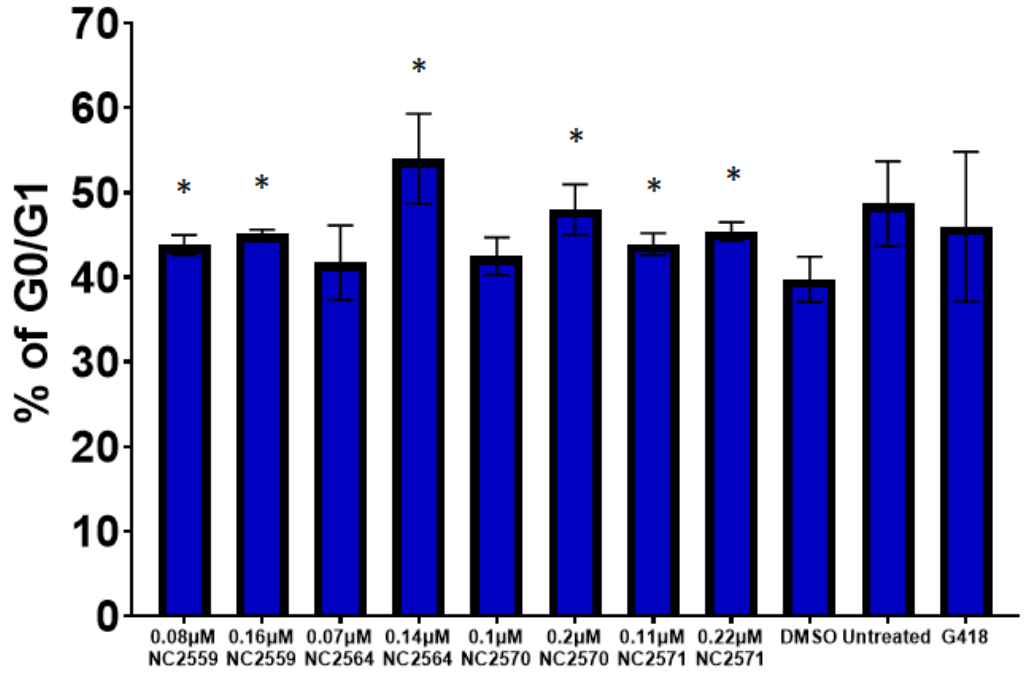
% of G0/G1
70
60
50
40
30
20
10
0
0.08μM NC2559
0.16μM NC2559
0.07μM NC2564
0.14μM NC2564
0.1μM NC2570
0.2μM NC2570
0.11μM NC2571
0.22μM NC2571
DMSO
Untreated
G418

c

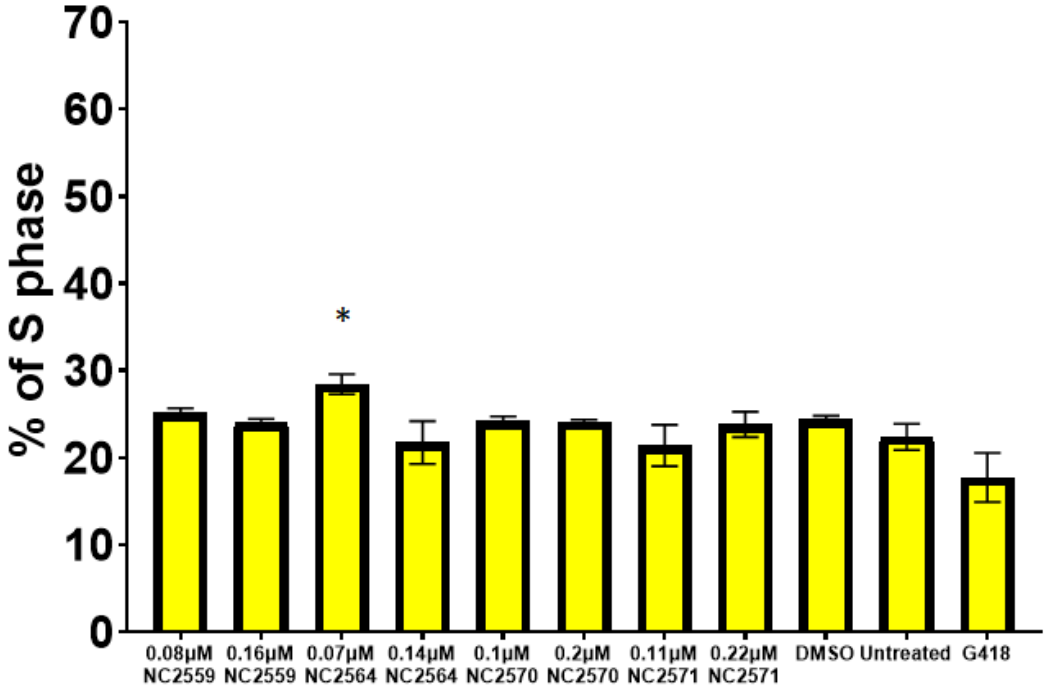
% of S phase
70
60
50
40
30
20
10
0
*
0.08μM NC2559
0.16μM NC2559
0.07μM NC2564
0.14μM NC2564
0.1μM NC2570
0.2μM NC2570
0.11μM NC2571
0.22μM NC2571
DMSO
Untreated
G418

d

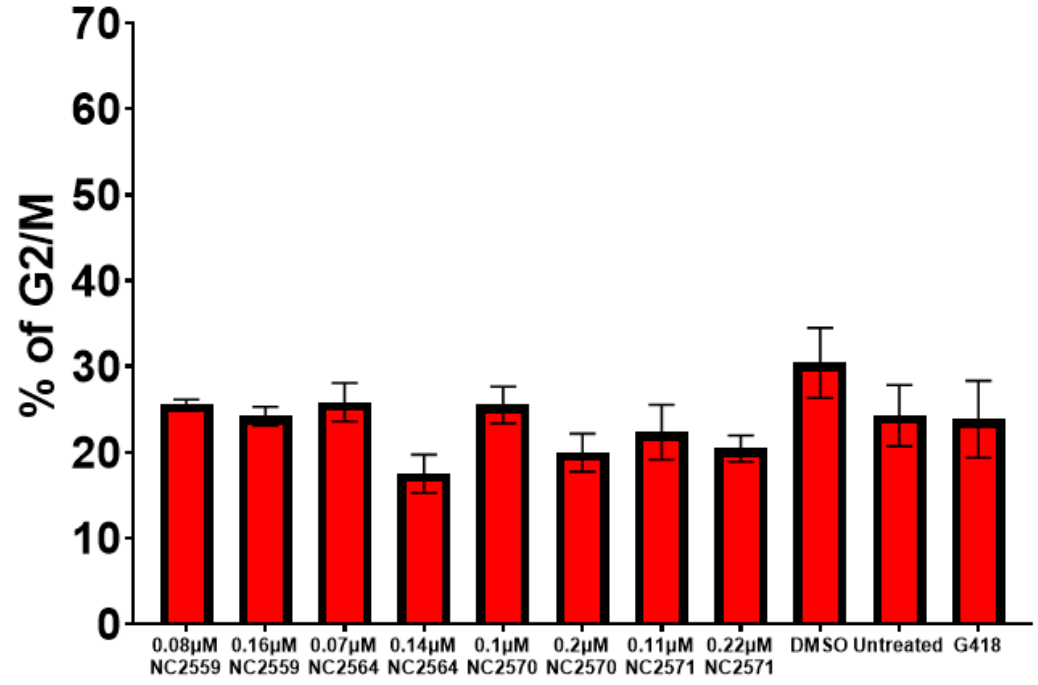
% of G2/M
70
60
50
40
30
20
10
0
0.08μM NC2559
0.16μM NC2559
0.07μM NC2564
0.14μM NC2564
0.1μM NC2570
0.2μM NC2570
0.11μM NC2571
0.22μM NC2571
DMSO
Untreated
G418

Figure 6. NC2559, NC2564, NC2570, and NC2571 mostly arrest HL-60 cells in G0/G1 phase interrupting cell cycle progression. Exposure of HL-60 cells for 96 h to the novel compounds causes the alteration of the cell cycle. **(a)** the four compounds produce the fragmentation of DNA as measured by the higher percentages of HL-60 cells after treatment with NC2559, NC2564, NC2570, and NC2571 compared to the DMSO. **(b)** NC2559, NC2564, NC2570, and NC2571 arrest the HL-60 cells in the G0/G1 phase as shown by the production of higher percentages of cells as compared to the DMSO. **(c)** NC2564 at 0.07 μM produced an arrest in the S phase. **(d)** the four compounds did not arrest HL-60 cells in the G2/M phase, however, there is a reduction of cells in this phase. * Represents *p*-value ≤ 0.021415 in comparison to DMSO.

Treatment with 0.08 μM and 0.16 μM of NC2559 caused the fragmentation of the DNA in 1.43% and 3.5% of the cell population (**Figure 6a**). NC2564 at 0.07 μM and 0.14 μM, NC2570 at 0.1 μM and 0.2 μM, and NC2571 at 0.11 μM and 0.22 μM, provoked DNA fragmentation in 2.9%, 5.9%, 3.3%, 5.8%, 2.8%, and 6.8% of the total cell population, respectively (**Figure 6a**). In comparison, 0.8% of the cells treated with DMSO at 0.1% displayed DNA fragmentation (**Figure 6a**). In addition, the positive control, G418, induced the fragmentation of 9.6% of the cells (**Figure 6a**). These data reveal that NC2559, NC2564, NC2570, and NC2571 significantly induced the fragmentation of the DNA as shown by the sub G0/G1 population (**Figure 6a**). Since DNA fragmentation is a hallmark of apoptosis[63], these results corroborate apoptosis as the cell death mechanism executed by the four compounds. The four compounds also arrested the cell cycle in the G0/G1 phase, before DNA duplication which occurs in the S phase[64]. 43.78% and 45.1% of the cell population remained in the G0/G1 phase after exposure to 0.08 μM and 0.16 μM of

NC2559 (**Figure 6b**). NC2564 at 0.07 µM and 0.14 µM produced 41.7% and 53.9% of the cells in the G0/G1 phase, respectively (**Figure 6b**). Moreover, cells were in the G0/G1 phase after treatment with NC2570 at 0.1 µM and 0.2 µM resulted in 42.5% and 47.9%, and NC2571 at 0.11 µM and 0.22 µM 44% and 45.4%. DMSO produced 39.7% of cells in G0/G1 phase and untreated cells 48.6%. Finally, the positive control G418 produced 45.9% of cells (**Figure 6b**). The comparison between DMSO and the values of NC2559 at 0.08 µM and 0.16 µM, NC2564 at 0.14 µM, NC2570 at 0.2 µM, and NC2571 at 0.11 µM and 0.22 µM produced a significant difference (**Figure 6b**) meaning that the compounds primarily arrest the cell cycle in the G0/G1 phase. We did not find a significant difference in cells treated with the four compounds and cells treated with the DMSO in the S phase, the only difference was when cells were treated with NC2564 at 0.07 µM, which produce 28.4% of the cells to be in that specific phase (**Figure 6c**). Unexpectedly, the positive control G418 did not arrest the cells in the S phase as previously shown[65], one possible explanation is that more cells were already dead after treatment with the G418 (**Figure 6a**). **Figure 6d** depicts the results for the G2/M phase. We did not see any significant difference in cell cycle arrest in this phase, since values after treatment were lower in this phase, these compounds do not arrest the cell cycle in the G2/M phase. Overall, these data corroborate apoptosis as the cell death mechanism being exerted by the four compounds as shown by the higher percentages of cells in the sub G0/G1 phase (**Figure 6a**). Furthermore, the four compounds induce the arrest of HL-60 cells in the G0/G1 phase of the cell cycle (**Figure 6b**). Compounds with similar structures were reported to not have any arresting effect in the cell cycle at 72 h[55], however, we did find arrest in the cell cycle after 96 h of exposure. Suggesting that time is a factor for these

compounds.

2.7 NC2559, NC2564, NC2570, and NC2571 Generated the Accumulation of Polyubiquitinated Proteins

Based on the homology of NC2559, NC2564, NC2570, and NC2571 with already published compounds, b-AP15[66], VLX1570[67], and the recently characterized piperidones P1 and P2[43], we inferred that these compounds could also act as proteasome activity inhibitors. The ubiquitin-proteasome pathway (UPP) is a pathway by which previously ubiquitin-tagged damaged, misfolded, or unneeded proteins are degraded[68]. As a matter of fact, targeting the UPP has established a crucial advance in the treatment of hematological cancers and solid tumors[69]. Therefore, it represents a potential strategy to develop novel anti-cancer drugs. The impairment of proteasome activity by looking at the accumulation of polyubiquitinated proteins has been previously used to characterize novel proteasome activity inhibitors[25,43,55,70]. Thus, to prove our hypothesis of the four compounds acting as proteasome activity inhibitors, we decided to follow the same approach and look for the accumulation of polyubiquitinated proteins after treatment with the compounds. We accomplished the experiment by using Western Blot. $3X10^6$ HL-60 cells were seeded in 6-well plates at a volume of 5 ml. Cells were treated for 8 h with 1 μM of NC2559, NC2564, NC2570, and NC2571. MG132 at 5 μM was used as a positive control and DMSO at 0.1% as vehicle control. After incubation cells were collected and pelleted at 1200 rpm for 5 minutes. The supernatant was discarded and cells were washed with 1 ml of PBS to remove all the remaining media. Cells were pelleted again at 1000 rpm for 5 minutes, the supernatant was discarded and the pellet was resuspended in 60 μL of 2X laemmli buffer (120 mM Tris-HCl, 0.1% β-mercaptoethanol, 4% SDS, 20%

glycerol, and 0.02% (v/v) bromophenol blue) following a vortex for 5 seconds and a quick centrifuge. Lysates were boiled for 10 minutes at 100°C and were analyzed by using the NanoDrop N-1000 system (Thermo, Fisher Scientific). 100 µg of protein were loaded in the SDS-PAGE and transferred to a polyvinylidene difluoride (PVDF) membrane. Subsequently, the PVDF membrane was blocked with a 10% milk/TBS solution overnight at 4°C to detect polyubiquitinated proteins. An α-ubiquitin mouse monoclonal antibody (Santa Cruz Biotech, Dallas, TX) in a 1:1000 dilution was used as the primary antibody. Membranes were incubated with the antibody for 1 h in constant movement followed by three 15-minute washes with TBS-T. Secondary polyclonal goat anti-mouse conjugated to peroxidase antibody (1:10000) (Thermo Scientific) was incubated for 1 h followed by three 15-minute washes with TBS-T. When incubation with secondary antibodies was finished, membranes were moistened with 1 ml of a BCL mix and analyzed with the iBrigth Imagining Systems (TermoFisher Scientific). After analysis of the Polyubiquitinated proteins, antibodies were removed by stripping the membrane over 30 minutes in constant movement. Actin, a housekeeping gene was used as a loading control. To detect actin, a monoclonal anti-β-actin-peroxidase conjugate antibody (1:25,000; Sigma Aldrich) was used, and antibodies were incubated with the membranes as aforementioned. Densitometry analyses were accomplished with the Image Studio Lite version 5.2 software by LI-COR, same areas were selected in the software to analyze the images. Anticipatedly, HL-60 cells treated with DMSO at 0.1% did not produce an accumulation of polyubiquitinated proteins (**Figure 7a, lane 1**). In addition, the positive control MG-132 produced the accumulation of polyubiquitinated proteins (**Figure 7a, lane 2**) with a 4.2-fold change compared to the vehicle control (**Figure 7b**). Treatment with 1 µM of NC2559,

NC2564, NC2570, and NC2571 produced the accumulation of polyubiquitinated proteins 2.8-, 2.7-, 2.2-, and 3.1-fold change, respectively (**Figure 7a, lanes 3-6, & Figure 7b**). All the fold changes were calculated respective to the vehicle. These results showed that the four compounds produce the accumulation of polyubiquitinated proteins in HL-60 cells. However, these results are not enough to prove that the proteasome activity is being inhibited by these compounds. Although the proteasome degrades 80% to 90% of the cellular proteins[71], ubiquitin tagging is not specific for the UPP since it is involved in lysosomal degradation and can be used by the autophagosome[72]. Therefore, the accumulation of polyubiquitinated proteins suggests that one of the major protein degradation pathways is being affected. To prove that proteasome activity is directly affected, further research is needed. We suggest following the same strategy as previously described[73] and using the proteasome activity assay kit (Abcam ab107921).

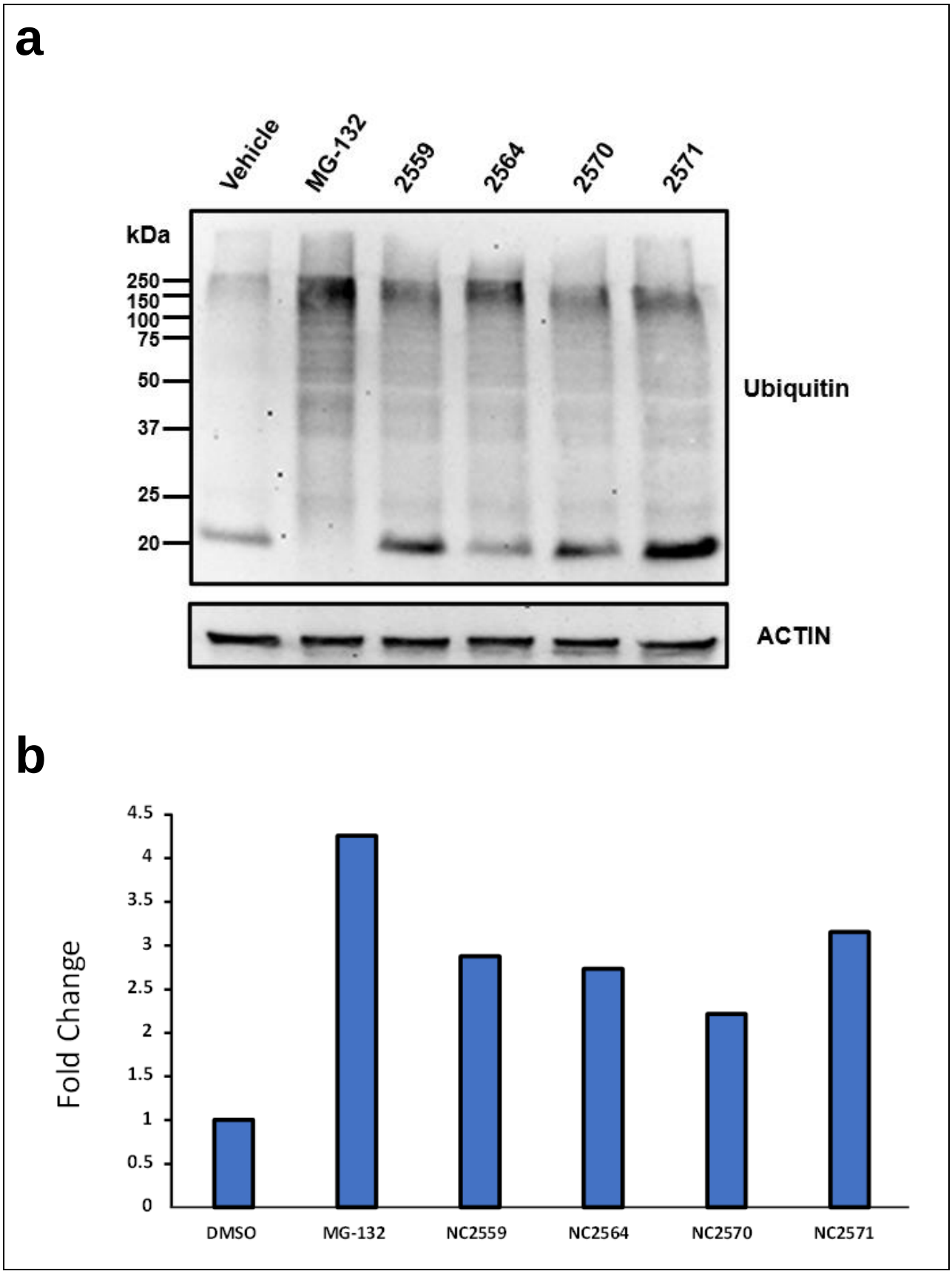
a
Vehicle
MG-132
2559
2564
2570
2571
kDa
250
150
100
75
50
37
25
20
Ubiquitin
ACTIN
b
Fold Change
4.5
4
3.5
3
2.5
2
1.5
1
0.5
0
DMSO
MG-132
NC2559
NC2564
NC2570
NC2571

Figure 7. NC2559, NC2564, NC2570, and NC2571 cause polyubiquitinated proteins accumulation. (a) Exposure of HL-60 cells to 1 μM of NC2559, NC2564, NC2570, and NC2572 for 8 h produced an accumulation of polyubiquitinated proteins (lanes 3 - 6). As expected, the proteasome inhibitor MG-132 produced an accumulation of polyubiquitinated proteins. In contrast, DMSO at 0.1% did not produce polyubiquitinated proteins. **(b)** Fold changes as measured by densitometry of the Western Blot relative to the vehicle, DMSO. The four compounds produced more than 2-fold change.

2.8 NC2559, NC2564, NC2570, and NC2571 Increase the Expression of the HMOX-1 Protein

Proteasome inhibition results in the accumulation of tagged proteins to be degraded which leads to the endoplasmic reticulum (ER) stress[74]. Moreover, the Heme Oxygenase 1 gene (HMOX-1) is overexpressed under oxidative stress conditions[75,76]. HMOX-1 overexpression and ER stress have been linked to being associated with proteasome inhibitors[25,43,77]. Considering that we found an impairment in the protein degradation pathway via the accumulation of polyubiquitinated proteins, we conjectured that HMOX-1 would be overexpressed after treatment with the four compounds. To prove our hypothesis, we ran a western blot analysis following the protocol discussed in the previous section with the *α-hmox-1* mouse monoclonal in a 1:200 dilution (Santa Cruz Biotech) as the primary antibody. Goat anti-mouse conjugated to peroxidase antibody (Thermo Scientific) and anti-β-actin-peroxidase conjugate antibody (1:25,000; Sigma Aldrich) were used as described above.

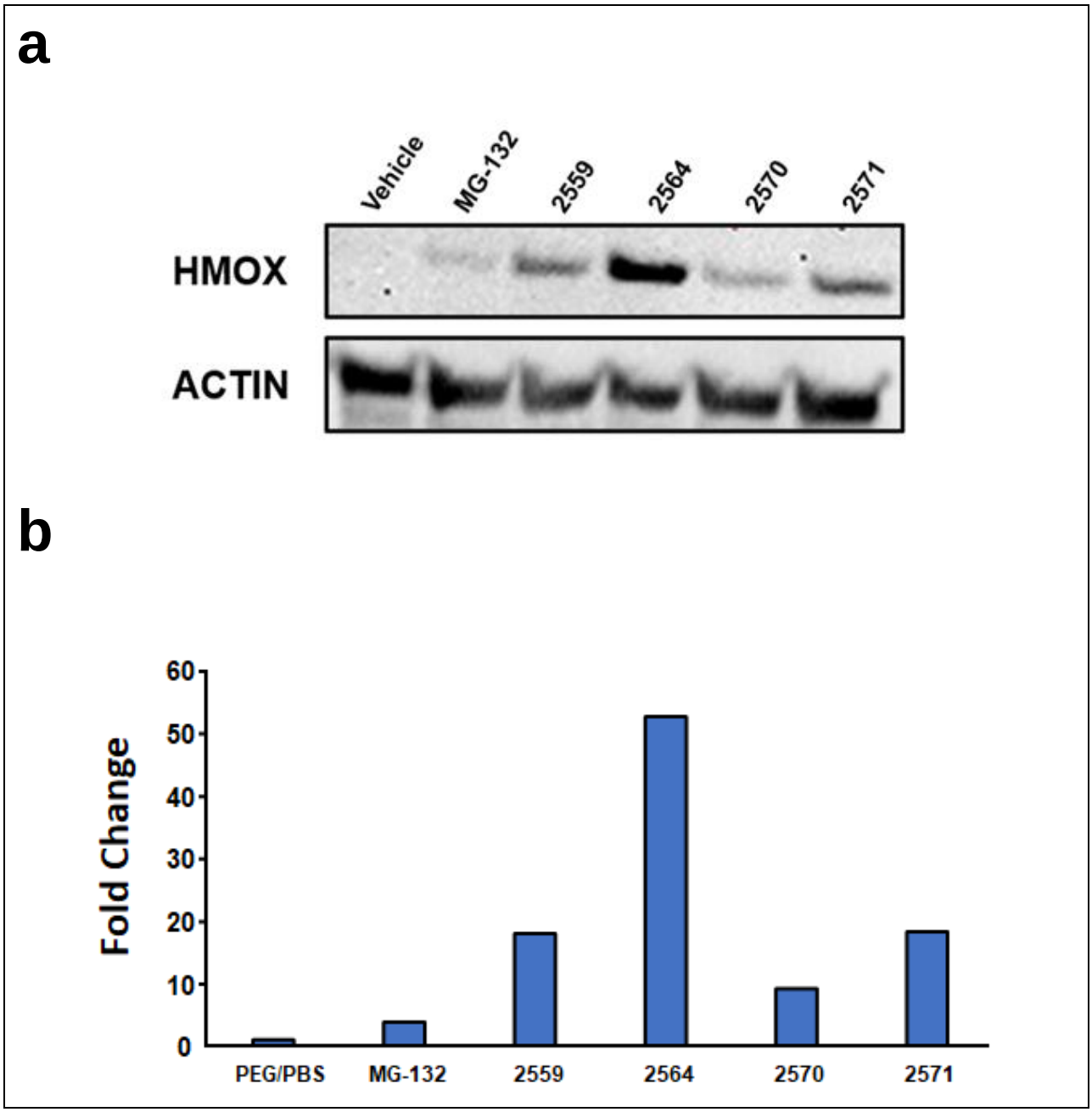

Figure 8. NC2559, NC2564, NC2570, and NC2571 cause the overproduction of HMOX-1. (a) Treatment for 8 h with 1 µM of the four compounds overproduces the protein HMOX-1, which has been associated to be overexpressed after treatment with proteasome inhibitors. Lanes 2-6 show the experimental compounds. As anticipated, treatment with DMSO did not produce HMOX-1 (lane 1). Even though the effect was not notorious as the experimental compounds, the proteasome inhibitor MG-132 at 5 µM

overproduced HMOX-1 (lane 2). **(b)** Densitometry analyses corroborate that the four compounds are overproducing HMOX-1 as shown by the fold changes relative to the DMSO. Interestingly, the positive control, a proteasome inhibitor, cause a less fold change than the experimental control but was higher than the DMSO.

The results showed that there is an overexpression of the HMOX-1 protein after treatment for 8 h. As we anticipated, the vehicle treatment (DMSO) did not produce HMOX-1 (**Figure 8a, lane 1).** On the other hand, HMOX-1 was overexpressed after treatment with the positive control MG-132 and the four experimental compounds (**Figure 8a, lanes 2-6**). The positive control produced a fold change of 3.8 respective to the DMSO (**Figure 8b**). The four experimental compounds demonstrated a much higher increase in the expression of HMOX-1 relative to those cells treated with DMSO. NC2559 produced a fold change of 17.9 (**Figure 8b**). Cells treated with NC2564 produced the highest overexpression of HMOX-1 with a difference of 52.64-fold change (**Figure 8b**). NC2570 and NC2571-treated cells produced a fold change of 9.14 and 18.2, respectively (**Figure 8b**). These data indicate that HMOX-1 is overexpressed after treatment with the novel piperidones. The overexpression of HMOX-1 has been linked to being associated with proteasome activity inhibition, however, to test the inhibition of the proteasome activity, we recommend further analysis of these compounds.

2.9 Discussion

Cancer remains a major health problem worldwide. Therefore, there is a need for new molecules that can kill cancer cells without affecting normal cells. In this chapter, a small library of fourteen piperidones derived from curcumin was tested on a panel of different cell lines. CC_{50} values were calculated to evaluate the cytotoxic activity of these compounds in cancer and non-cancerous cell lines. The fourteen compounds have cytotoxicity at relatively small concentrations spanning the nanomolar and micromolar range. HL-60 and CCRF-CEM which are hematological cancer cell lines were the most sensitive of the tested cell lines (**Table 1**). The fourteen compounds also showed strong cytotoxicity toward COLO 205 and HT29, two cell lines derived from colon cancer patients, and MCF7, derived from a patient with breast cancer (**Table 2**). Even though the compounds killed the non-cancerous cells Hs27 and CCD-112CoN at micromolar concentrations, the effects were not as strong as in the other tested cells (**Table 3**). The comparison of the CC_{50}s between the HL-60 and CCRF-CEM cell lines to the Hs27 cell line to calculate selectivity, resulted in SCIs greater than 1 (**Table 4**), thus, indicating that the four compounds have preferentially activity towards cancer cells than non-cancerous cells. NC2559, NC2564, NC2570, and NC2571 (**Figure 1**) were chosen for further characterization in the HL-60 cell line after considering cytotoxicity, selectivity, and sensitiveness. A literature review indicated that similar compounds were reported to induce apoptosis as the cell death mechanism[42,43,55,78], for this reason, we tested the ability of the four compounds to induce apoptosis. Two important events in the apoptotic pathway, phosphatidylserine (PS) externalization, and caspase 3 activation were evaluated to determine if apoptosis was induced by the experimental compounds. The

data demonstrated that a significantly greater percentage of cells was positive for PS externalization (**Figure 2**) and caspase 3 activation (**Figure 3**) with compound treatment in comparison with the solvent DMSO. Moreover, the four compounds induced the fragmentation of the DNA as shown in the sub G0/G1 population (**Figure 6**). These results demonstrate that apoptosis occurs after cells are exposed to these compounds. Apoptosis is triggered due to two major pathways the extrinsic apoptotic pathway, triggered by external factors that activate cell death receptors, and the intrinsic apoptotic pathway which is executed through the mitochondria[52]. One of the major events in the activation of the intrinsic pathway is the depolarization of the mitochondrial membrane potential[53] thereby, we tested if the four compounds cause this event. The data showed that the four compounds were responsible for a higher percentage of cells experiencing mitochondrial membrane depolarization, indicating that the compounds activate the apoptotic intrinsic pathway (**Figure 4**). The overproduction of ROS can lead to impairment in mitochondria function and induce programmed cell death[57]. Thus, we evaluated the ROS production after treatment with the four compounds. The chemical compounds were able to significantly increase the production of ROS (**Figure 5**). We were also able to corroborate apoptosis with the cell cycle analysis. Cell cycle analysis also demonstrated that the four novel molecules were able to arrest the cell cycle in the G0/G1 phase (**Figure 6b**). Finally, related molecules have been reported to induce the accumulation of polyubiquitinated proteins leading to the inhibition of the ubiquitin-proteasome pathway. Exposure to piperidones was responsible for the accumulation of polyubiquitinated proteins in HL-60 cells as measured by western blot (**Figure 7**). In addition, the HMOX-1 protein was overproduced after treatment with the four compounds (**Figure 8**) suggesting

that the compounds could be inhibiting the ubiquitin-proteasome pathway, however, more experiments would have to be accomplished to confirm this. The results proved that one of the three major protein degradation pathways could be the target of these compounds. Overall, these four compounds have potent cytotoxicity and selectivity towards cancer cells and not non-cancerous cells. The analyzed compounds in this chapter demonstrated to have lower CC_{50}s than previously reported compounds[43], making them very attractive as anti-cancer drugs. Nonetheless, *in vivo* studies are needed before being considered as potential anti-cancer drugs. *In vivo* testing with similar compounds has demonstrated promising results[79]. Consequently, we consider these compounds as potential candidates to be tested using *in vivo* models.

Chapter 3: Evaluation of cytotoxicity of a commercial chemical library, identification, and characterization of one hit compound

3.1 Evaluation of a Chemical Library to Identify a Hit Compound

In this chapter, 5000 compounds from the chemical library, ChemBridge DIVERset were tested in the cancer cell line CCRF-CEM to find a highly potent compound. The primary screening was accomplished by using the DNS assay[40]. CCRF-CEM cells ($1X10^4$) were seeded in 96-well plates at a final volume of 100 µL of media per well, then incubated overnight under cell culture conditions. The experiments included the experimental compounds at a concentration of 5 µM, 1% of DMSO as the vehicle control, untreated cells as a negative control, and 1 millimolar (mM) of H_2O_2 as a positive control of cell death. After treatments, the plates were placed and left under cell culture conditions for a 24 h exposure. Two hours before the period of incubation was completed, a mix containing Hoechst 33342 and PI diluted in PBS was put into each well. Then, four contiguous images of each well were captured using the IN Cell Analyzer 2000 system (GE Healthcare, Pittsburg PA, USA) and analyzed with Analyzer Workstation 3.2 software (GE Healthcare). The primary screening revealed ten potent compounds that killed more than 50% of the total cell population and these were selected to be further analyzed (data not shown). Thereafter, a secondary screening was performed following the aforementioned procedure and cell line to identify a hit compound. The cytotoxic activity of the ten compounds was determined by calculating the cytotoxic concentration needed to kill half the total population known as the CC_{50}. Using an online tool (https://www.johndcook.com/interpolator.html) we determined the CC_{50} by using one concentration that kills more than 50% of the population and one that kills less than 50%.

CC_{50}s were determined as the average of at least three comparisons of concentrations. The secondary screening of the ten compounds led to the identification of the most potent compound. This compound was designated B6 (**Figure 9**).

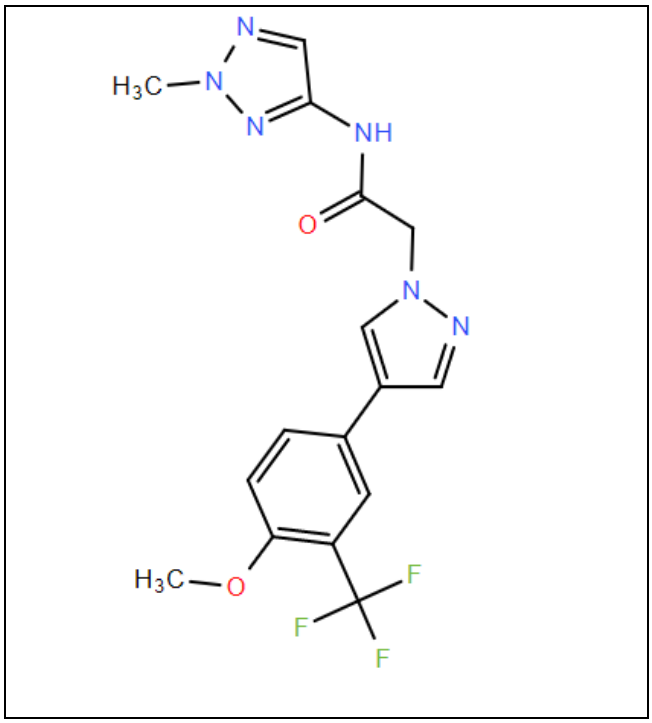

Figure 9. B6 chemical structure. The chemical structure of 2-{4-[4-methoxy-3-(trifluoromethyl)phenyl]-1H-pyrazol-1-yl}-N-(2-methyl-2H-1,2,3-triazol-4-yl)acetamide also known as B6.

3.2 Evaluation of the Cytotoxicity of B6 Compounds on a Panel of Different Cancer and Non-cancerous Cell Lines.

Once we identified a potent compound, we tested it against a panel of different cell lines to calculate the CC_{50}s and define its cytotoxic activity. We selected twenty-three cell lines for this analysis. The following hematological cancer cell lines were used: Ramos, HL-60, CCRF-CEM, Nalm6, Jurkat, KCL22, and K562. The following breast cancer cell lines were used: MDA-MB-231, MCF7, HCC70, and T47D, the metastatic LM2-4 cell derived

from the MDA-MB-231, and a PTX-resistant MDA-MB-231. The following also were used: two cell lines derived from patients with colon cancer, (COLO 205 and HT29), a lung cancer cell line A549, a liver cancer cell line HepG2, one melanoma cell line A375, the pancreatic PANC-1, a prostate cancer cells PC3, and finally three non-cancerous cell lines derived from breast, colon tissues, and the foreskin (MCF10A, CCD-112CoN, and Hs27, respectively). Different types of media were used to grow the cell lines. For the hematological cancer cells, we used RPMI medium supplemented with 10% FBS, except for HL-60 which was supplemented with 20% FBS. The HCC70 and COLO 205 cell lines were also grown using RPMI. For MDA-MB-231, HepG2, Hs27, PANC-1, A375, A549, MCF7, LM2-4, and MDA-MB-231 resistant to PTX, DMEM was used with 10% FBS. Additionally, 10 µg/ml of insulin was added to the media for the MCF-7 cell line. The MCF10A cell line was grown using DMEM F/12 media containing 10% FBS, 10 µg/ml of insulin, 20 ng/ml of epidermal growth factor (EGF), and 0.5 µg/ml of hydrocortisone. HT-29 was grown in McCoy's media supplemented with 10% FBS. Moreover, every cell media was supplemented with 100 U/ml of penicillin and 100 µg/ml of streptomycin. All cell lines were grown at 37°C in a humidified environment with 5% CO_2 and were monitored every day to avoid 100% confluency. For the hematological cancers, cell viability was measured by using propidium iodide (PI) before every experiment, only cells with 95% or more viability were used. Furthermore, for adherent cells, 1X trypsin was used to detach the cells. To avoid 100% confluency, media was changed every 2-3 days and cells that were not needed were discarded.

To accomplish cytotoxic evaluation, we used the DNS assay[40]. We utilized different time points since we tested two different types of cancer cells, adherent and non-adherent.

Cells that are derived from patients with hematological cancers were tested for 48 h of exposure to B6 and cells derived from patients with solid tumors were exposed for 72 h to the compound (**Table 6**). Overall, all the cell lines were sensitive to the B6 compound treatment with CC_{50} values in the micromolar range, which is a good indicator of cytotoxicity.

Table 6. CC_{50} values of B6 on a panel of different cell lines

	48 hours			**72 hours**	
Cell Line			**Cell Line**		
	CC_{50}	**Standard Deviation**		**CC_{50}**	**Standard Deviation**
CEM	0.42 µM	0.011547	**MDA-MB-231**	0.93 µM	0.07800
KCL22	0.72 µM	0.032016	**MCF10A**	4.40 µM	0.25131
HL-60	0.82 µM	0.015275	**Hs27**	17.92 µM	1.18245
RAMOS	0.75 µM	0.022279	**HT-29**	0.47 µM	0.2100
NALM6	2.07 µM	0.097660	**COLO 205**	0.30 µM	0.063
Jurkat	0.32 µM	0.001876	**MCF7**	0.23 µM	0.059
K562	4.37 µM	0.624	**A375**	0.34 µM	0.047
			A549	0.17 µM	0.037
			PANC-1	0.28 µM	0.076
			CCD-112CoN	0.34 µM	0.056
			T47D	0.63 µM	0.136
			HCC70	0.74 µM	0.015
			HepG2	0.36 µM	0.15
			PC3	0.92 µM	0.06
			LM2-4	0.78 µM	0.11
			MDA-MB-231 PTX-resistant	0.38 µM	0.0287

The B6 compound has different CC_{50} values in the tested cancer cell lines. The most sensitive cancer cell line for leukemias/lymphomas was Jurkat where B6 has a CC_{50} of

0.32 μM and the less sensitive was K562 with a CC_{50} of 4.37 μM (**Table 6**). For the cells that were derived from solid tumors, the most sensitive was A549 with a CC_{50} of 0.17 μM and the less sensitive was MDA-MB-231 with a CC_{50} of 0.93 μM (**Table 6**). In addition, two non-cancerous cell lines, Hs27 and MCF10A, were less sensitive to treatment with B6 which resulted in CC_{50}s of 17.92 μM and 4.4 μM, respectively. Non-cancerous cells being less sensitive means that the compound has better activity toward cancer cells and not non-cancerous cells. However, CCD-112CoN, a non-cancerous fibroblast colon cell line was very sensitive to B6 in which the compound has a CC_{50} of 0.34 μM (**Table 6**). These results suggest that B6 has potent activity in all the cancer cells that were tested and it is less aggressive in 2/3 of the non-cancerous cell lines. For this reason, B6 is considered a good candidate to be tested as a potent drug with anti-cancer properties. Although MDA-MB-231 was the least sensitive among the adherent cells, it was still used for further characterization of the B6 compound due to our laboratory having experience with this cell line in transcriptome analysis[80,81]. Furthermore, the comparison of the CC_{50} values of MDA-MB-231 and MCF10A gave us an SCI value of 4.73, which means that the B6 compound has selectivity in this breast cancer cell line.

3.3 B6 Induces the Externalization of Phosphatidylserine (PS) in MDA-MB-231 Cells

It has been reported that some compounds with a pyrazole moiety can induce apoptosis as the cell death mechanism in different cell lines[82–84]. Therefore, we tested the ability of the B6 compound to induce apoptosis in the MDA-MB-231 cell line by the Annexin V-FITC assay, which measures the externalization of phosphatidylserine (PS). The experiment was performed by seeding MDA-MB-231 cells ($1X10^5$) at a volume of 1 ml of media in 96-well plates. Plates were left overnight under cell culture conditions to allow

the cells to attach to the plates. Next, cells were treated with 10 μM and 20 μM of B6, DMSO at 0.1% final concentration as the vehicle control, and 1 mM of H_2O_2 as the positive control and were left for a period of 24 h. The B6 compound at a concentration of 10 μM and 20 μM induced the externalization of phosphatidylserine in 59.4% and 59.7% of MDA-MB-231 cells, respectively. DMSO treatment induced the externalization of the PS in 9% of the cell population. As expected, the positive control induced PS externalization in 49.9% of the cells. Furthermore, in untreated cells, just 3.4% of the cells demonstrated this event (**Figure 10**). The comparison between the experimental treatments and DMSO showed a significant difference in the populations displaying externalized PS (**Figure 10**), indicating that B6 induces the externalization of PS in MDA-MB-231 cells.

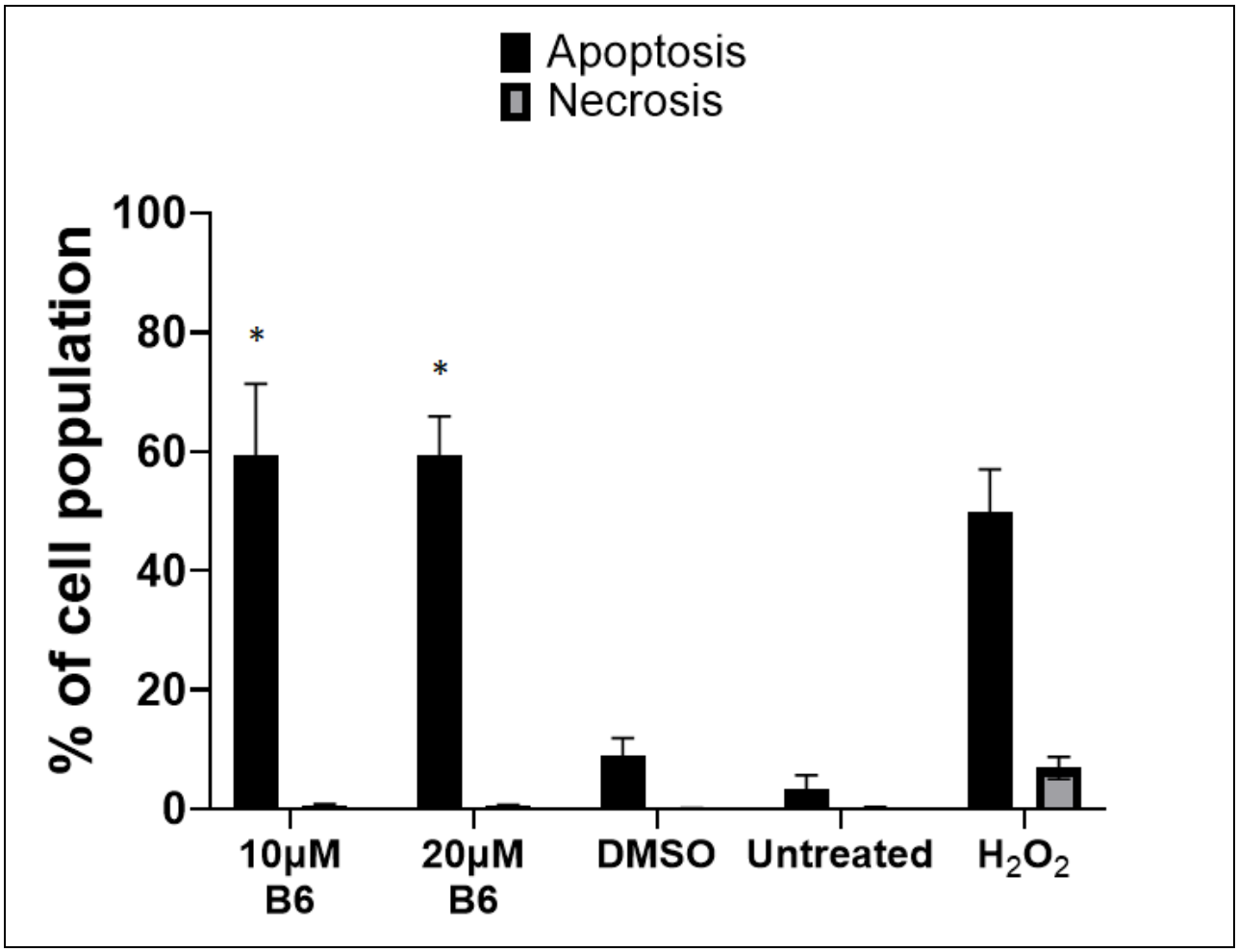

Figure 10. B6 induces apoptosis as measured by phosphatidylserine (PS) externalization. Annexin V-FITC assay analyzed by flow cytometry shows the externalization of the phospholipid phosphatidylserine (PS). Treatment of MDA-MB-231 cells with B6 at concentrations of 10 μM and 20 μM for 24 h induces apoptosis as shown by PS externalization. Each bar represents the average of at least three technical replicates. * Indicates *p*-value is ≤.001002 compared to DMSO

3.4 B6 Activates Caspase 3 in MDA-MB-231 Cells

Caspase 3 is activated during the apoptotic pathway to promote the cleavage of the ICAD protein and activate the CAD which cleaves the DNA[51]. To corroborate apoptosis as the

cell death mechanism executed by B6, we tested the activation of caspase 3, by using the fluorogenic reagent NucView 488 Caspase 3 substrate assay kit (Biotium, Hayward, CA). To assess the activation of caspase 3, $1X10^5$ MDA-MB-231 cells were seeded in 24-well plates at a volume of 1 ml of complete media and were left under cell culture conditions overnight. Then, cells were treated with 10 µM and 20 µM of the B6 compound. After 7 h of exposure, media was collected in 5 ml cytometry tubes, and cells were trypsinized with 1X trypsin to be detached and put back into cell culture conditions. After being detached, cells were collected and centrifuged at 1200 rpm for 5 minutes, the supernatant was discarded and a mixture of 200 µL of PBS containing 5 µM of the NucView 488 Caspase 3 substrate was added to each tube. Successively, tubes were incubated in the dark for 30 minutes at room temperature. After, cells were washed with PBS and resuspended with 300 µL of warm PBS to be immediately read by flow cytometry. Caspase 3 was activated after exposure of the MDA-MB-231 cells to both concentrations of the B6 compound,10 µM activated caspase 3 in 7.51% of the cells and 20 µM in 9.91% of the cells (**Figure 11**). In contrast, the vehicle at 0.1% activated caspase 3 in just 3.9% of the total cells (**Figure 11**). There was a significant difference between the DMSO and B6 compound. These data suggest that caspase 3 is activated by the compound B6, corroborating apoptosis as the cell death mechanism.

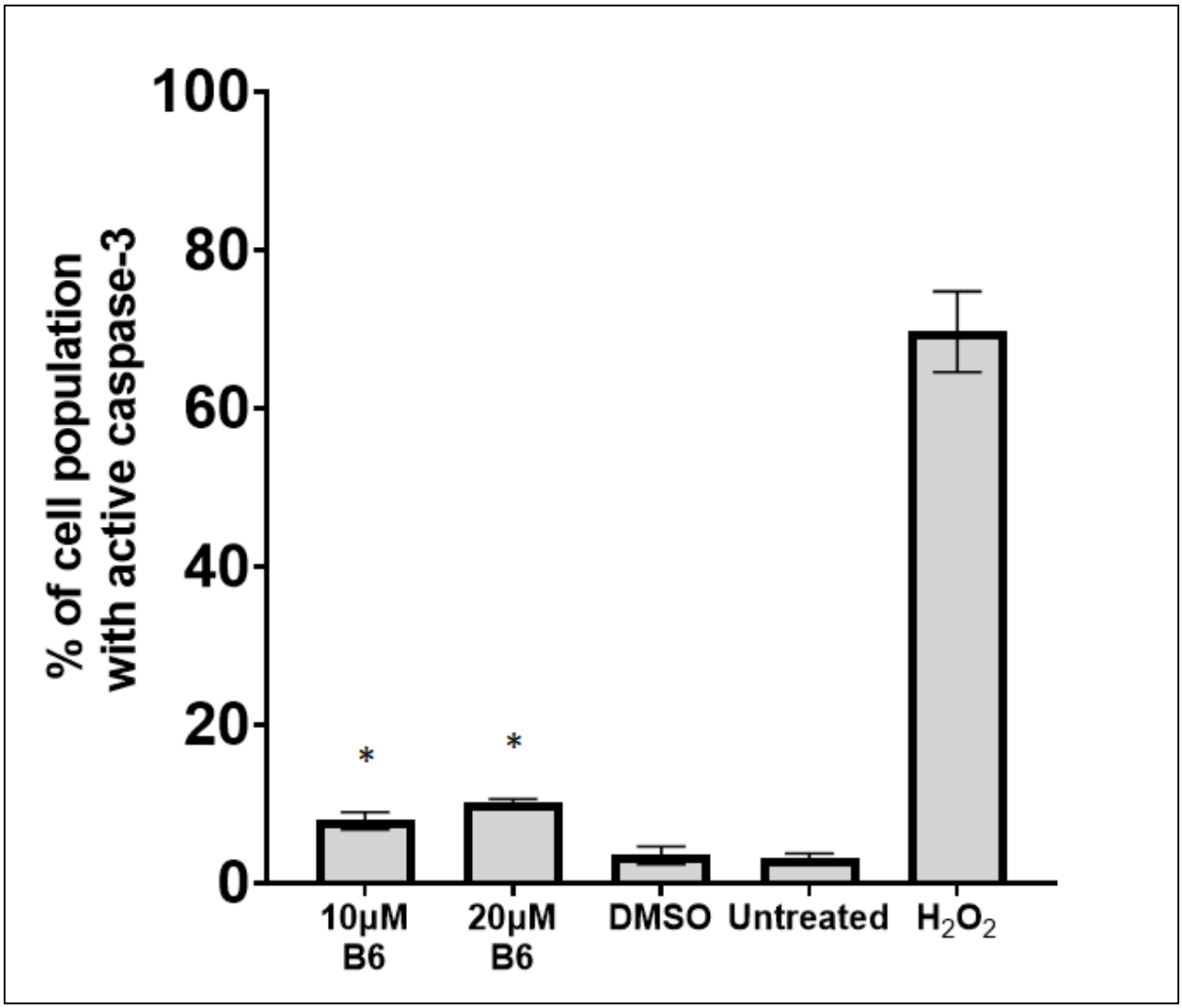

Figure 11. B6 induces activation of caspase 3. The fluorogenic reagent NucView 488 Caspase 3 substrate was used to detect the activation of caspase 3 via flow cytometry. MDA-MB-231 cells treated with 10 μM and 20 μM of B6 compound significantly induced the activation of caspase 3 as compared to the DMSO, corroborating apoptosis as the cell death mechanism exerted by B6. * Denotes *P*-value ≤ 0.00421. The average of three replicates is represented by each bar.

3.5 B6 Does Not Induce Mitochondrial Membrane Potential Depolarization

After demonstrating that B6 causes apoptosis in the MDA-MB-231 cell line, we sought to understand which apoptotic pathway was being elicited by the compound. As already mentioned, apoptosis can be triggered by internal signals in the cell that is dependent on the mitochondria (intrinsic pathway), or by extracellular signals mediated by cell death receptors (extrinsic pathway)[52]. We hypothesized that B6 could be triggering apoptosis via the intrinsic pathway since one of the hallmarks in the intrinsic pathway is the depolarization of the mitochondrial membrane potential[53,54] that can be initiated by internal signals induced by chemotherapeutic agents[52]. To assess the mitochondrial membrane potential, we used the cationic JC-1 dye[56]. We seeded MDA-MB-231 cells at a density of $1X10^5$ cells per 1 ml of media in 24-well plates and were put under cell culture conditions. The next day, cells were treated with 10 µM and 20 µM of B6, 0.1% of DMSO, and 1 mM of H_2O_2 for 7 h. Next, media was collected in flow cytometry tubes and 1X trypsin was added to each well to allow the detachment of the cells. Following detachment, cells were spun down for 5 minutes at 1200 rpm, the supernatant was discarded, and cells were incubated with 400 µL of PBS having 2 µM of the dye JC-1. Exposure to 10 µM of B6 produced the depolarization of the mitochondrial membrane potential in 6.7% of the cells and, treatment with 20 µM of B6 in 10.7%, whereas DMSO at 0.1% caused depolarization of the mitochondrial membrane potential in 8.04% (**Figure 12**). There was not a significant difference between DMSO and B6, suggesting that B6 does not induce apoptosis through the intrinsic pathway.

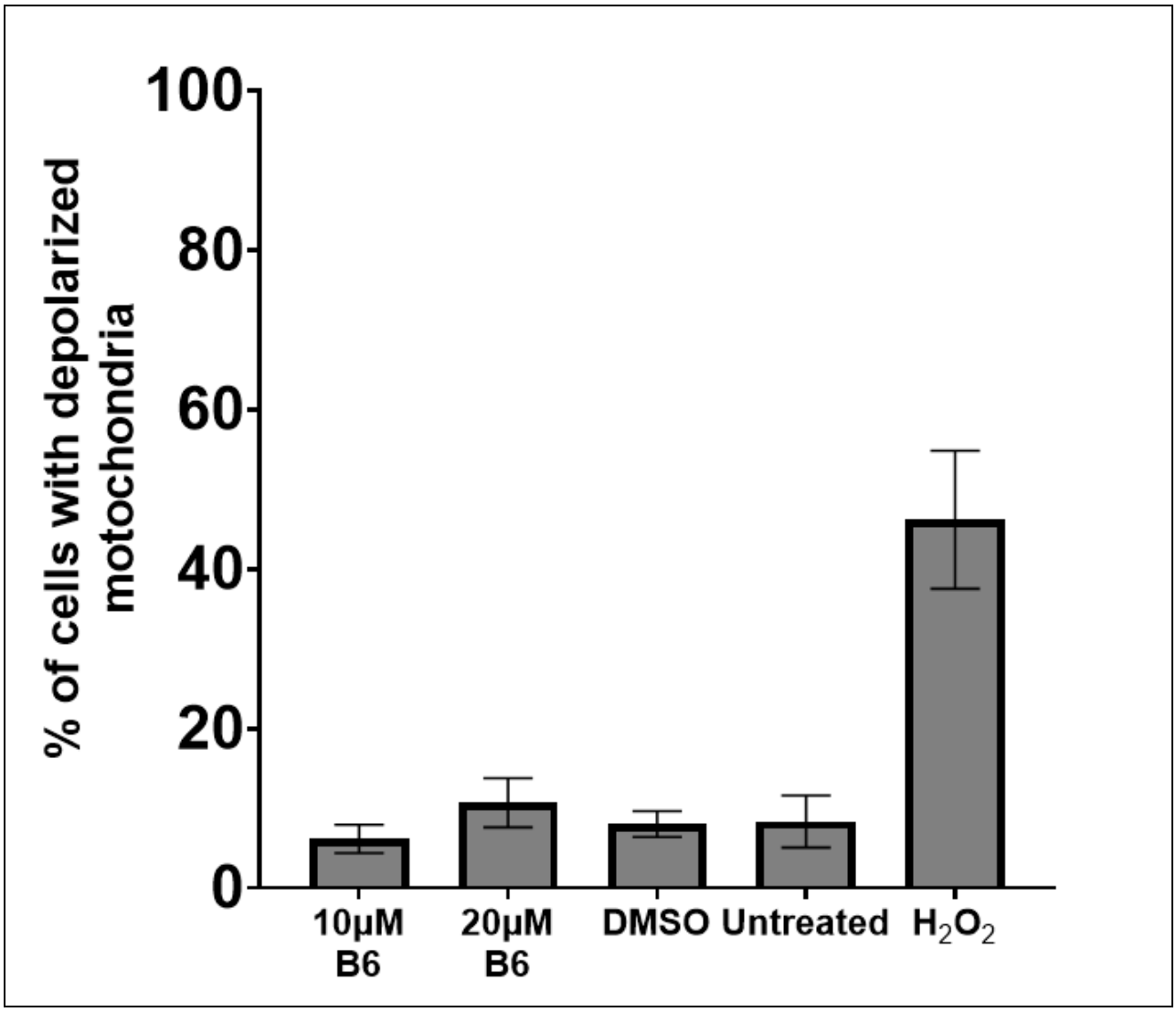

Figure 12. B6 does not induce mitochondrial membrane depolarization. B6-treated MDA-MB-231 cells at 10 μM and 20 μM did not produce any significant change in the induction of the mitochondrial membrane depolarization.

3.6 B6 Does Not Overproduce Reactive Oxygen Species (ROS)

The JC-1 assay showed that the mitochondrial membrane was not being depolarized by the B6 compound (**Figure 12**). Mitochondria are responsible for the production of 90% of cellular ROS[85]. In addition, ROS overproduction is related to mitochondrial dysfunction and loss of the mitochondrial membrane potential[80,86]. Therefore, we sought to prove mitochondrial dysfunction by detecting ROS production. We conjectured there will be no overproduction of ROS after the treatment of MDA-MB-231 cells with B6. To prove this, we measured the ROS production by using the fluorescent dye 2', 7' dichlorodihydrofluorescein diacetate (H_2DCFDA). The assay was performed by seeding $1X10^5$ MDA-MB-231 cells in 24-well plates at a volume of 1000 µL of media per well. Plates were put under cell culture conditions overnight. The next day, cells were treated for 6 h with 10 µM and 20 µM of B6, DMSO at 0.1% as the vehicle control, untreated cells as a negative control, and H_2O_2 at 1 mM as a positive control. Next, media collected in 5 ml tubes and 200 µL of 1X trypsin was added to each well, and plates were put back into cell culture conditions to allow cells to be detached. Once cells were detached, 200 µL of media was added to each well, and cells were collected in their respective tube and centrifuged at 1200 rpm for 5 minutes at room temperature. Then, the supernatant was discarded and cells were incubated for 45 minutes under cell culture conditions with 10 µM of 2', 7' dichlorodihydrofluorescein diacetate (H_2DCFDA) dissolved in 1 ml of warm PBS. Afterward, cells were centrifuged again using the abovementioned conditions to remove the excess dye, and 400 µL of warm PBS was added to each tube to resuspend the cell. Tubes were analyzed using flow cytometry. B6 exposure at 10 µM and 20 µM caused ROS production in 1.93% and 2.5% of the cell population, respectively. DMSO at

0.1% concentration produced 0.8% of the total cells. In contrast, the positive control of 1 mM of H_2O_2 caused ROS production in 64.79% of the total cells (**Figure 13**). These data indicate that B6 did not overproduce ROS in MDA-MB-231 cells, correlating that there is no mitochondrial membrane depolarization.

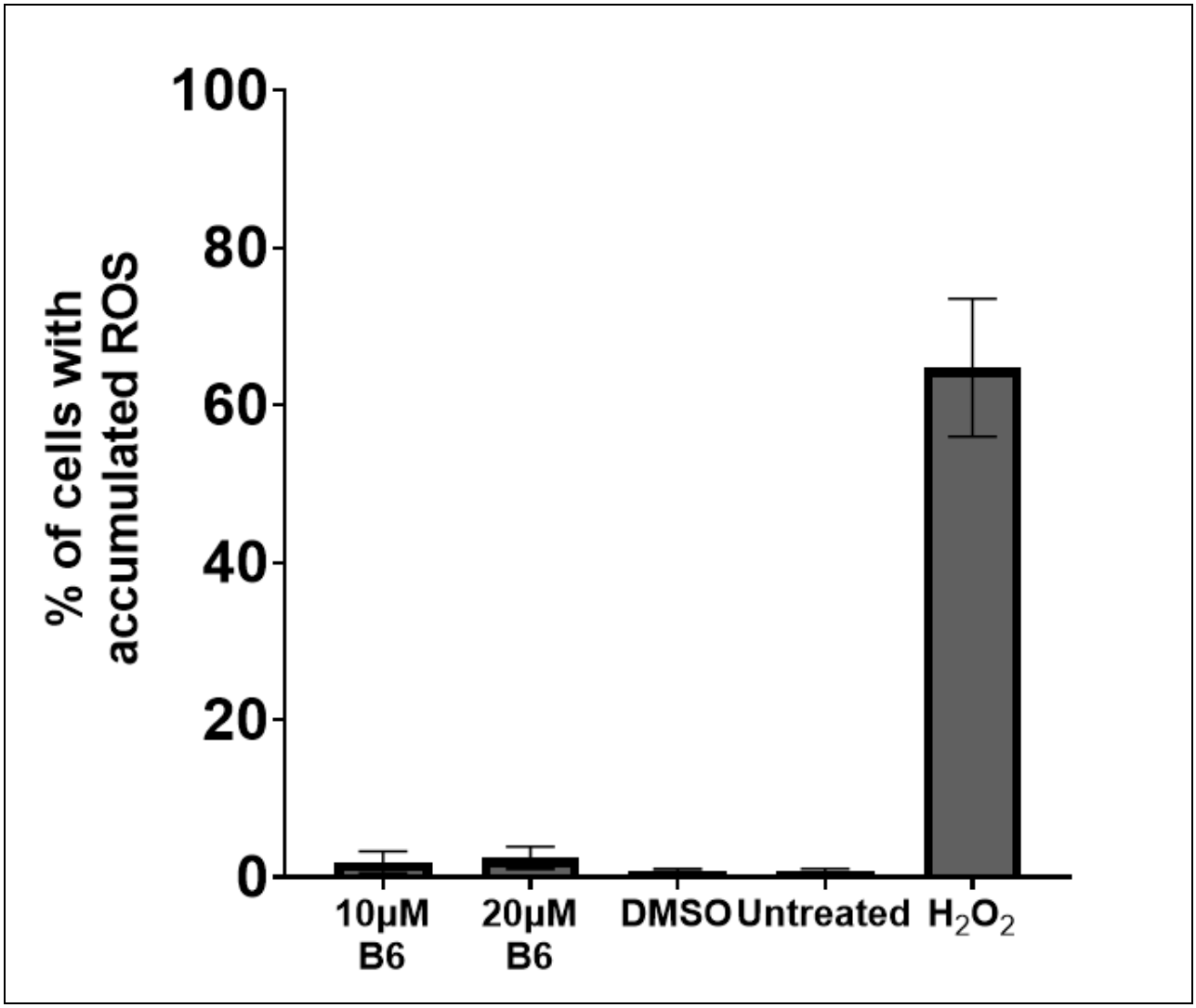

Figure 13. B6 does not overproduce Reactive Oxygen Species. Treatment with B6 at a concentration of 10 μM and 20 μM did not overproduce reactive oxygen species as measured by flow cytometry using the dye H_2DCFDA. Comparison to the DMSO did not produce a significant difference. Cells treated with H_2O_2 at a concentration of 1 mM

produced ROS at higher percentages.

3.7 B6 Alters the Progression of the MDA-MB-231 Cell Cycle and Arrests Cells in S and G2/M Phases

To assess the cell cycle MDA-MB-231 cells were seeded in 24-well plates at a density of $1X10^5$ cells per 1 ml of media. Plates were left overnight under cell culture conditions. After, cells were treated for 72 h with B6, etoposide as a positive control, DMSO as a vehicle control and untreated cells as a negative control. After incubation time, media was collected in 5 ml flow cytometry tubes, 200 µL of 1X trypsin was added to each well, and plates were put back to cell culture conditions to detach the cells. Following the detachment of the cells, 200 µL of complete media was added to each well. Then, cells were collected and centrifuged at 1200 rpm for 5 minutes at room temperature, followed by the removal of the supernatant. Next, a mixture containing 200 µL NIM-DAPI and 200 µL of PBS was added to each tube to resuspend. Samples were read via flow cytometry for this analysis. In this experiment, we decided to use half (5 µM), a quarter (2.5 µM), and an eighth (1.25 µM) of the CC_{50} value of B6 in MDA-MB-231 cells at 24 h (**Figure 14**). B6 at 1.25 µM, 2.5 µM, and 5 µM, caused DNA fragmentation in 9.22%, 5.5%, and 5.9% of the cells, respectively (**Figure 14a**). The positive control, etoposide in 28.6% of the cells. In contrast, DMSO at 0.1% in 0.41% of the cell population (**Figure 14a**). We found a statistically significant difference between both, the concentrations of B6 and the vehicle (DMSO), which indicates that B6 causes the fragmentation of the DNA in MDA-MB-231 cells (**Figure 14a**). The purpose of the experiment was to find in which phase of the cell cycle the compound B6 arrests the cells, however, we did not see higher percentages of cells being in the G0/G1 phase after treatment with B6, thus, we decided

not to compare the values of that specific phase (**Figure 14b**). Nonetheless, we found that the other two phases were being affected by the B6 compound (**Figure 14c-d**). Treatment with B6 at 1.25 µM, 2.5 µM, and 5 µM, produced 19.8%, 15.34%, and 24.6% of the cells to remain in the S phase (**Figure 14c**). Etoposide is a compound that has been shown to arrest the cell cycle in the S phase[87], therefore, we expected it to produce higher percentages than the DMSO and untreated controls. In fact, 21.8% of the cells were in the S phase after treatment with etoposide (**Figure 14c**). As anticipated, fewer cells were in the S phase after treatment with DMSO (10.2%) and without treatment (10.3%) (**Figure 14c**). These data reveal that B6 produces an arrest in the S phase in a similar manner as etoposide. In addition to the S phase, the percentages of cells treated with B6 were higher than those of the controls in the G2/M phase. **Figure 14d** displays the percentage of cells that correspond to the G2/M phase. 53.25%, 71.5%, and 66.47% of cells were in the G2/M phase after treatment with 1.25 µM, 2.5 µM, and 5 µM of B6, respectively. On the other hand, 29.86% of the cells were in the G2/M phase after being treated with 0.1% of DMSO, and 15.4% of the cells with etoposide. Also, 28.78% of untreated cells were in the G2/M phase. These results led to the conclusion that B6 arrests the cell cycle in the S phase and the G2/M phase, showing higher percentages in the G2/M phase, suggesting that B6 favorably arrests the cell cycle in the G2/M phase. During this phase, the mitotic complex and the mitotic spindle are formed[88]. Therefore, the B6 compound could be interfering with one of these events.

a

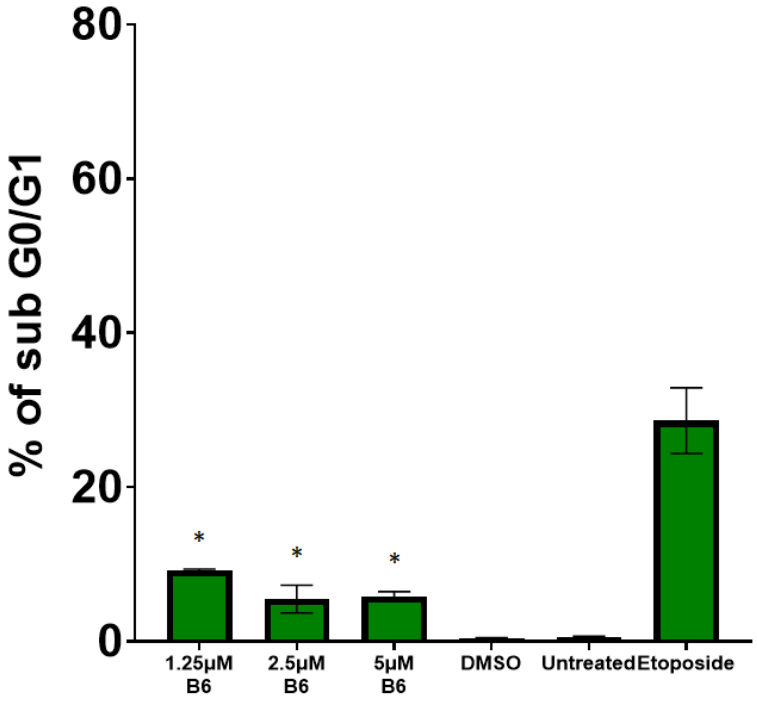
% of sub G0/G1
80
60
40
20
0
*
*
*
1.25μM B6
2.5μM B6
5μM B6
DMSO
Untreated
Etoposide

b

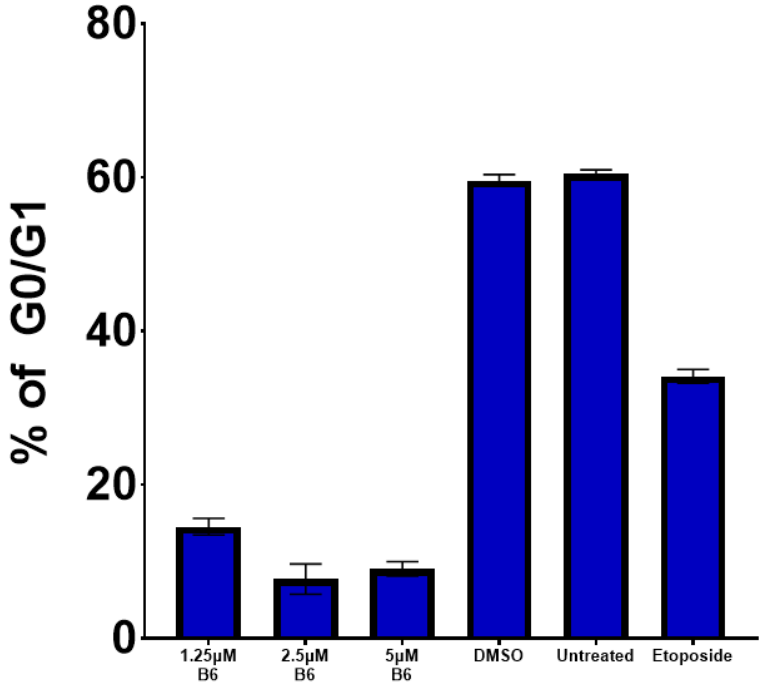
% of G0/G1
80
60
40
20
0
1.25μM B6
2.5μM B6
5μM B6
DMSO
Untreated
Etoposide

c

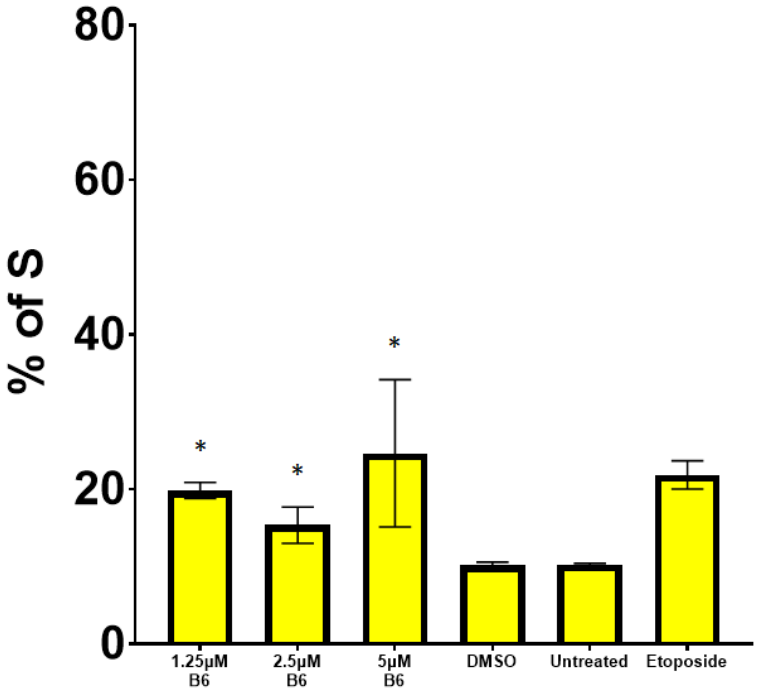
80
60
40
20
0
% of S
*
*
*
1.25μM B6
2.5μM B6
5μM B6
DMSO
Untreated
Etoposide

d

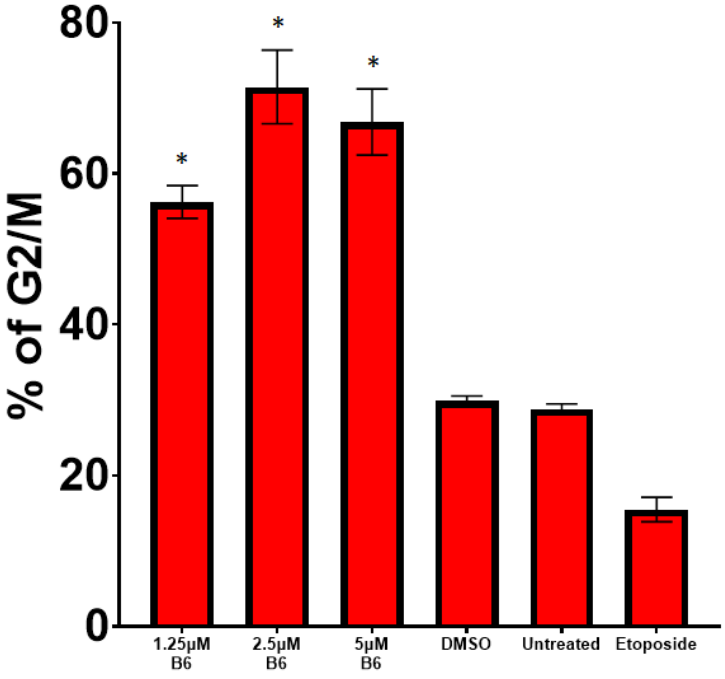
80
60
40
20
0
% of G2/M
*
*
*
1.25μM B6
2.5μM B6
5μM B6
DMSO
Untreated
Etoposide

Figure 14. B6 alters the MDA-MB-231 cell cycle by arresting cells in S and G2/M phases. Exposure of MDA-MB-231 cells to B6 for 72 h causes the alteration of the cell cycle. **(a)** B6 at 1.25 µM, 2.5 µM, and 5 µM significantly causes the fragmentation of the DNA as measured by hypodiploid cells that are present in the sub G0/G1 phase, this corroborates apoptosis as the cell death mechanism. **(b)** B6 treatment did not arrest cells in the G0/G1 phase, however, there are fewer cells in this phase after treatment with the three concentrations of B6. MDA-MB-231 cells exposed to B6 at the aforementioned concentrations significantly arrest the cells in the S phase **(c)** and the G2/M phase **(d)** nonetheless, the effect is more notorious in the G2/M phase. These results suggest that B6 could act at that specific phase. * Means *p*-value is ≤ 0.029368 compared to DMSO.

3.8 Evaluation of the Transcriptome Profile After Treatment with B6

The identification of potential drug targets is crucial in drug discovery. The transcriptome is defined as the collection of the total RNA molecules in a cell or a cell population[89,90]. RNA sequencing has been widely used in drug research[89]. As a matter of fact, our laboratory has previously used this approach to identify the target of chemical compounds[80,81,91]. Therefore, we decided to analyze the transcriptome profile of B6-treated cells to identify the compound's potential target. Two separate transcriptome analyses were to be accomplished, one at each time point indicated (6 h or 24 h) to see the effects of compound treatment at a short and a longer period. The analysis of the transcriptome was accomplished by seeding $1X10^6$ MDA-MD-231 cells at a volume of 5 ml in T-25 flasks. After seeding, T-25 flasks were left under cell culture conditions overnight. The next day, cells were treated for 6 h or 24 h with 0.1% of DMSO and 20 µM of the B6 compound and were put back into cell culture conditions. After incubation, media

was collected in 15 ml conical tubes, and cells were detached by adding 1 ml of 1X trypsin to each flask, and they were put back into incubation. Then, 1 ml of complete media was added to each flask, and cells were collected to their respective tubes followed by centrifugation at 1200 rpm for 5 minutes and the supernatant was discarded. Next, cells were washed with 1ml of warm PBS to remove leftover media and centrifuged under the abovementioned conditions. PBS was discarded. The extraction of RNA was done by using the RNeasy Mini Kit (Qiagen; Germantown, MD, USA; 74104) and following the manufacturer's RNA isolation instructions. RNA quantity and purity were measured by a NanoDrop spectrophotometer (Thermo Fisher; ND-ONE-W). From here, we followed the protocol as previously reported[80]. We considered samples with a purity of A260/A280 ratio between 1.8 and 2.1 for RNA-sequencing. The concentrations of the RNA were quantified using RNA BR Assay Kit for Qubit 3.0 (Invitrogen; Q10210) and integrity (RINe > 7.0) with RNA Screen Tape (Agilent; Santa Clara, CA, USA; 5067-5576) in a 2200 TapeStation (Agilent; G2964AA). To convert the RNA into cDNA, the TruSeq Stranded mRNA library prep kit (Illumina, San Diego, CA, USA; 20020594). After, the cDNA libraries were sequenced using the NextSeq 500 High Output Kit v2.5 (Illumina; I20024907) following the manufacturer's instructions, and the NextSeq 500 system (Illumina). For RNAseq data analysis, the raw reads were trimmed using Trimmomatic (v0.38)[92], aligned, and quantified within RSEM[93] using Bowtie2[94]. Differential analysis was performed using DESeq2[95]. A list of significant genes was extracted using a p-adjusted cutoff of less than 0.05 and fold change greater than 2. B6-treated MDA-MB-231 cells revealed a total of 116 genes that were significantly up-regulated whereas 87 genes were down-regulated after 6 h of treatment. In addition, 24 h of exposure to the B6

displayed a significant up-regulation of 198 and down-regulation of 532. Further analyses revealed differentially expressed genes (DEGs) at both times (**Figure 15**). 61 genes were up-regulated, whereas 47 were down-regulated at both times (**Table 7**). These data suggest that there is a pattern in the transcriptome profile after the time of exposure to the B6 compound.

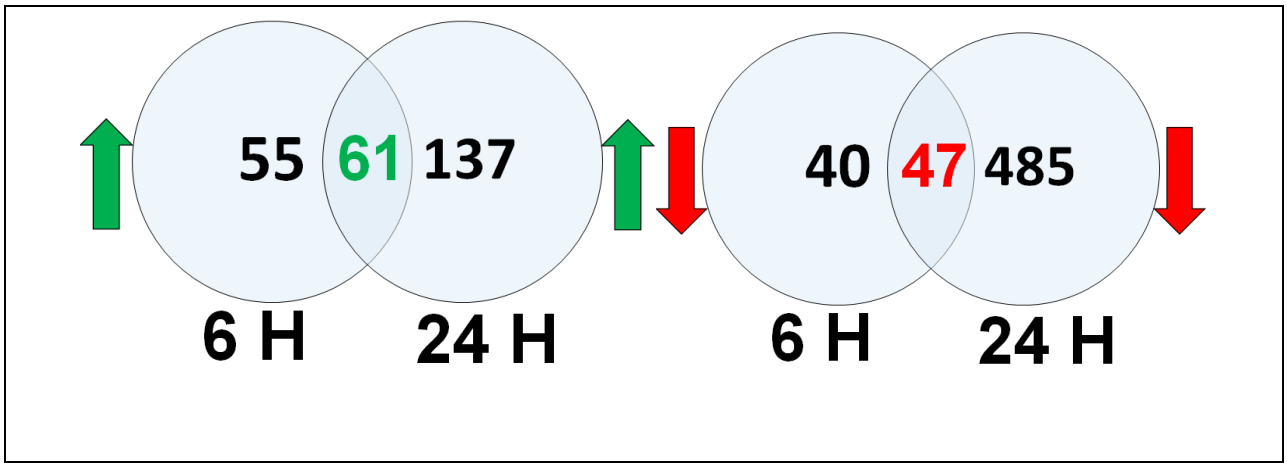

Figure 15. Total of up-regulated and down-regulated genes B6 exposure at 6 and 24 h after. Up-regulated 116 genes and 198 genes after 6 h and 24 h of treatment with B6, respectively. In contrast, B6 down-regulated 87 and 532 genes at 6 and 24 h. 61 genes were up-regulated at both times, whereas 47 were down-regulated.

Table 7. Overlapping differential expressed genes of MDA-MB-231 after treatment with B6 for 6 and 24 h

Up-regulated Genes			Down-regulated genes		
ADAMTS1	IL24	RGMB-AS1	ADAMTS15	ID1	SMAD6
ADAMTS6	ITGB3	S1PR1	ADORA1	ID3	SYT2
AKAP12	KISS1	SEMA7A	APOL3	IFIT1	TMEM37
ALS2CL	KRTAP2-1	SERPINB2	APOL6	IFIT2	TSC22D3
ARHGAP22	KRTAP2-3	SERPINE1	ATF3	IFIT3	VIPR1
C1orf110	LAMA1	SH3BP5L	ATOH8	KLRK1	ZC3H12D
CALD1	LCP1	SH3RF2	BCL3	LINC01085	ZFP36
CD177	LINC00702	SLC20A2	BMF	LOC100506895	
CD274	LINC00704	SMTN	BMP4	LOC284454	
CREB5	LOC152225	SOCS2	CIITA	MAP2K6	
DDR2	NAV3	SPHK1	CMKLR1	METTL7A	
DUSP8	NEDD4L	SPOCD1	CSRNP3	OASL	
ETS1	NLRP3	TAGLN	CX3CL1	OSR2	
FGF1	PDZD2	TMEM171	CXCL10	PARD6B	
FGF5	PLAT	TNFSF15	CXXC4	PCDH18	
FHL2	PLAUR	TRPC4	CYP1B1	PDE4B	
GLIPR1	PLXNA2	UBASH3B	DBP	PDE7B	
HAS2	PROSER2	VCAN	EGR1	PIK3C2B	
HAS2-AS1	PTPRR	ZNF804A	FOS	PLEKHS1	
HBEGF	RELN		FOSB	SLCO4C1	
IL1A	RGMB		GGT3P	SLITRK5	

3.9 B6 Displays a Similar Transcriptome Profile with Tubulin Inhibitors

The connectivity map (CMap) is a resource that facilitates the identification of the mode of action of drugs[96]. CMap works by comparing the expression signatures of a specific perturbagen to a large database that contains the DEGs patterns of several cell lines treated with a wide range of chemical compounds[96,97]. Drugs that interact with the same target usually generate a similar gene expression pattern[98]. Up to now, the CMap has produced a collection comprising more than 1.5M gene expression profiles from around 5,000 compounds tested in several cell types[99]**.** Thus, to identify the potential target of the B6 compound we compared the DEGs of MDA-MB-231 cells treated with B6 to those

in the Connectivity Map (CMap). To compare the gene expression profile from B6 in MDA-MB-231 cells, we uploaded the up-regulated and down-regulated genes that were differentially expressed at both times, 6 and 24 h to the https://clue.io/ webpage. The top 25 compounds based on the median tau score were selected (**Figure 16**). The comparison with the CMap revealed that 13 out of the top 25 compounds were tubulin inhibitors (**Figure 16**). Tubulin inhibitors are a class of compounds that interfere with tubulin. These have become an efficient strategy to develop anti-cancer drugs[100]. In our analysis, we found, vindesine, nocodazole, vincristine, vinorelbine, and vinblastine, (**Figure 16**), compounds that have similar gene expression signatures to B6. Since the comparison of the gene expression profile produced by B6 in MDA-MB-231 is similar to those of tubulin inhibitors, we hypothesized that B6 could behave as a tubulin inhibitor.

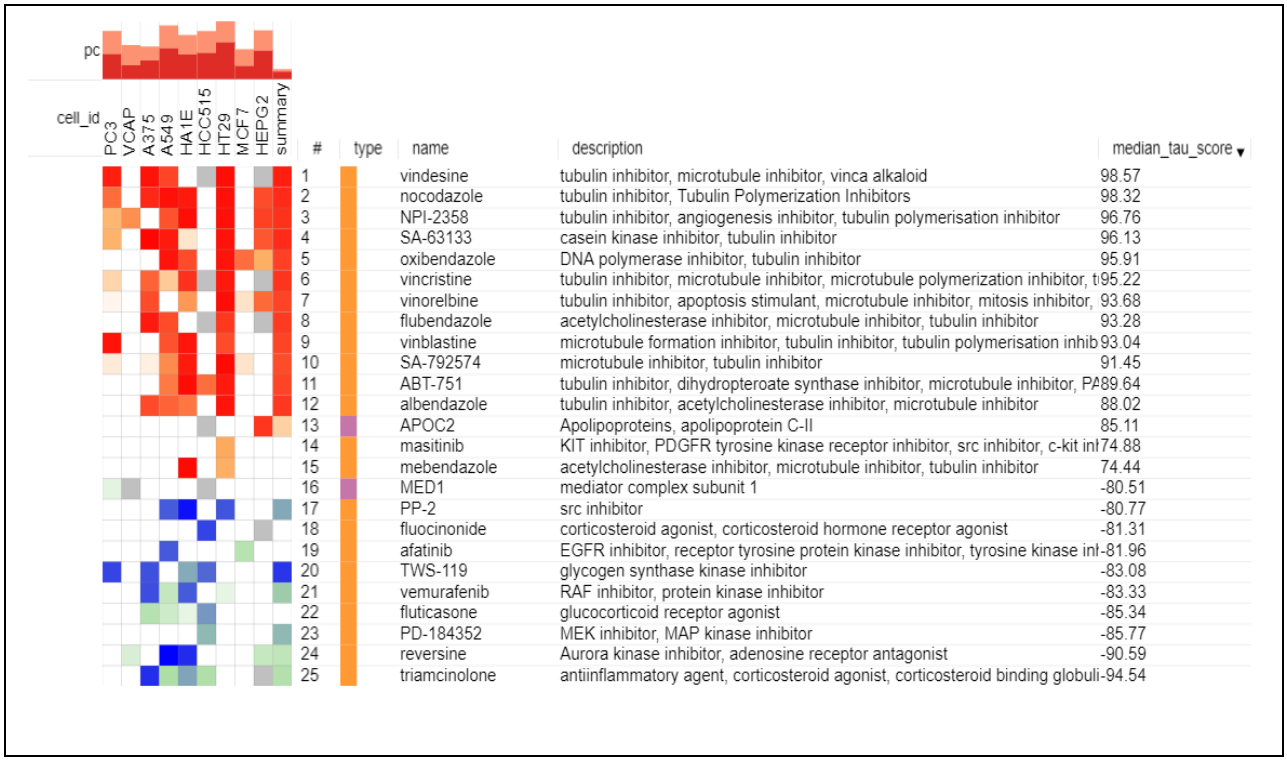

#	type	name	description	median_tau_score
1		vindesine	tubulin inhibitor, microtubule inhibitor, vinca alkaloid	98.57
2		nocodazole	tubulin inhibitor, Tubulin Polymerization Inhibitors	98.32
3		NPI-2358	tubulin inhibitor, angiogenesis inhibitor, tubulin polymerisation inhibitor	96.76
4		SA-63133	casein kinase inhibitor, tubulin inhibitor	96.13
5		oxibendazole	DNA polymerase inhibitor, tubulin inhibitor	95.91
6		vincristine	tubulin inhibitor, microtubule inhibitor, microtubule polymerization inhibitor, t	95.22
7		vinorelbine	tubulin inhibitor, apoptosis stimulant, microtubule inhibitor, mitosis inhibitor,	93.68
8		flubendazole	acetylcholinesterase inhibitor, microtubule inhibitor, tubulin inhibitor	93.28
9		vinblastine	microtubule formation inhibitor, tubulin inhibitor, tubulin polymerisation inhib	93.04
10		SA-792574	microtubule inhibitor, tubulin inhibitor	91.45
11		ABT-751	tubulin inhibitor, dihydropteroate synthase inhibitor, microtubule inhibitor, PA	89.64
12		albendazole	tubulin inhibitor, acetylcholinesterase inhibitor, microtubule inhibitor	88.02
13		APOC2	Apolipoproteins, apolipoprotein C-II	85.11
14		masitinib	KIT inhibitor, PDGFR tyrosine kinase receptor inhibitor, src inhibitor, c-kit inl	74.88
15		mebendazole	acetylcholinesterase inhibitor, microtubule inhibitor, tubulin inhibitor	74.44
16		MED1	mediator complex subunit 1	-80.51
17		PP-2	src inhibitor	-80.77
18		fluocinonide	corticosteroid agonist, corticosteroid hormone receptor agonist	-81.31
19		afatinib	EGFR inhibitor, receptor tyrosine protein kinase inhibitor, tyrosine kinase inl	-81.96
20		TWS-119	glycogen synthase kinase inhibitor	-83.08
21		vemurafenib	RAF inhibitor, protein kinase inhibitor	-83.33
22		fluticasone	glucocorticoid receptor agonist	-85.34
23		PD-184352	MEK inhibitor, MAP kinase inhibitor	-85.77
24		reversine	Aurora kinase inhibitor, adenosine receptor antagonist	-90.59
25		triamcinolone	antiinflammatory agent, corticosteroid agonist, corticosteroid binding globuli	-94.54

Figure 16. B6 CMap comparison revealed a similar transcriptome profile of known tubulin inhibitors. Gene expression profile of overlapping genes MDA-MB-231 cells after treatment with B6 for 6 and 24 h shows that B6 has a gene expression signature similar to tubulin inhibitors. 13 out of the top 25 compounds are tubulin inhibitors, suggesting that B6 could be a tubulin inhibitor.

3.10 In silico Screening Shows an Interaction of B6 with Tubulin

Computational methods like molecular docking and molecular dynamics are routinely used for drug discovery, they provide tools to understand the interaction between proteins and ligands[101]. The purpose of molecular docking and molecular dynamics is to analyze how molecular structures such as a drug and an enzyme fit together[102]. Molecular dynamics simulations can be used to predict the binding affinity of drug-target interactions[103]. Therefore, Molecular dynamics can be used to identify the target of drugs[104]. Due to the prediction of the CMap of B6 as a tubulin inhibitor, we utilized an in silico model to confirm and identify the interaction between B6 and tubulin. We used the Schrödinger software (Schrödinger, LLC, New York, NY, USA) to accomplish molecular docking as previously described[55,78]. For this analysis, we examined compound B6, doxorubicin as a negative control, and 89U as a positive control using the Ligprep interface of the software with OPLS3 at 7± 2 using Epik. Other included options were set as default on the software. The structure of tubulin was obtained from the protein databank (PBD:5XLZ) (https://www.rcsb.org/structure/5XLZ) and was prepared as previously described[105]. Tubulin was crystallized in a complex with 10-[(4-methoxy-3-oxidanyl-phenyl)methylidene]anthracen-9-one, also known as 89U. We docked on the same site where 89U is present. The sitemap tool in the Schrodinger software was used

to define the receptor grid generation. Molecular docking and Molecular mechanics were performed by using the glide tool and the prime tool on Maestro 11.5, respectively. According to the Schrodinger website, a good Glidescore is -10 or lower[106], and since Glidescore and docking scores are similar[107], we considered -10 a good binding score. After docking simulations, the best interactions for each molecule were selected. **Figure 17** shows the interactions of each molecule. As expected, the positive control, 89U, showed a good binding score of -10.9. 89U interacts mostly with hydrophobic residues (**Figure 17b**). Since doxorubicin is a topoisomerase II inhibitor[108], we decided to use it as a negative control. Indeed, doxorubicin showed a score of -1.1, meaning it does not have a good affinity for tubulin. The docking analyses showed that the B6 compound has a docking score of -12.3. Interestingly, B6 showed a better score than the ligand that was used to crystallize tubulin. The docking interaction diagrams show that B6 interacts mainly with hydrophobic amino acid residues: Phe367, Ile316, Ile368, Leu240, Leu316, Leu 246, Leu253, Ala248, Ala314, Ala315, Ala352, Val236, and Cys239. Additionally, B6 creates hydrogen bonds with Thr178, Asn247, and Asp249 (**Figure 17a**). These data revealed that B6 tightly interacts with the tubulin protein in an in silico model, especially some hydrophobic residues.

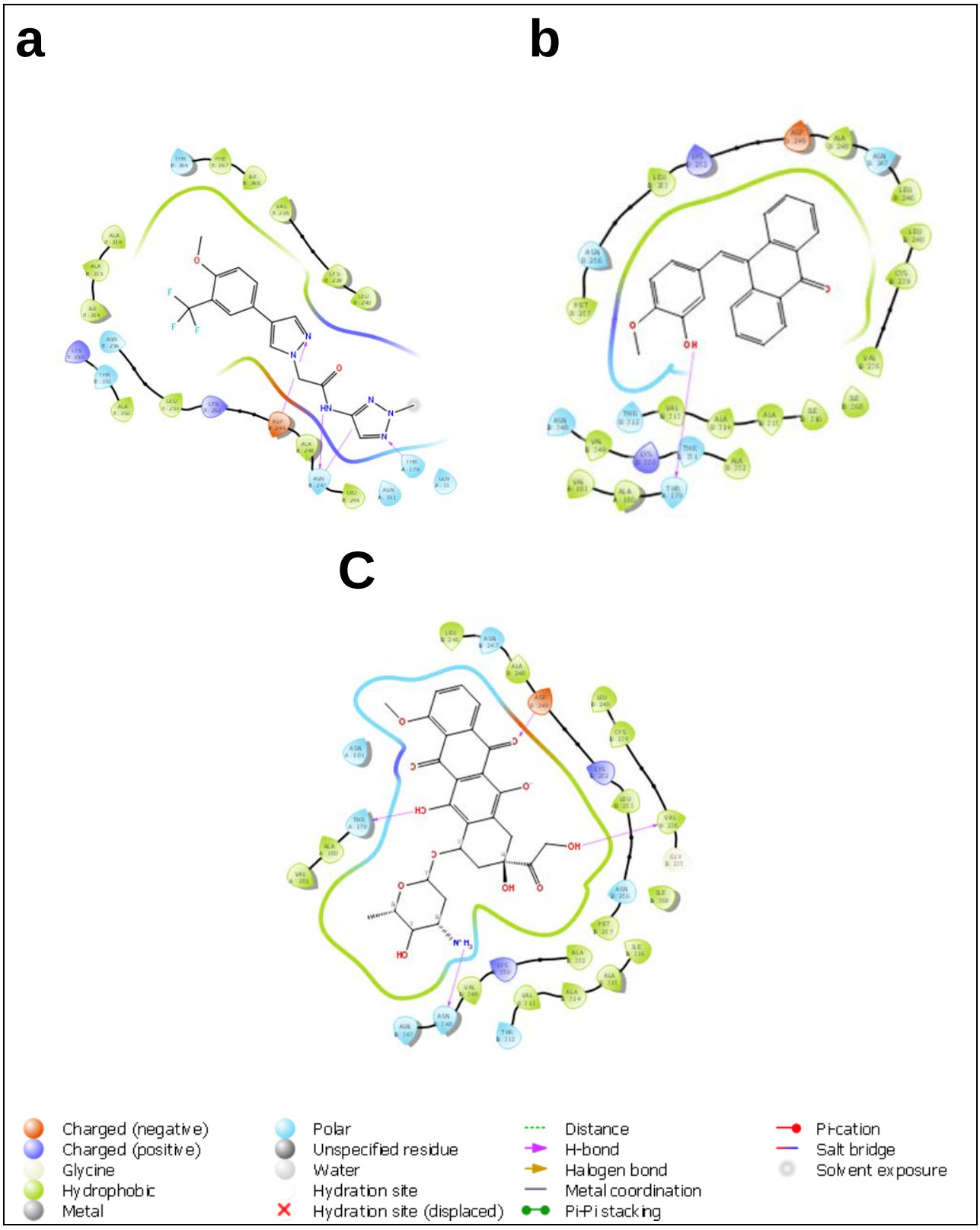
a
b
C
Charged (negative)
Charged (positive)
Glycine
Hydrophobic
Metal
Polar
Unspecified residue
Water
Hydration site
Hydration site (displaced)
Distance
H-bond
Halogen bond
Metal coordination
Pi-Pi stacking
Pi-cation
Salt bridge
Solvent exposure

Figure 17. In silico screening reveals B6 interacts with tubulin. Molecular docking using the Schrödinger software shows that **(a)** B6 interacts with the tubulin with a docking score of -12.345. **(b)** 89U, which is the ligand used to crystallize tubulin protein had a docking score of -10.926, whereas **(c)** the topoisomerase II inhibitor, Doxorubicin, had a score of -1.166. Surprisingly, B6's docking score was better than the ligand used to crystallize the tubulin protein.

3.11 B6 Disturbs Microtubule Organization on MDA-MB-231 cells

To prove our hypothesis of B6 acting as a tubulin inhibitor, we conjectured that the compound could be producing an alteration in the microtubule organization of MDA-MB-231 cells. Indeed, previous research showed that the microtubules are directly disrupted by tubulin inhibitors[109,110]. Disruption of the microtubules can be assessed by taking direct images of the microtubules through fluorescence microscopy[111–113]. Thus, we decided to test our hypothesis by using the same approach and directly taking photographs of the microtubule organization of MDA-MB-231 cells treated with the B6 compound. The experiment was accomplished by seeding $2X10^3$ cells at a volume of 100 µL of media per well in 96-well plates (BD Falcon, 353216) and left overnight under cell culture conditions. The following day, cells were treated for 4 h with 20 µM of B6, Paclitaxel (PTX) at 1 µM as a stabilizer of microtubule polymerization control, DMSO at 1% as solvent control, and untreated cells as a negative control. Cells were then fixed by adding 100 µL of 8% formaldehyde to each well and were incubated for 20 minutes at room temperature. Next, formaldehyde and media were removed and each well was washed three times with 200 µL of a combination of 0.1% Tween 20 detergent in PBS for 10 minutes at room temperature. This allows the removal of any leftover media and formaldehyde and the

permeabilization of cells. After three washes, a blocking solution containing 5% bovine serum albumin in TBS-T (Tris-buffered saline with 0.1% Tween 20) was added to each well, and plates were placed for an incubation time of 1 h on a rocking platform at room temperature. Following incubation, the blocking solution was removed and 50 µL of a mixture containing PBS 0.1% Tween 20, DAPI (5 µg/ml), phalloidin conjugated to Alexa Fluor 568 (0.165 µM), and an anti-tubulin monoclonal antibody conjugated to Alexa Fluor-488 was added to each well to stain the cells. Plates were incubated overnight on a rocking platform at 4°C. After incubation, the mixture was recovered from each well, and cells were washed three times as before. Pictures were captured with a laser scanning confocal microscope (LSM-700, Zeiss) by using an EC Plan-Neofluar 40X/1.30 oil DIC objective and helped by the Zen 2009 6.0 software (Zeiss). Unsurprisingly, the microtubule organization remains unaltered in cells treated with 1% of DMSO and in untreated cells (**Figure 18**). Cells treated with PTX showed that the microtubules were in the periphery of the cells, however, the cytoskeleton pattern disappeared (**Figure 18**). In cells treated with 10 µM of B6, the tubular structure of the microtubules vanished (**Figure 18**). The tubulin in these cells was shapeless (**Figure 18**). In addition, we noticed voids in these pictures (**Figure 18**). Nonetheless, the microfilament structure remained unaltered with all three treatments (**Figure 18**). These images suggest that B6 alter the microtubule organization while producing no damage to the microfilaments, reinforcing our hypothesis of B6 targeting microtubules.

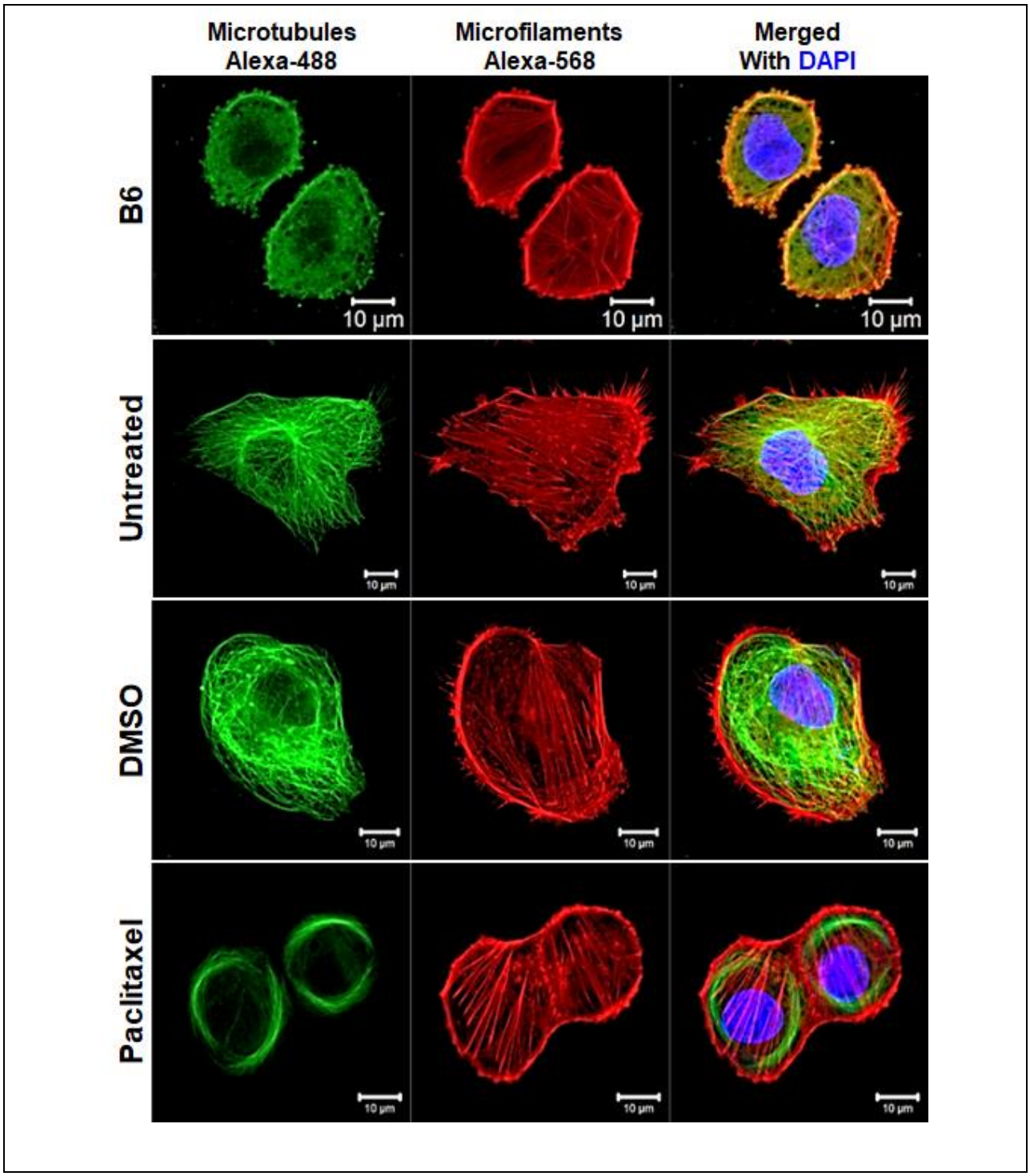

Figure 18. B6 disturbs Microtubule organization on MDA-MB-231 cells. Cells were stained with α-tubulin-Alexa-488 (microtubules), phalloidin-Alexa-568 (microfilaments), and DAPI (nucleus). Exposure of MDA-MB-231 cells to B6 for 4 h disrupts the microtubule

organization. Treatment with 1% of DMSO did not produce the disruption of the tubular structure of the microtubules. In addition, untreated cells keep an intact morphology after 4 h. The tubulin polymerization enhancer, Paclitaxel, disappeared the cytoskeleton morphology of the MDA-MB-231 cells. Interestingly, the effect of B6 was seen just in the microtubules, suggesting that tubulin is the target of B6.

3.12 B6 Inhibits Tubulin Polymerization

Finally, to test the potential activity of B6 as a tubulin polymerization inhibitor, we used a tubulin polymerization Assay Kit (cat. # BK006p) purchased from Cytoskeleton Inc. (Denver, CO). Before running the assay, a general tubulin buffer (GT) containing 80 mM of piperazine-N,N′-bis(2-ethanesulfonic acid) (PIPES), 2 mM of Magnesium Chloride (Mg_2CL), and 0.5 mM or Ethylene glycol-bis(b-amino-ethyl ether) N,N,N', N'- tetra-acetic acid (EGTA), was reconstituted with 10ml of sterile distilled water. Also, GTP was reconstituted with sterile water given a concentration of 100 mM, and 10 mg of lyophilized tubulin protein was reconstituted with 10 µL of GTP at 100 mM and 1.1 ml general tubulin buffer (GT). GTP stocks were kept at -80°C and tubulin was frozen by using liquid nitrogen and was kept at -70°C. Before starting the assay, we pre-warmed the sample plate at 37°C for 30 minutes. Then, the tubulin polymerization buffer (TP) was cold prepared by mixing general tubulin buffer, tubulin glycerol buffer, and GTP at a final concentration of 15% glycerol and 1 mM, respectively. Next, 10 µL of general tubulin Buffer was added to each well. Treatments for the assay included B6 at 10 µM, 0.9% of DMSO as vehicle control, 10 µM of PTX as a tubulin stabilizer, and 3 µM of vinblastine as a positive control. After treatment, tubulin was diluted and mixed with ice-cold TP for a final concentration of 3 mg/ml, then 100 µL of the solution was rapidly added to all wells with the treatments.

Plates were placed in the spectrophotometer at 37°C and read for 1 h, taking reads every minute at a 340 nm wavelength. An automatic mix was done before the first read. **Figure 19** depicts the curves for the vehicle control, a tubulin stabilizer PTX, a tubulin polymerization inhibitor, vinblastine, and the B6 compound. According to some authors, the process of tubulin polymerization occurs in two main steps: nucleation and elongation[114,115]. However, this assay's protocol and separate authors mention three phases in tubulin polymerization occur: nucleation, growth, and steady state[116]. Here we decided to follow the protocol's phases to explain the results. Polymerization of the tubulin protein is directly correlated with absorbance, therefore if polymerization happens, there is an increase in the absorbance at 340 nm. Expectedly, the growth phase of tubulin polymerization after PTX treatment started immediately, before the vehicle control (**Figure 19**). DMSO, vinblastine, and B6 had a growth phase starting after 4 minutes, which means that the nucleation phase lasted 4 minutes. However, DMSO reached its steady state after 14 minutes with an absorbance of 0.3662. In contrast, the steady state of B6 was reached after 20 minutes. After 60 minutes of treatment, DMSO and B6 had significantly different absorbance values of 0.3702 and 0.3247, respectively (**Figure 19**). Interestingly, the B6 compound produced a similar curve to the well-known tubulin inhibitor vinblastine (**Figure 19**). The curve for both compounds never reached the absorbance values of the vehicle control. Therefore, these data reveal that B6 is a tubulin polymerization inhibitor.

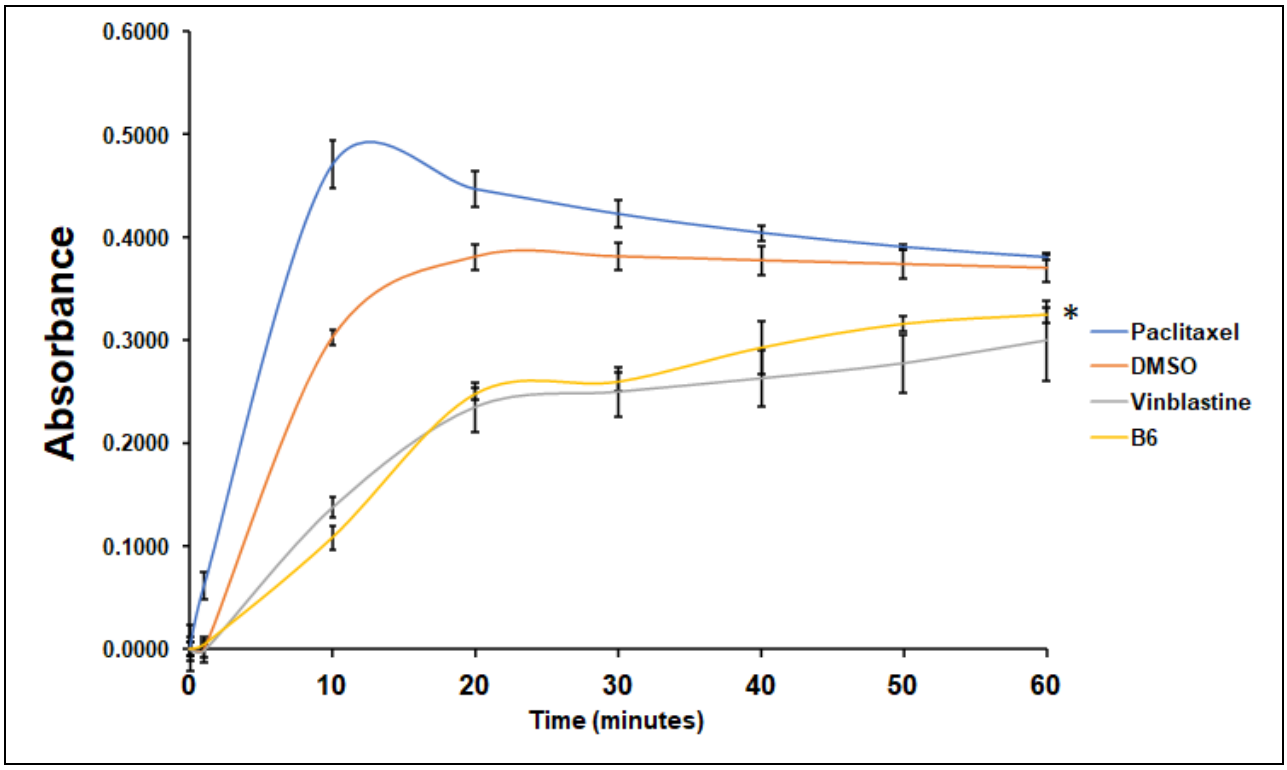

Figure 19. B6 inhibits tubulin polymerization. Curves of four different treatments for tubulin polymerization. Absorbance is directly correlated with tubulin polymerization. As expected PTX enhanced the polymerization of tubulin. B6 produced less tubulin polymerization in comparison to the vehicle DMSO. Indeed, B6 and the well-known tubulin polymerization inhibitor, vinblastine, have similar curves. These results corroborate that B6 is a tubulin polymerization inhibitor. To compare B6 and DMSO, three replicates were used for each reading every 10 minutes. * Represents the comparison between the DMSO and the B6 at each time (10 minutes) * ≤ 0.000144.

3.13 Developing an *in vivo* Model to Test Drugs with Anti-cancer Activity

After the identification of a chemical compound with activity against cancer *in vitro*, the next step in preclinical research is *in vivo* experiments[117]. Preclinical research studies are very important because they provide sufficient information about the toxicity and dosage of any compound. *In vivo* studies can be performed in rodent and nonrodent mammalian models to define different aspects of the compound's behavior such as the pharmacokinetic profile, general safety, and toxicity patterns[118]. Therefore, we decided to develop an *in vivo* model using mice to grow tumors and test the potency and toxicity of our compound. To do this, we acquired J:NU homozygous for Fox1 (nu) mice, also known as nude mice from Jackson Laboratories. A xenograft model of the metastatic cell line LM2-4, which is derived from the MDA-MB-231 breast cancer cell line, containing a luciferase activity reporter[119] was generated. **Figure 20** depicts the general procedure that was used to grow the tumors in nude mice. First, cells were grown *in vitro* by using DMEM media supplemented with 10% FBS, 100 U/ml of penicillin, and 100 µg/ml of streptomycin, at 37°C in a humidified environment with 5% CO_2. Cells were detached with 1X trypsin and collected in 15 ml conical tubes, then centrifuged for 5 minutes at 1200 rpm. The supernatant was removed and cells were washed twice with PBS. The tubes were placed on ice until injection. The mice were handled under a biosafety cabinet level 2 to maintain aseptic conditions. Before the injection, we anesthetized each mouse with Isoflurane and oxygen. Then, the left flank of each mouse was cleaned with ethanol followed by an injection of 200 µL of PBS with $2X10^6$ cells. Mice were woken up and monitored for any abnormal behavior. All mice were treated ethically according to IACUC's recommendation. We monitored tumor growth by visual inspection and by

palpation of the injected zone every day. When the first tumors were noticeable, we measured them with a caliper. To determine the size of the tumor, we used the formula Length x width x width = tumor volume (mm^3).

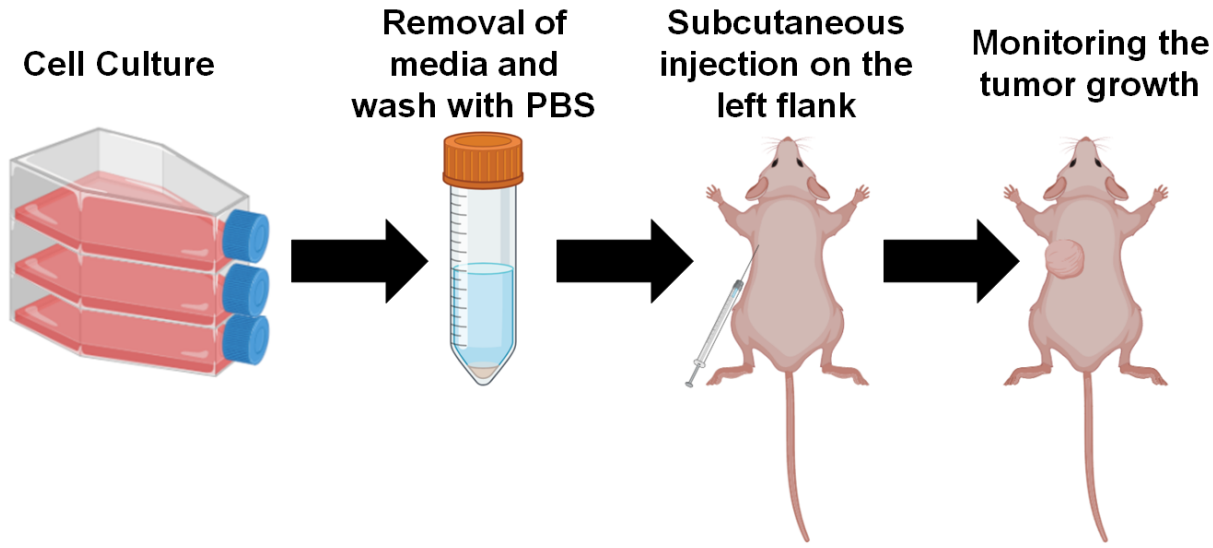

Figure 20. General procedure to grow tumors in Nude mice. Followed strategy to create an *in vivo* model to test novel compounds with anti-cancer activity. Cells were cultured under general cell culture conditions; they were detached and media was removed. After washing with fresh PBS, cells were quantified and resuspended at a density of $2X10^6$ cells per 200 µL of PBS. Mice were anesthetized to be injected with the tumor cells. Once injected, mice were monitored every day, by visual inspection and palpation of the injected zone. This figure was created with Biorender.com.

Two weeks after the injection of the cells, we observed the first tumors in the mice. **Figure 21a** shows a mouse with a tumor of around $50mm^3$. Tumors reached the desired volume of 100 mm^3 within one month. When tumors reached 100 mm^3, we randomized the mice and used them to test the B6 compound. The goal of the experiment was to measure if the size of the tumors decreases after treatment with the B6 compound in comparison

with the solvent. Moreover, we wanted to see if the compound was toxic to the mice. We weighed the mice with a balance to determine if there was a weight decrease after compound treatment. In addition, we also monitored the metastasis of cells in other parts of the body. To accomplish this, we used luciferin at a concentration of 15 mg/ml and placed the mice inside the *In vivo* imaging system (IVIS). This allowed us to monitor the luciferase activity of the LM2-4 Luc cells and determine if there was metastasis (**Figure 21b**).

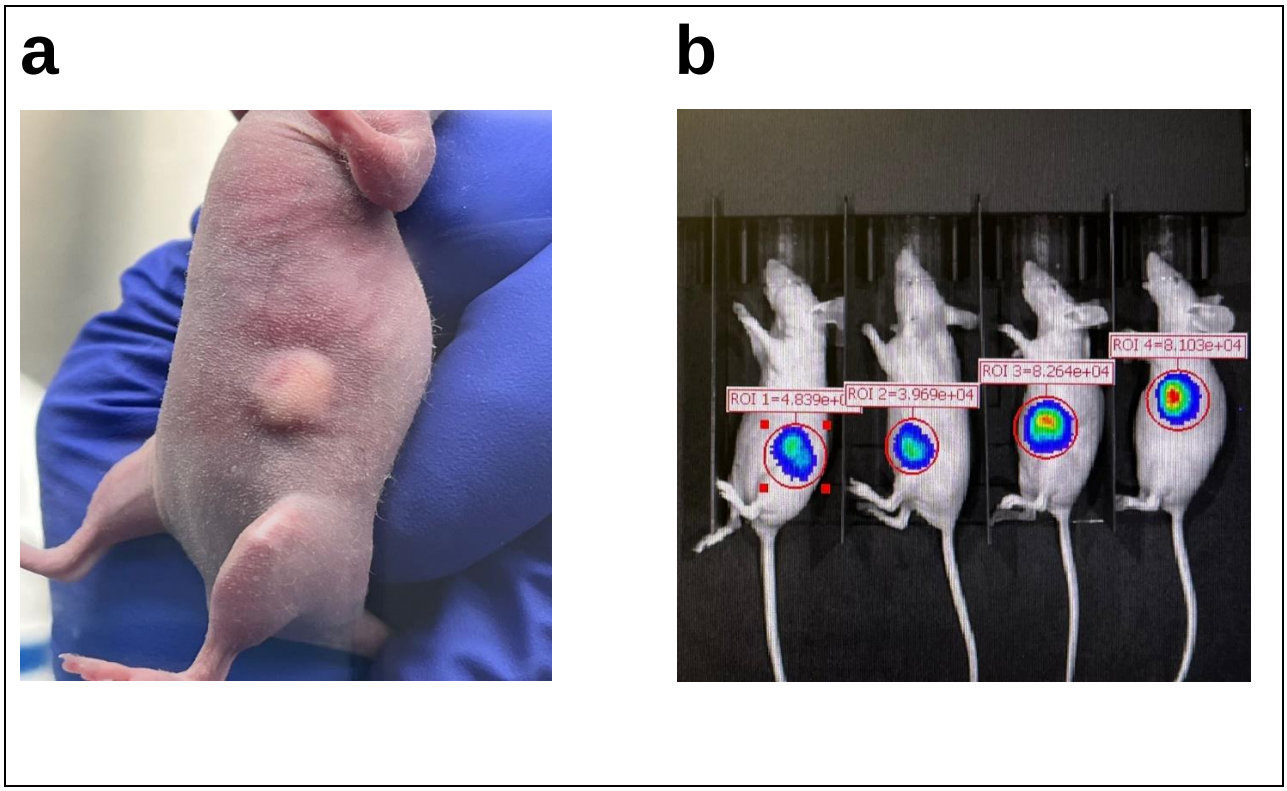

Figure 21. Nude mice displaying subcutaneous tumors derived from metastatic cell line LM2-4. (a) a mouse with a tumor of ~50mm^3 after 2 weeks of injection. **(b)** four mice were injected with 15 mg/ml of luciferin to monitor the tumor growth, regions of interest for each mouse are visible. Pictures were taken using the IVIS system.

The mice developed the desired size tumor of 100 mm^3 within a month, therefore, we proceeded to test the B6 compound. To test the compound in mice we decided to try using different solvents. It was decided not to use DMSO because DMSO at a concentration higher than 25% is harmful to the mice[120]. We attempted to use PBS but the compound failed to dissolve. We tried PBS/PEG-400 solution at different concentrations but the compound came out of solution as the concentration of PBS increased. Finally, through a literature review, we found that another compound with poor aqueous solubility, PTX, is dissolved in a mixture consisting of 50% of Cremophor EL® (a polyoxyethylated castor oil) and 50% ethanol[121,122]**.** Since PTX is FDA-approved, we decided to use the formulation to deliver this compound. We deliver the compound at a concentration of 25 mg/kg through an intraperitoneal route. Unfortunately, we were forced to end the study early due to endpoint criteria established at the beginning. We were therefore unable to get data about the reduction of the tumor size. Although the study was not carried out to completion, we established a model to test novel compounds with anti-cancer activity within our laboratory. We hope this model helps our lab to test novel compounds that are discovered.

3.14 Discussion

Cancer is still a deadly disease if untreated. Chemotherapy remains the standard cancer treatment, however, many chemical compounds produce resistance to themselves in cancer patients. Moreover, indiscriminately killing cells by chemotherapeutic agents is produced by currently used drugs. Therefore, there is an urgent need for new molecules with anti-cancer properties[24]. In this study, we analyzed more than 5000 compounds from the chemical library ChemBridge DIVERset to identify a hit compound. A novel compound, B6, was tested on a panel of different cell lines, encompassing cancer and non-cancerous cell lines. Hematological cancer cells were treated for 48 h, whereas cells derived from solid tumors were for 72 h (**Table 6**). The B6 compound showed potent activity at both times and for all cancer cells. In addition, the less sensitive cells were two non-cancerous cells which indicate the selectivity of B6 towards cancer cells and not non-cancerous cells (**Table 6**). Even though the cell line MDA-MB-231 was less sensitive than other cell lines, we decided to use it as our model cell line to characterize this compound based on our experience characterizing novel compounds using this cell line[80,81]. Previously characterized compounds containing a pyrazole moiety have been shown to induce apoptosis[82–84], therefore we analyzed the ability of the B6 compound to induce apoptosis. The B6 compound induced the externalization of the phospholipid phosphatidylserine (PS) from the inner part of the cell membrane to the exterior (**Figure 10**). This event is one of the hallmarks of apoptosis and serves as an eat-me signal to remove apoptotic cells by phagocytes[44,46]. We corroborate apoptosis as the cell death mechanism by analyzing the activation of caspase 3. There were significantly more cells with caspase 3 active after treatment with the B6 (**Figure 11**). These results corroborate

that the B6 compound induces apoptosis as the main cell death mechanism. The induction of apoptosis by small compounds is nearly preferred to the induction of necrosis because cells are eliminated through an order process[123]. Necrotic cells trigger the activation of the immune system which leads to the damage of surrounding tissue[123]. Since apoptosis is documented to occur through extrinsic signals (extrinsic pathway) and intrinsic signals (intrinsic pathway)[52], we sought to discover which one was exerted by the B6 compound. Mitochondrial membrane depolarization is characteristic of the intrinsic pathway[53]; however, the B6 compound did not cause this effect in MDA-MB-231 cells (**Figure 12**). ROS, primarily produced by the mitochondria were not produced after treatment with the B6 compound (**Figure 13**). These results suggest that B6 did not induce the intrinsic pathway. Therefore, at this point, we do not know which apoptotic pathway is being induced. However, the evidence shows that apoptosis is the cell death mechanism being exerted by B6. Furthermore, we were able to further corroborate apoptosis by analyzing the cell cycle. The higher percentages of cells in the sub G0/G1 (hypodiploid) phase of the cell cycle show that B6 causes the fragmentation of the DNA (**Figure 14a**), which is a hallmark of apoptosis. This analysis also showed that B6 arrests the cell cycle in the S and G2/M phases (**Figure 14c and 14d**), however, we saw higher percentages of cells in the G2/M phase (**Figure 14d**). Compounds with the same target have a similar gene expression signature[98], thus, to identify the mode of action of B6 we performed transcriptome analyses of cells treated with the B6 compound to identify DEGs. MDA-MB-231 cells that were treated with B6 at 6 and 24 h showed an up-regulation of 116 and 198 genes, respectively. On the other hand, there were 87 and 532 down-regulated genes at 6 and 24 h. Further analyses showed that 61 and 47 genes

were up-regulated and down-regulated at both times (**Figure 15**), meaning that the expression followed a pattern. The Connectivity Map (CMap) is a collection of gene profiles of cells that were treated with compounds whose target has been identified[96,97]. For this reason, we submitted the list of up-regulated and down-regulated genes that were present at both times of B6 treatment. The results revealed that B6 has a gene expression signature similar to tubulin inhibitors (**Figure 16**). Moreover, molecular docking by using tubulin protein on Schrödinger software showed that B6 has a docking score of -12.345 a better score than 89U (-10.926) which is the molecule that was used to crystallize tubulin. In addition, molecular mechanics revealed B6 mostly interacts with hydrophobic amino acid residues (**Figure 17a**). These results predicted that B6 is a tubulin inhibitor, therefore, we decided to perform proof-of-concept experiments in a wet lab setting. Previous data with tubulin inhibitors showed them to disrupt the tubular structure of the microtubules[109,110]. We analyzed the microtubule structure by using fluorescent microscopy. Cells treated with the B6 compound displayed a different structural pattern of the microtubules compared to those treated with DMSO or untreated cells (**Figure 18**). The tubular structure completely disappeared after 4 h of treatment with B6 (**Figure 18**). In addition, we also noticed voids in the pictures of cells that were exposed to B6 (**Figure 18**). These data show that B6 disrupts the microtubule structure. Finally, to corroborate the B6 as a tubulin inhibitor, we performed a tubulin polymerization inhibition assay. This assay uses absorbance to test the polymerization of tubulin. Absorbance is directly correlated to tubulin polymerization. The assay revealed that B6 inhibits the polymerization of the tubulin, there was a noticeable difference when compared with the vehicle control DMSO (**Figure 19**). B6's curves were lower than DMSO's. Interestingly,

B6 produced a curve similar to that of the well-known tubulin polymerization inhibitor, vinblastine (**Figure 19**). These data reveal that B6 inhibits tubulin polymerization. Microtubules are essential for the segregation of the chromosomes during mitosis[124], which correlates with tubulin inhibitors arresting the cell cycle in the G2/M phase[125,126]. Cancer cells have an altered cell cycle, they divide faster, hence, compounds that stop cell division are considered important anti-cancer agents. The B6 compound arrested the cell cycle preferentially in The G2/M phase. Preclinical trials include *in vivo* testing; therefore, we developed an *in vivo* model to test our compound (**Figure 20**). In this model, we formed tumors by injecting LM2-4 with luciferase activity cells in nude mice. After 2 weeks we observed tumors in the mice (**Figure 21a**). In addition, this model was created to test metastasis inhibition after B6 compound treatment (**Figure 21b**). However, the study to determine the effects of compound treatment on tumor growth could not be completed due to end study criteria. Nonetheless, we consider we have identified a good compound to be used in anti-cancer research. For future research we consider modification of the actual chemical structure 1) to have better solubility and 2) to be less toxic in an *in vivo* model. We do hope this novel compound can be used as an additional weapon in the cancer fight.

Limitations and Future Directions

Before a drug can go to the clinical phase, limited damage to humans has to be proven[117]. Therefore, conducting preclinical research in both *in vitro* and *in vivo* models is crucial in drug development[117]. Our work with the five novel presented compounds showed these to have potent cytotoxicity on a panel of different cell lines. In addition, they showed to be preferentially selective towards cancer cells and not non-cancerous cells. The results presented in this project, are the initial steps that will require further investigation to get a better insight into the characteristics of the compounds. For the four novel piperidones, we managed to reveal that polyubiquitinated proteins were accumulated after exposure to the leukemia cells. In addition, HMOX-1 was overproduced. These are traits of well-known proteasome inhibitors. However, we did not measure the proteasome activity directly, thus, a proteasome inhibition assay would be essential to conclude these are proteasome inhibitors. Another way to prove that these four novel compounds interact with the proteasome is by using surface plasmon resonance[127]. Our *in vivo* experiments showed that to test a compound a good solvent is needed. Similar compounds have been proven to be soluble in Polyethylene glycol 400 and PBS (PEG/PBS)[128]. In addition, these compounds were found to improve the survival of mice in a pilot experiment. Therefore, we consider the four novel compounds to be studied in the next step of the preclinical trial, *in vivo* studies.

B6 was proven to inhibit tubulin polymerization. Tubulin inhibitors are gaining special attention in cancer research for their ability to prevent mitosis. The compound B6 showed promising results as was shown by the lower CC_{50} values on several cancer cells. However, we could not dissolve the compound in a saline solution as PBS, this shows

that B6 has poor solubility. *In vivo* analyses showed that mice treated with 25 mg/kg of B6 seemed to have health problems. We decided to stop the pilot experiment; therefore, we could not get good results. For future work with this compound, we propose both 1) to find a good solvent and 2) to add additional groups to the drug to create more soluble analogs of the compound. The molecular docking results can be used as a reference, in this way, we can potentially know which groups are essential for B6's activity. The creation of novel molecules using B6 as bases will need another complete evaluation of their cytotoxic activity, nonetheless, having described a molecule with a known target will make this process faster.

References

1. Cancer - Symptoms and causes - Mayo Clinic. https://www.mayoclinic.org/diseases-conditions/cancer/symptoms-causes/syc-20370588.

2. What Is Cancer? - National Cancer Institute. https://www.cancer.gov/about-cancer/understanding/what-is-cancer.

3. Hanahan, D. & Weinberg, R. A. Leading Edge Review Hallmarks of Cancer: The Next Generation. (2011) doi:10.1016/j.cell.2011.02.013.

4. Hanahan, D. & Weinberg, R. A. Hallmarks of cancer: The next generation. *Cell* **144**, 646–674 (2011).

5. Loeb, K. R. & Loeb, L. A. *Significance of multiple mutations in cancer*. *Carcinogenesis* vol. 21 (2000).

6. Hanahan, D. Hallmarks of Cancer: New DimensionsHallmarks of Cancer: New Dimensions. *Cancer Discov.* **12**, 31–46 (2022).

7. Anand, P. *et al.* Expert Review Cancer is a Preventable Disease that Requires Major Lifestyle Changes. doi:10.1007/s11095-008-9661-9.

8. Irigaray, P. *et al.* Lifestyle-related factors and environmental agents causing cancer: An overview. *Biomed. Pharmacother.* **61**, 640–658 (2007).

9. Debela, D. T. *et al.* New approaches and procedures for cancer treatment: Current perspectives. *SAGE Open Med.* **9**, 205031212110343 (2021).

10. Sung, H. *et al.* Global Cancer Statistics 2020: GLOBOCAN Estimates of Incidence and Mortality Worldwide for 36 Cancers in 185 Countries. *CA. Cancer J. Clin.* **71**, 209–249 (2021).

11. Cancer. https://www.who.int/news-room/fact-sheets/detail/cancer.

12. Siegel, R. L., Miller, K. D., Fuchs, H. E. & Jemal, A. Cancer statistics, 2022. *CA. Cancer J. Clin.* **72**, 7–33 (2022).

13. Mariotto, A. B., Robin Yabroff, K., Shao, Y., Feuer, E. J. & Brown, M. L. Projections of the cost of cancer care in the United States: 2010-2020. *J. Natl. Cancer Inst.* **103**, 117–128 (2011).

14. Mariotto, A. B., Enewold, L., Zhao, J., Zeruto, C. A. & Yabroff, K. R. CANCER EPIDEMIOLOGY, BIOMARKERS & PREVENTION | Medical Care Costs Associated with Cancer Survivorship in the United States. doi:10.1158/1055-9965.EPI-19-1534.

15. Liu, B. *et al.* Protecting the normal in order to better kill the cancer. *Cancer Medicine* vol. 4 1394–1403 (2015).

16. Billings, J. A. Clinical review Recent advances. *BMJ* **321**, 555–558 (2000).

17. Schirrmacher, V. From chemotherapy to biological therapy: A review of novel concepts to reduce the side effects of systemic cancer treatment (Review). *Int. J. Oncol.* **54**, 407–419 (2019).

18. Huang, C.-Y. *et al.* A review on the effects of current chemotherapy drugs and natural agents in treating non-small cell lung cancer. *Article* **7**, 12–23 (2017).

19. National Cancer Institute. Radiation Therapy for Cancer - NCI. *Radiation Therapy to Treat Cancer was originally published by the National Cancer Institute* https://www.cancer.gov/about-cancer/treatment/types/radiation-therapy (2019).

20. Chen, H. H. W. & Kuo, M. T. *Improving radiotherapy in cancer treatment: Promises and challenges*. www.impactjournals.com/oncotarget (2017).

21. Abbott, M. & Ustoyev, Y. Cancer and the Immune System: The History and Background of Immunotherapy. *Seminars in Oncology Nursing* vol. 35 150923 (2019).

22. Koury, J. *et al.* Immunotherapies: Exploiting the immune system for cancer treatment. *Journal of Immunology Research* vol. 2018 (2018).

23. How does chemotherapy work? - InformedHealth.org - NCBI Bookshelf. *Institute for Quality and Efficiency in Health Care* https://www.ncbi.nlm.nih.gov/books/NBK279427/ (2022).

24. Bukowski, K., Kciuk, M. & Kontek, R. Molecular Sciences Mechanisms of Multidrug Resistance in Cancer Chemotherapy. doi:10.3390/ijms21093233.

25. Gutierrez, D. A. *et al.* A new pyridazinone exhibits potent cytotoxicity on human cancer cells via apoptosis and poly-ubiquitinated protein accumulation. *Cell Biol Toxicol* **35**, 503–519 (2019).

26. How Does Chemo Work? | Types of Chemotherapy. *American Cancer Society* https://www.cancer.org/treatment/treatments-and-side-effects/treatment-types/chemotherapy/how-chemotherapy-drugs-work.html (2019).

27. Gao, G., Chen, L. & Huang, C. *Anti-cancer Drug Discovery: Update and Comparisons in Yeast, Drosophila, and Zebrafish*. (2014).

28. Mayr, L. M. & Bojanic, D. Novel trends in high-throughput screening. *Curr. Opin. Pharmacol.* **9**, 580–588 (2009).

29. Szymański, P., Markowicz, M. & Mikiciuk-Olasik, E. Adaptation of High-Throughput Screening in Drug Discovery-Toxicological Screening Tests. *Int. J. Mol. Sci* **13**, 427–452 (2008).

30. Hughes, J. P., Rees, S. S., Kalindjian, S. B. & Philpott, K. L. Principles of early drug discovery. *British Journal of Pharmacology* vol. 162 1239–1249 (2011).

31. Razali, N. S. C. *et al.* Curcumin piperidone derivatives induce anti-proliferative and anti-migratory effects in LN-18 human glioblastoma cells. *Sci. Rep.* **12**, 13131 (2022).

32. Tomeh, M. A., Hadianamrei, R. & Zhao, X. A review of curcumin and its derivatives as anticancer agents. *International Journal of Molecular Sciences* vol. 20 (2019).

33. KSandur, S. *et al.* Curcumin, demethoxycurcumin, bisdemethoxycurcumin, tetrahydrocurcumin and turmerones differentially regulate anti-inflammatory and anti-proliferative responses through a ROS-independent mechanism. *Carcinogenesis* **28**, 1765–1773 (2007).

34. Kostrzewa, T. *et al.* Curcumin and Its New Derivatives: Correlation between Cytotoxicity against Breast Cancer Cell Lines, Degradation of PTP1B Phosphatase and ROS Generation. *J. Mol. Sci* 22 (2021) doi:10.3390/ijms221910368.

35. Giordano, A. & Tommonaro, G. Curcumin and cancer. *Nutrients* vol. 11 (2019).

36. Karrouchi, K. *et al.* molecules Synthesis and Pharmacological Activities of Pyrazole Derivatives: A Review. doi:10.3390/molecules23010134.

37. Bennani, F. E. *et al.* Overview of recent developments of pyrazole derivatives as an anticancer agent in different cell line. *Bioorganic Chemistry* vol. 97 103470 (2020).

38. Alsayari, A., Asiri, Y. I., Bin Muhsinah, A. & Zaheen Hassan, M. Anticolon Cancer Properties of Pyrazole Derivatives Acting through Xanthine Oxidase Inhibition. (2021) doi:10.1155/2021/5691982.

39. Ou, S.-H. I. Drug Design, Development and Therapy Dovepress Crizotinib: a novel and first-in-class multitargeted tyrosine kinase inhibitor for the treatment of anaplastic lymphoma kinase rearranged non-small cell lung cancer and beyond. *Drug Des. Devel. Ther.* **5**, 471–485 (2011).

40. Lema, C., Varela-Ramirez, A. & Aguilera, R. J. *Differential nuclear staining assay for high-throughput screening to identify cytotoxic compounds*.

41. Hess, J. D. *et al.* Identification of a Unique Cytotoxic Thieno[2,3-c]Pyrazole Derivative with Potent and Selective Anticancer Effects In Vitro. *Biology (Basel).* **11**, (2022).

42. Robles-Escajeda, E. *et al.* A novel curcumin-like dienone induces apoptosis in triple-negative breast cancer cells. *Cell. Oncol.* doi:10.1007/s13402-016-0272-x.

43. Contreras, L. *et al.* Induction of apoptosis via proteasome inhibition in leukemia/lymphoma cells by two potent piperidones. *Cell. Oncol.* **41**, 623–636 (2018).

44. Van Engeland, M., Nieland, L. J. W., Ramaekers, F. C. S., Schutte, B. & Reutelingsperger, C. P. M. Annexin V-affinity assay: A review on an apoptosis detection system based on phosphatidylserine exposure. *Cytometry* vol. 31 1–9 (1998).

45. Boada-Romero, E., Martinez, J., Heckmann, B. L. & Green, D. R. The clearance of dead cells by efferocytosis. *Nature Reviews Molecular Cell Biology* vol. 21 398–414 (2020).

46. Birge, R. B. *et al.* Phosphatidylserine is a global immunosuppressive signal in efferocytosis, infectious disease, and cancer. *Cell Death and Differentiation* vol. 23 962–978 (2016).

47. Robles-Escajeda, E., Lerma, D., Nyakeriga, A. M., Ross, J. A. & Kirken, R. A. Searching in Mother Nature for Anti-Cancer Activity: Anti-Proliferative and Pro-Apoptotic Effect Elicited by Green Barley on Leukemia/Lymphoma Cells) Searching in Mother Nature for Anti-Cancer Activity: Anti-Proliferative and Pro-Apoptotic Effect Elicited by Green Barley on Leukemia/Lymphoma Cells. *PLoS One* **8**, 73508 (2013).

48. Villanueva, P. J. *et al.* Pyronaridine exerts potent cytotoxicity on human breast and hematological cancer cells through induction of apoptosis. *PLoS One* **13**, (2018).

49. Kumar, S. Caspase function in programmed cell death. *Cell Death and Differentiation* vol. 14 32–43 (2007).

50. Porter, A. G. & Jänicke, R. U. Emerging roles of caspase-3 in apoptosis. *Cell Death and Differentiation* vol. 6 99–104 (1999).

51. Jänicke, R. U., Sprengart, M. L., Wati, M. R. & Porter, A. G. Caspase-3 Is Required for DNA Fragmentation and Morphological Changes Associated with Apoptosis. *J. Biol. Chem.* **273**, 9357–9360 (1998).

52. Pistritto, G., Trisciuoglio, D., Ceci, C., Alessia Garufi & D'Orazi, G. Apoptosis as anticancer mechanism: Function and dysfunction of its modulators and targeted therapeutic strategies. *Aging (Albany. NY).* **8**, 603–619 (2016).

53. Tait, S. W. G. & Green, D. R. Mitochondria and cell death: Outer membrane permeabilization and beyond. *Nature Reviews Molecular Cell Biology* vol. 11 621–632 (2010).

54. Nunes, L. M. *et al.* A novel class of piperidones exhibit potent, selective and pro-apoptotic anti-leukemia properties. *Oncol. Lett.* **11**, 3842–3848 (2016).

55. Swain, R. M. *et al.* Two novel piperidones induce apoptosis and antiproliferative effects on human prostate and lymphoma cancer cell lines. *Invest. New Drugs* (2022) doi:10.1007/s10637-022-01266-y.

56. Sivandzade, F., Bhalerao, A. & Cucullo, L. Analysis of the Mitochondrial Membrane Potential Using the Cationic JC-1 Dye as a Sensitive Fluorescent Probe. *BIO-PROTOCOL* **9**, (2019).

57. Redza-Dutordoir, M. & Averill-Bates, D. A. Activation of apoptosis signalling pathways by reactive oxygen species. *Biochimica et Biophysica Acta - Molecular Cell Research* vol. 1863 2977–2992 (2016).

58. Ott, M., Gogvadze, V., Orrenius, S. & Zhivotovsky, B. Mitochondria, oxidative stress and cell death. *Apoptosis* vol. 12 (2007).

59. Tetz, L. M., Kamau, P. W., Cheng, A. A., Meeker, J. D. & Loch-Caruso, R. Troubleshooting the dichlorofluorescein assay to avoid artifacts in measurement of

toxicant-stimulated cellular production of reactive oxidant species. *J. Pharmacol. Toxicol. Methods* **67**, (2013).

60. Barnum, K. J. & O'Connell, M. J. Cell cycle regulation by checkpoints. *Methods Mol. Biol.* **1170**, 29–40 (2014).

61. Vermeulen, K., Van Bockstaele, D. R. & Berneman, Z. N. *The cell cycle: a review of regulation, deregulation and therapeutic targets in cancer*. *Cell Prolif* vol. 36 (2003).

62. Hoose, S. A., Duran, C., Malik, I., Eslamfam, S. & Shasserre, S. C. Systematic Analysis of Cell Cycle Effects of Common Drugs Leads to the Discovery of a Suppressive Interaction between Gemfibrozil and Fluoxetine. *PLoS One* **7**, 36503 (2012).

63. Jian Hua, Z. *REVIEW DNA fragmentation in apoptosis*. *Cell Research* vol. 10 (2000).

64. Fischer, M., Dang, C. V. & DeCaprio, J. A. Control of Cell Division. *Hematol. Basic Princ. Pract.* 176–185 (2018) doi:10.1016/B978-0-323-35762-3.00017-2.

65. Iglesias-Figueroa, B. F. *et al.* Recombinant human lactoferrin induces apoptosis, disruption of F-actin structure and cell cycle arrest with selective cytotoxicity on human triple negative breast cancer cells. *Apoptosis* **24**, 562–577 (2019).

66. D'Arcy, P. *et al.* Inhibition of proteasome deubiquitinating activity as a new cancer therapy. *Nat. Med.* **17**, 1636–1640 (2011).

67. Wang, X. *et al.* The proteasome deubiquitinase inhibitor VLX1570 shows selectivity for ubiquitin-specific protease-14 and induces apoptosis of multiple myeloma cells OPEN. (2016) doi:10.1038/srep26979.

68. Marques, C. *et al.* The triage of damaged proteins: degradation by the ubiquitin-proteasome pathway or repair by molecular chaperones. *FASEB J.* (2006) doi:10.1096/fj.05-5080fje.

69. Crawford, L. J., Walker, B. & Irvine, A. E. Proteasome inhibitors in cancer therapy. *Journal of Cell Communication and Signaling* vol. 5 101–110 (2011).

70. Wada, N. *et al.* Shikonin, dually functions as a proteasome inhibitor and a necroptosis inducer in multiple myeloma cells. *Int. J. Oncol.* **46**, 963–972 (2015).

71. Jang, H. H. Regulation of Protein Degradation by Proteasomes in Cancer. *J. Cancer Prev.* **23**, 153–161 (2018).

72. Clague, M. J. & Urbé, S. Leading Edge Minireview Ubiquitin: Same Molecule, Different Degradation Pathways. *Cell* **143**, 682–685 (2010).

73. Kyca, T. *et al.* Insight into bortezomib focusing on its efficacy against p-gp-positive mdr leukemia cells. *Int. J. Mol. Sci.* **22**, (2021).

74. Lipchick, B. C., Fink, E. E. & Nikiforov, M. A. Oxidative stress and proteasome inhibitors in multiple myeloma. *Pharmacol. Res.* **105**, 210–215 (2016).

75. Chiang, S. K., Chen, S. E. & Chang, L. C. A dual role of heme oxygenase-1 in cancer cells. *International Journal of Molecular Sciences* vol. 20 (2019).

76. Liu, X. M. *et al.* Endoplasmic reticulum stress stimulates heme oxygenase-1 gene expression in vascular smooth muscle: Role in cell survival. *J. Biol. Chem.* **280**, 872–877 (2005).

77. Brnjic, S. *et al.* Induction of tumor cell apoptosis by a proteasome deubiquitinase inhibitor is associated with oxidative stress. *Antioxidants Redox Signal.* **21**, 2271–2285 (2014).

78. Contreras, L. *et al.* Three novel piperidones exhibit tumor-selective cytotoxicity on leukemia cells via protein degradation and stress-mediated mechanisms. *Pharmacol. Reports* **3**, 159–174 (2022).

79. Subramaniam, D. *et al.* Diphenyl difluoroketone: A curcumin derivative with potent in vivo anticancer activity. *Cancer Res.* **68**, 1962–1969 (2008).

80. Gutierrez, D. A. *et al.* Identification of a Potent Cytotoxic Pyrazole with Anti-Breast Cancer Activity That Alters Multiple Pathways. *Cells* **11**, (2022).

81. Villanueva, P. J. *et al.* The Antimalarial Drug Pyronaridine Inhibits Topoisomerase II in Breast Cancer Cells and Hinders Tumor Progression In Vivo HHS Public Access. *Clin Cancer Drugs* **8**, 50–56 (2021).

82. Mellini, P. *et al.* Pyrazole-based inhibitors of enhancer of zeste homologue 2 induce apoptosis and autophagy in cancer cells. *Philos. Trans. R. Soc. B Biol. Sci.* **373**, 1–8 (2018).

83. Balbi, A. *et al.* Synthesis and biological evaluation of novel pyrazole derivatives with anticancer activity. *Eur. J. Med. Chem.* **46**, 5293–5309 (2011).

84. Wang, C. R., Wang, Z. F., Shi, L., Wang, Z. C. & Zhu, H. L. Design, synthesis, and biological evaluation of pyrazole derivatives containing acetamide bond as potential BRAFV600E inhibitors. *Bioorg. Med. Chem. Lett.* **28**, 2382–2390 (2018).

85. Martinotti, S. *et al.* Mitochondrial Reactive Oxygen Species and Their Contribution in Chronic Kidney Disease Progression Through Oxidative Stress. *Front. Physiol.* | *www.frontiersin.org* **1**, 627837 (2021).

86. Murphy, M. P. Mitochondrial dysfunction indirectly elevates ROS production by the endoplasmic reticulum. *Cell Metab.* **18**, 145–146 (2013).

87. Smith, P. J. *et al. Etoposide-induced cell cycle delay and arrest-dependent modulation of DNA topoisomerase H in small-cell lung cancer cells*. *Br. J. Cancer* vol. 914 (1994).

88. Ventura, E. & Giordano, A. Cell Cycle. *Ref. Modul. Life Sci.* (2019) doi:10.1016/B978-0-12-809633-8.90189-4.

89. Yang, X. *et al.* Article 19 1 (2020) High-Throughput Transcriptome Profiling in Drug and Biomarker Discovery. *Front. Genet* **11**, 19 (2020).

90. Srivastava, A., George, J. & Karuturi, R. K. M. Transcriptome analysis. in *Encyclopedia of Bioinformatics and Computational Biology: ABC of Bioinformatics* vols 1–3 792–805 (Academic Press, 2018).

91. Contreras, L. *et al.* Induction of apoptosis via proteasome inhibition in leukemia/lymphoma cells by two potent piperidones. *Cell. Oncol.* **41**, 623–636 (2018).

92. Bolger, A. M., Lohse, M. & Usadel, B. Trimmomatic: A flexible trimmer for Illumina sequence data. *Bioinformatics* **30**, 2114–2120 (2014).

93. Parrish, N., Hormozdiari, F. & Eskin, E. Assembly of non-unique insertion content using next-generation sequencing. *Bioinforma. Impact Accurate Quantif. Proteomic Genet. Anal. Res.* 21–40 (2014) doi:10.1201/b16589.

94. Langmead, B. & Salzberg, S. L. Fast gapped-read alignment with Bowtie 2. *Nat. Methods* **9**, 357–359 (2012).

95. Love, M. I., Huber, W. & Anders, S. Moderated estimation of fold change and dispersion for RNA-seq data with DESeq2. *Genome Biol.* **15**, 1–21 (2014).

96. Lim, N. & Pavlidis, P. Evaluation of connectivity map shows limited reproducibility in drug repositioning. *Sci. Rep.* **11**, 17624 (2021).

97. Subramanian, A. *et al.* A Next Generation Connectivity Map: L1000 Platform and the First 1,000,000 Profiles. *Cell* **171**, 1437-1452.e17 (2017).

98. Wang, K., Sun, J., Zhou, S., Wan, C. & Qin, S. Prediction of Drug-Target Interactions for Drug Repositioning Only Based on Genomic Expression Similarity. *PLoS Comput Biol* **9**, 1003315 (2013).

99. Connectivity Map (CMAP) | Broad Institute. https://www.broadinstitute.org/connectivity-map-cmap (2018).

100. Ibrahim, T. S., Hawwas, M. M., Malebari, A. M. & Taher, E. S. Potent Quinoline-Containing Combretastatin A-4 Analogues : Design , Synthesis , Antiproliferative , and Anti-Tubulin Activity.

101. Singh, S., Bani Baker, Q. & Singh, D. B. *Molecular docking and molecular dynamics simulation*. *Bioinformatics* (INC, 2022). doi:10.1016/b978-0-323-89775-4.00014-6.

102. Ferreira, L. G., Dos Santos, R. N., Oliva, G. & Andricopulo, A. D. Molecular docking and structure-based drug design strategies. *Molecules* vol. 20 13384–13421 (2015).

103. De Vivo, M., Masetti, M., Bottegoni, G. & Cavalli, A. Role of Molecular Dynamics and Related Methods in Drug Discovery. (2016) doi:10.1021/acs.jmedchem.5b01684.

104. Salo-Ahen, O. M. H. *et al.* Molecular dynamics simulations in drug discovery and pharmaceutical development. *Processes* vol. 9 1–63 (2021).

105. David, T. I. *et al.* Molecular docking analysis of phyto-constituents from Cannabis

sativa with pfDHFR. *print) Bioinformation* **14**, 574–579 (2018).

106. Schrödinger. What is considered a good GlideScore? *Schrödinger, Inc.* https://www.schrodinger.com/kb/639 (2010).

107. What is the difference between the docking score and GlideScore from the results of a docking run? | Schrödinger. https://www.schrodinger.com/kb/348.

108. Nitiss, J. L. Targeting DNA topoisomerase II in cancer chemotherapy. *Nature Reviews Cancer* vol. 9 338–350 (2009).

109. Stanton, R. A., Gernert, K. M., Nettles, J. H. & Aneja, R. ChemInform Abstract: Drugs that Target Dynamic Microtubules: A New Molecular Perspective. *ChemInform* **42**, no-no (2011).

110. Kapoor, S., Srivastava, S. & Panda, D. Indibulin dampens microtubule dynamics and produces synergistic antiproliferative effect with vinblastine in MCF-7 cells: Implications in cancer chemotherapy. *Sci. Rep.* **8**, 2–13 (2018).

111. Alatrash, N. *et al.* Disruption of microtubule function in cultured human cells by a cytotoxic ruthenium(ii) polypyridyl complex. *Chem. Sci.* **11**, 264–275 (2020).

112. Ma, Y., Zhou, Y., Xie, C., Chen, D. & Li, J. Novel microtubule-targeted agent 6-chloro-4-(methoxyphenyl) coumarin induces G2-M arrest and apoptosis in HeLa cells. *Nat. Publ. Gr.* (2012) doi:10.1038/aps.2011.176.

113. Bausch, E., Kohlhof, H., Hamm, S., Krauss, R. & Baumgartner, R. A Novel Microtubule Inhibitor 4SC-207 with Anti-Proliferative Activity in Taxane-Resistant Cells. *PLoS One* **8**, 79594 (2013).

114. Bonfils, C., Bec, N., Lacroix, B., Harricane, M. C. & Larroque, C. Kinetic analysis of tubulin assembly in the presence of the microtubule-associated protein TOGp. *J. Biol. Chem.* **282**, 5570–5581 (2007).

115. Campanacci, V. *et al.* Insight into microtubule nucleation from tubulin-capping proteins. *Proc. Natl. Acad. Sci. U. S. A.* **116**, 9859–9864 (2019).

116. Anichina, K. *et al.* 1H-benzimidazole-2-yl hydrazones as tubulin-targeting agents: Synthesis, structural characterization, anthelmintic activity and antiproliferative activity against MCF-7 breast carcinoma cells and molecular docking studies. *Chem. Biol. Interact.* **345**, 109540 (2021).

117. FDA. The Drug Development Process | FDA. *U.S. Food and Drug Administration* https://www.fda.gov/patients/learn-about-drug-and-device-approvals/drug-development-process (2018).

118. Steinmetz, K. L. & Spack, E. G. The basics of preclinical drug development for neurodegenerative disease indications. *BMC Neurol.* **9**, 1–13 (2009).

119. Fricke, I. B. *et al.* Spatiotemporal assessment of spontaneous metastasis formation using multimodal in vivo imaging in HER2+ and triple negative metastatic breast cancer xenograft models in mice. *PLoS One* **13**, (2018).

120. Zhu, Y. P. *et al.* Letter to the Editor: Administration of TGF-ß Inhibitor Mitigates Radiation-induced Fibrosis in a Mouse Model. *Clin. Orthop. Relat. Res.* **479**, 1862–1863 (2021).

121. Fda & Cder. TAXOL ® (paclitaxel) INJECTION (Patient Information Included).

122. Lu, Y. *et al.* Development and evaluation of transferrin-stabilized paclitaxel nanocrystal formulation. *J. Control. Release* **176**, 76–85 (2014).

123. Elmore, S. Apoptosis: A Review of Programmed Cell Death. *Toxicol. Pathol.* **35**, 495–516 (2007).

124. Kline-Smith, S. L. & Walczak, C. E. Mitotic spindle assembly and chromosome segregation: Refocusing on microtubule dynamics. *Mol. Cell* **15**, 317–327 (2004).

125. Salerni, B. L., Bates, D. J., Albershardt, T. C., Lowrey, C. H. & Eastman, A. Vinblastine Induces Acute, Cell Cycle Phase - Independent Apoptosis in Some Leukemias and Lymphomas and Can Induce Acute Apoptosis in Others when Mcl-1 is Suppressed. *Mol. Cancer Ther.* **9**, 791–802 (2010).

126. Thomas, E. *et al.* A novel resveratrol based tubulin inhibitor induces mitotic arrest and activates apoptosis in cancer cells. *Sci. Rep.* **6**, (2016).

127. Vallelian, F. *et al.* Proteasome inhibition and oxidative reactions disrupt cellular homeostasis during heme stress. (2015) doi:10.1038/cdd.2014.154.

128. Calderon, Ruben Israel, "Elucidating The Molecular Mechanism Of Action By Which RS1-208b Induces Apoptosis In Hematological Cancers" (2016). *Open Access Theses & Dissertations*. 614. https://scholarworks.utep.edu/open_etd/614

Curriculum Vita

Edgar Alonso Borrego Puerta was born in Durango, Dgo. Mexico. He obtained his bachelor's degree in biology from Instituto Tecnologico del Valle del Guadiana in 2014. In the fall of 2016, he joined the master's in Biology program at the University of Texas at El Paso. Edgar started working in Dr. Renato Aguilera's lab in the spring of 2017 whose main focus is anti-cancer drug discovery. While doing his master's, Edgar decided to pursue a doctoral degree and he transferred to the Ph.D. program in Biosciences at UTEP in the fall of 2019. During his doctoral career, Edgar participated in seven publications, and he is the co-first author in one of those publications.

Mr. Borrego was a teaching assistant for various laboratories during most of his graduate student years. He was also the instructor of record for the Molecular Cell Biology laboratory in the spring and summer of 2022 and he was the lecturer for Molecular Cell Biology in the summer of 2022. Edgar received a scholarship from the Government of Durango in 2017 and 2019. He was also awarded the UTEP Graduate School Dodson Grant for Research in the Spring of 2021. Edgar also mentored undergraduate students that are now pursuing their doctoral careers.

Edgar's dissertation work has a provisional patent and is expected to contribute to developing novel compounds with anti-cancer properties. After graduation, he plans to continue his career as a postdoctoral fellow.